

**KINETICS OF PHASE SEGREGATION IN A
QUENCHED ALLOY**

by

Anton Buhagiar B.Sc., M.Sc.

The Open University, Milton Keynes.

A Thesis in Statistical Mechanics

submitted for the Ph.D. degree at the Open University

Supervisor: O. Penrose

May 1980



University of Malta
L-Universita' ta' Malta

University of Malta Library – Electronic Thesis & Dissertations (ETD) Repository

The copyright of this thesis/dissertation belongs to the author. The author's rights in respect of this work are as defined by the Copyright Act (Chapter 415) of the Laws of Malta or as modified by any successive legislation.

Users may access this full-text thesis/dissertation and can make use of the information contained in accordance with the Copyright Act provided that the author must be properly acknowledged. Further distribution or reproduction in any format is prohibited without the prior permission of the copyright holder.

Acknowledgements

I dedicate this work to my parents, Paul and Pauline Buhagiar, to my uncle Carmelo Portelli, to my mother's cousin Carmena Micallef, and to my sister Mary Anne Buhagiar. Their encouragement and material support enabled me to pursue my tertiary education in Malta and in England.

I would also like to thank the Open University for awarding me a grant to read for the Ph.D. degree. This was a generous grant which covered my tuition and living expenses during the four and a half years which I spent at the OU between 1975 and 1980.

I would also like to thank my English colleagues and friends, Matthew Esplen, Lynne Graham, John Garne, Alf Vella, Brian Staff, Ian Breffit, Michael and Lily Buckley who helped me to settle in England, and to get used to the English way of life.

Above all, I would like to express my sincerest gratitude to my supervisor, Professor Oliver Penrose, without whose patience and kind expertise, this work would not have been possible.

A. Buhagiar, 1980.

Note to reader

The present document is a version of my 1980 thesis which was printed on a manual typewriter. This version was typeset in T_EX for better neatness and accessibility. It is practically identical to the original typewritten version: the only changes made were to correct typographical errors, and to improve clarity where necessary.

The main results of this thesis are summarised in the paper by my supervisor and myself:

Penrose O. and Buhagiar A. (1983) *Kinetics of Nucleation in a Lattice Gas Model: Microscopic Theory and Simulation Compared*, Journal of Statistical Physics, Vol. 30, No 1, Pages 219-241.

This T_EX version of my thesis is dedicated to my wife Violet, my children, Stefania and Paul, and my daughter-in-law, Maria, who afforded me with constant care and support during these past years.

A. Buhagiar, 2019.

Abstract

We model the time evolution of a lattice gas or binary alloy quenched from an infinite temperature to a temperature T less than T_c , the critical temperature. The alloy is represented on a simple cubic lattice of N sites by the Ising Model with Kawasaki dynamics assuming nearest neighbour attraction.

The Becker-Döring equations are used to model the rate of change of the distribution of cluster sizes in the quenched lattice gas. The coefficients of these equations are calculated from first principles by solving a diffusion problem for the concentration of particles near a given cluster. These coefficients are found for cluster sizes up to 6, and extrapolated to larger cluster sizes. The resulting version of the Becker-Döring equations are then solved numerically for $T = 0.59T_c$, for three separate densities, ρ , of the lattice gas: $\rho = 0.05, 0.075$ and 0.10 . Simulations of the lattice gas with these parameters were carried out by Marro and others.

At each density, the differential equations give quite good predictions of the cluster size distribution in the corresponding simulation, when the critical cluster size, usually denoted by l^* , is the same in both. The cluster size distribution in terms of l^* predicted by the Becker-Döring equations also compares very well with that observed in real alloys (Ni-Al), and is an improvement on the theory of Lifshitz and Slyozov, which consistently underestimates the number of large clusters.

The critical cluster size, $l^*(t)$, is compared between the simulations and the differential equations at the same value of the time t . For the lower density, $\rho = 0.05$, $l^*(t)$ is very well predicted by the Becker-Döring equations. For the higher densities, $\rho = 0.075$ and 0.10 , $l^*(t)$ was found to be approximately linear over the whole time range. However, the Becker-Döring equations underestimate the rate of growth of $l^*(t)$ by a factor of 0.3.

KEYWORDS: Lattice gas; binary alloy; clusters; kinetics; phase transitions; nucleation; Becker-Döring equations; Lifshitz-Slyozov theory.

Contents

Acknowledgements

Note to Reader

Abstract

Contents

Preface

Declaration of Originality

List of Figures

List of Tables

Chapter I: Introduction

- I. 1 Motivation of this work
- I. 2 The kinetic Ising Model of a lattice gas
- I. 3 Equilibrium properties of the Kawasaki model
- I. 4 Validity of the distribution (I, 6) for small clusters under conditions of steady state for various temperatures and densities
- I. 5 Fundamental equations of the Lifshitz-Slyozov theory

Chapter II: The Becker-Döring equations

- II. 1 The kinetic equations
- II. 2 Existence of a phase transition for $\rho > \rho_s$
- II. 3 The free energy

Chapter III: The kinetic coefficients $a_l(0)$ in the limit of zero density

- III. 1 Microscopic formulation
- III. 2 Boundary conditions

- III. 3 Calculation of the kinetic coefficients, $a_l(0)$
- III. 4 Comparison of $a_l(0)$ with the diffusion theory for a spherical cluster

Chapter IV: Calculation of $a_1(0)$ and $a_2(0)$ in terms of the parameter

$$\gamma \equiv \frac{p-1}{p_0} - 1, \text{ using the Green's function } G(r)$$

- IV. 1 The Green's function $G(\mathbf{r})$
- IV. 2 Calculation of $a_1(0)$ in terms of γ using $G(\mathbf{r})$
- IV. 3 Calculation of $a_2(0)$ in terms of γ using $G(\mathbf{r})$

Chapter V: Comparison of the Becker-Döring differential equations with the simulation of a quenched alloy at the same value of l^*

- V. 1 Numerical solution of the differential equations
- V. 2 Empirical estimates of $\mu(l^*)$
- V. 3 Comparison of the concentrations c_l of the large clusters in the simulation and the differential equations at the same value of l^*

Chapter VI: Calculation of $\mu(l^*)$: comparison of l_{sim}^* and l_{de}^* at the same value of the simulation time t

- VI. 1 Statistical mechanics of a lattice gas on the Bethe lattice
- VI. 2 Equilibrium distribution of small clusters on the Bethe lattice
- VI. 3 The diffusion constant on the Bethe lattice as a function of ξ
- VI. 4 Comparison of l_{sim}^* and l_{de}^* at the same value of the simulation time t

Chapter VII: Comparison of the Becker-Döring equations with the
Lifshitz-Slyozov theory and with real alloys

- VII. 1 Reduction of the Becker-Döring equations to (I, 13)
- VII. 2 Comparison of A , K and A/K for simulation and differential equations
- VII. 3 Comparison of the cluster size distribution predicted by the Becker-Döring equations with that of real alloys

Discussion and Conclusions

References

Preface

This thesis is an attempt to improve the theory of coarsening in quenched alloys due to Lifshitz and Slyozov.

We model the time evolution of a lattice gas or binary alloy quenched from an infinite temperature to a temperature $T < T_c$, the critical temperature. The alloy is represented by the Ising Model with Kawasaki dynamics assuming nearest neighbour attraction. The basic kinetic process is the interchange of two unlike particles on adjacent sites, and is Markovian. The time unit is one attempted interchange per lattice site. The model is described in Chapter I.

In Chapter II, we set up the Becker-Döring system of differential equations which assumes the droplets of the new phase to grow or shrink by absorbing or emitting one particle at a time. For each size of droplet, the relevant differential equation contains two kinetic coefficients, a_l and b_l which are related to the probability that an l -droplet absorbs or emits one particle. These coefficients, which also depend on the density ρ of particles on the lattice, are related by a detailed balance condition.

In Chapter III, we calculate $a_l(0)$, the value of a_l in the limit of zero density. As in the Lifshitz-Slyozov theory, we assume the absorption of monomers by a central cluster to be diffusion-controlled. We then express $a_l(0)$ as the solution of a lattice diffusion problem describing the motion of monomers (that is clusters of size $l = 1$) near a specified l -cluster with suitable boundary conditions at infinity and at the surface of the cluster. The coefficients $a_l(0)$, $1 \leq l \leq 6$, were found in this way, and shown to obey the relation $a_l(0)^3 \propto l$. This property was used to extrapolate $a_l(0)$ for $l > 6$. We then

compared the results for $1 \leq l \leq 6$ with the predictions of classical diffusion theory for spherical clusters.

Using Green's functions, we also obtained in Chapter IV a closed formula for $a_1(0)$ and $a_2(0)$ in terms of the transition probabilities and of the temperature. These estimates compared very favourably with the corresponding estimates obtained in Chapter III.

The Becker-Döring equations are solved numerically in Chapter V for densities $\rho = 0.05, 0.075$ and 0.10 . The solutions are compared with corresponding computer simulations (Marro, 1975) of a binary alloy. The comparison is done between instants when the critical cluster size, l^* , is the same in the differential equations and the simulation. For given l^* , the cluster size distribution predicted by the differential equations is very similar to that observed in the simulations. The quantity l^* is an important parameter which characterises the supersaturation. Clusters larger than l^* tend to grow at the expense of those smaller than l^* , which tend to shrink. According to the theory of Lifshitz and Slyozov, l^* grows linearly with time, t .

In Chapter VI, we complete the comparison by finding l^* as a function of the simulation time, t . To determine $l^*(t)$, we need to know the variation of a_l with l^* . We find that a_l is negative for small l^* , or high supersaturation, indicating the presence of spinodal decomposition initially. For higher values of l^* , however, $26 \lesssim l^* \lesssim 200$, a_l is approximately constant, with $a_l \approx 2a_l(0)$. The quantity $l^*(t)$ is then compared between the simulations and the Becker-Döring equations:

- For the lower density, $\rho = 0.05$, $l^*(t)$ is very well predicted by the Becker-Döring equations. However, $l^*(t)$ is only linear over the range

$80 \lesssim l^* \lesssim 200$, $4000 \lesssim t \lesssim 7000$, possibly due to the fact that the system is undergoing spinodal decomposition in the early stages of the nucleation.

- For the higher densities, $\rho = 0.075$ and 0.10 , it was found that $l^*(t)$ is linear in both simulation and differential equations, over the whole duration of the simulation ($0 \leq l^* \lesssim 200$, $0 \leq t \lesssim 6000$). However, the Becker-Döring equations underestimate the rate of growth of $l^*(t)$ by a factor of 0.3 .

In Chapter VII, the cluster size distribution in terms of l^* predicted by the Becker-Döring equations are compared with the cluster size distribution observed in real alloys (Ni-Al, Cd-Ag). It is found that the agreement is very good, and that our equations are an improvement on the theory of Lifshitz and Slyozov, which tends to underestimate the number of large clusters.

Declaration of Originality

Original work is contained in Chapters III, IV, V, VII, Section VI.4, and parts of Sections I.3 and I.4. The first three sections of Chapter VI are almost entirely due to my supervisor, Professor Oliver Penrose. Chapters I and II are of an introductory nature. The simulations were done by Marro et al. (1975).

The most important reference on which this work is based is the paper by Penrose et al. (1978), and we follow the formulation in that paper throughout. Other important references are:

- the review article by Penrose and Lebowitz (1978) which serves as a good introduction to the work contained in this thesis;
- the paper by Kalos et al. (1978) where the steady state distribution formula (I, 6) is given;
- the paper by Ardell and Nicholson (1966) which compares the cluster-size distribution in Ni-Al alloys with the predictions of the Lifshitz-Slyozov theory;
- the paper by Lifshitz and Slyozov (1961), which explains nucleation by diffusion in a supersaturated solution.

This thesis is not substantially the same as any which has already been submitted to any other university.

A. Buhagiar, 1980.

List of Figures

Chapter I

- Fig. (I, i): Illustration of a quench from temperature $T_1 > T_c$ to $T < T_c$ on the phase diagram of an alloy AB.
- Fig. (I, ii): A graph of w_s against $\frac{V}{kT}$ for the range $0.7 \leq \frac{V}{kT} \leq 2.0$.
- Fig. (I, iii): A graph of C against $\frac{V}{kT}$ for the range $0.7 \leq \frac{V}{kT} \leq 2.0$.

The constants w_s and C occur in the formula

$$\frac{Q_l}{Q_{l+1}} = w_s \left(1 + \frac{C}{(l-2)^{1/3}} \right).$$

Chapter III

- Fig. (III, i): Graphs of $a_l(0)^3$ against l for the range

$$-0.8 \leq \gamma \equiv \frac{p_{-1}}{p_0} - 1 \leq 0.8.$$

The points lie on a straight line with a small intercept, for each value of γ , as predicted by (III, 24).

- Fig. (III, ii): Graphs of $\frac{p_0}{a_l(0)}$ against $\frac{p_0}{p_{-1}}$ for $1 \leq l \leq 6$ over the range $0.2 \leq \frac{p_{-1}}{p_0} \leq 2$. The graphs for each integer l are all straight lines meeting on the line $\frac{p_0}{p_{-1}} = -1$.

Chapter IV

- Fig. (IV, i): Illustration showing a monomer at the origin with its nearest neighbours and second nearest neighbours. The two symmetries of the second nearest neighbours with respect to the central monomer are also shown.

- Fig. (IV, ii): Illustration showing a dimer at $(0, 0, 0)$ and $(1, 0, 0)$ and its ten nearest neighbours. We also show the four symmetries of the second nearest neighbours with respect to the central dimer.

Chapter V

- Fig. (V, i): Graph of t_{de} , the time in the differential equations with coefficient $a_l(0)$, against the simulation time $t (\equiv t_{sim})$, when the value of l^* is the same in the simulation and the differential equations. The slope of this graph gives an empirical estimate for $\mu(l^*)$. It is seen that $\mu(l^*)$ is practically constant for $t > 1000$. Densities $\rho = 0.05, 0.075$ and 0.10 .
- Fig. (V, ii): Comparison, at same l^* , of c_l for $l > 20$ for the simulation and the differential equations for $0 \leq t \leq 7000$. Densities $\rho = 0.05, 0.075$ and 0.10 .

Chapter VI

- Fig. (VI, i): Graph of $\mu(l^*)$ against l^* . The quantity $\mu(l^*)$ is effectively constant and is ≈ 2 in the range $50 \leq l^* \leq 200$.
- Fig. (VI, ii): Graph of $\frac{1}{6D_c}$ against t_{de} . The area under this graph up to t_{de} gives the simulation time t according to the theory of this chapter. Densities $\rho = 0.05, 0.075$ and 0.10 .
- Figures (VI, iii), (VI, iv), (VI, v): Graph of l_{sim}^* and l_{de}^* against simulation time t for densities $\rho = 0.05, 0.075$ and 0.10 , respectively.
- Fig. (VI, vi): Graph of t_{de} against simulation time $t_{sim} (\equiv t)$, as predicted by the theory in this chapter, for densities $\rho = 0.05, 0.075$ and 0.10 .

0.10. All three cases are approximated by the straight line, $t_{de} = \mu(l^*)(t_{sim} + t_0)$, with average slope $\mu(l^*) \cong 2.5$ and $t_0 \cong 1400$. Compare with Fig. (V, i) and (V, 3).

Chapter VII

- Fig. (VII, i): Graph of $g(l, l^*)$ against the argument $f \equiv \ln(l^*) + \phi\left(\frac{l}{l^*}\right)$ for the simulation at various values of l^* , and for the differential equations. The constant A/K is taken to be 4.0. This is a ‘universal’ curve independent of l^* . Density $\rho = 0.075$.
- Fig. (VII, ii): Graph of the slope of the previous figure against f , for simulation and differential equations. For a given value of A/K , the concentrations c_l are proportional to the ordinates in this figure. Density $\rho = 0.075$.
- Fig. (VII, iii): Graph of $l^{*1/3} l^{2/3} c_l$ against $\left(\frac{l}{l^*}\right)^{1/3}$ for our differential equations and for Ni-Al alloys (Ardell and Nicholson, 1966). The predictions of Lifshitz and Slyozov are also given. The ordinates at $l = l^*$ are all scaled down to 1.

List of Tables

Chapter I

- Table (I, i): The constants w_s and C in (I, 7) for temperatures in the range $0.7 \leq \frac{V}{kT} \leq 2.0$.
- Table (I, ii): Prediction of the steady state formula (I, 6) with simulation values of c_l . Density $\rho = 0.075$, and infinite temperature, $T = \infty$.
- Table (I, iii): Comparison of the distribution of small clusters in a simulation with the steady state distribution given by (I, 6), with a differential equation, described in Chapter II, which uses (I, 6) for its equilibrium concentrations. This is done for density $\rho = 0.10$ and temperature $T = 0.59T_c$.

Chapter III

- Table (III, i): Kinetic coefficients $a_l(0)$ in the limit of zero density for simulation parameters $\frac{V}{kT} = 1.5$, and transition probabilities $p(\mathbf{x}, \mathbf{y}) = \frac{p_i}{3}$, with p_i given in (I, 1) and (I, 2).
- Table (III, ii): Table of $a_l(0)$, the kinetic coefficients in the limit of zero density, for $1 \leq l \leq 6$, for parameters γ in the range $-0.8 \leq \gamma \leq 0.8$. Constants M and N in the equation (II, 24), $\frac{a_l(0)}{D} = (M + Nl)^{1/3}$, are obtained by least squares for each temperature. $D = \frac{p_0}{3} = \frac{1}{6}$ is the diffusion constant for monomers.
- Table (III, iii): List of $a_{\lambda\lambda+}$ for clusters λ of sizes $l = 3$ and 4 , for values of γ in the range $-0.8 \leq \gamma \equiv \frac{p-1}{p_0} - 1 \leq 0.8$. We also give $a_3(0)$ and $a_4(0)$ calculated from the Gibbs average (III, 20) of the individual $a_{\lambda\lambda+}$.

Chapter IV

- Table (IV, i): Table of Green's function for relevant values of \mathbf{r} :
the functions $G(\mathbf{r})$, defined in (IV, 2),
the functions $H^i(\mathbf{r})$, defined in (IV, 5), for $a_1(0)$,
the functions $G^i(\mathbf{r})$, defined in (IV, 22), for $a_2(0)$.
- Table (IV, ii): The kinetic coefficients $a_1(0)$ and $a_2(0)$ in the limit of zero density calculated by the Green's function method, compared with S.O.R. calculations from Chapter III. The closed formulae are given by (IV, 17) and (IV, 29).

Chapter V

- Table (V, i): Position of local maxima and minima in the $c_l - l$ curves, and concentrations at these two points for the differential equations and the simulation. Densities $\rho = 0.075$ and 0.10 .

Chapter VI

- Table (VI, i): Equilibrium parameters for the Bethe lattice with coordination number $q = 6$. These are compared with corresponding values obtained from a simulation of a lattice gas on a simple cubic lattice (Kalos et al., 1978). Temperatures $\frac{V}{kT} = 1.5, 1.0926$ and 0.99438 .
- Table (VI, ii): Steady state parameters on the Bethe lattice calculated in terms of ξ at $\frac{V}{kT} = 1.5$. In particular, we give c_1, l^* and $\mu(l^*) \equiv 6D_c$.
- Table (VI, iii): Values of l_{de}^* and l_{sim}^* corresponding to the same simulation time t . Densities $= \rho = 0.05, 0.075$ and 0.10 .

Chapter VII

- Table (VII, i): Comparison of the prediction of formulae (VII, 18) with simulation values of g obtained from Table VII of Penrose et al. (1978).

Chapter I: Introduction

I.1 Motivation of this work

A binary alloy, which we call AB, such as ZnAl or NiAl, is spatially homogeneous when it is in thermal equilibrium at a temperature $T_1 > T_c$ the critical temperature, that is it consists of one thermodynamic phase. If the system is suddenly quenched to a lower temperature, $T < T_c$, it remains spatially homogeneous. Thermal equilibrium, however, requires the coexistence of two phases, one A-rich and one B-rich phase, whenever the fraction ρ of A-atoms is in the range $\rho_A < \rho < \rho_B$, where ρ_A and ρ_B are the concentrations of the A and B phases as time $t \rightarrow \infty$. This quench is shown in Fig. (I, i), which gives the densities ρ_A and ρ_B for temperatures T below T_c . The nature of the time evolution of a quenched alloy is very important in metallurgy.

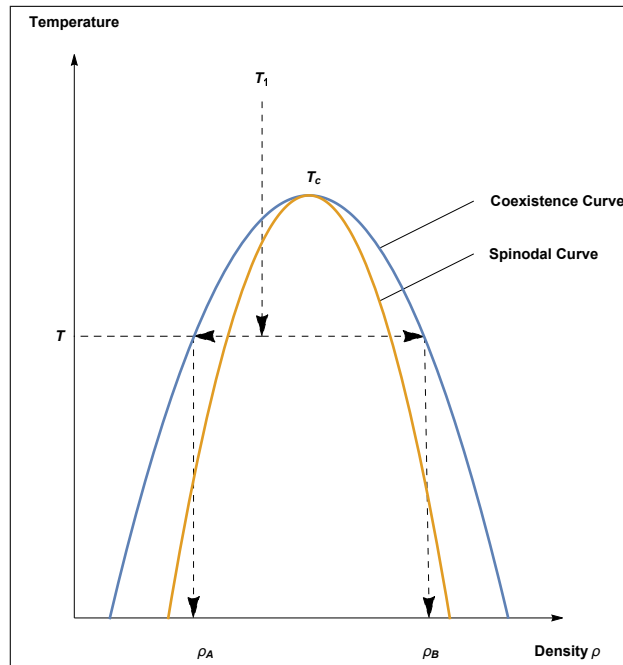


Fig. (I, i). Illustration of a quench from temperature $T_1 > T_c$ to $T < T_c$ on the phase diagram of an alloy AB.

The kinetics of this physical system can be studied by a set of kinetic equations put forward by Becker and Döring in 1935. These equations are well established as the basis for successful treatments of some topics in phase transition kinetics, such as metastability and Ostwald ripening. These equations assume that droplets of the new phase grow or shrink by absorbing or emitting one particle at a time. For each size of droplet, the equations contain two kinetic coefficients, one giving the probability per unit time that it will absorb a particle, the other giving the probability that it will emit a particle.

The normal methods for calculating these coefficients depend on treating the droplets as if they were spheres of the new phase. This assumption is, however, obviously invalid for ‘droplets’ consisting of only a few particles, and is in any case difficult to relate to the basic microscopic model. The difficulty of establishing such a relationship has already led to much controversy in the treatment of metastability. Refer for example to Lothe and Pound (1962).

It is the purpose of this work to describe, for a particular microscopic model, how the kinetic coefficients can be calculated directly from microscopic quantities. These kinetic coefficients, when used in the Becker-Döring theory, give a system of differential equations which can be integrated numerically to predict how the distribution of cluster sizes varies with time. These predictions are then compared with the results of computer simulations of the same microscopic model carried out by Kalos et al. (1978), and also with experimental results on real alloys.

The model to which our results apply is the Ising model with Kawasaki dynamics. This is a model of a binary alloy in which each lattice site is

occupied by one atom, and the state changes with time according to a Markov process where the allowed transitions are interchanges of the atoms on two neighbouring sites. The model is mathematically equivalent to a lattice gas, with each site either empty or occupied by a particle, in which case the allowed transitions are jumps of any particle to any neighbouring empty site. In either case, a nearest neighbour attractive law is assumed, and the transition probabilities are chosen in accordance with a detailed balancing condition which includes a specification of the temperature.

The Becker-Döring theory assumes that the new phase consists of widely separated droplets or nuclei immersed in the old phase. This requires one of the components of the alloy, the one which predominates in the new phase, to have a relatively small concentration. At such concentrations, it is convenient to use a lattice gas picture regarding the minority atoms as ‘particles’ and the majority atoms as ‘empty sites’. We can then describe the configurations in terms of clusters, a cluster being defined as a maximal connected set of particles (i.e. minority atoms), and to identify the clusters with the ‘droplets’ in the Becker-Döring theory. It was pointed out by Lifshitz and Slyozov (1961) and by Wagner (1961) that the rate of change of the average number of particles in a large spherical cluster can be found by treating the motion of the other particles nearby as a diffusion problem. We therefore apply a similar idea to the motion of the particle near a cluster of any size or shape: we express the Becker-Döring kinetic coefficients in terms of the solution of a lattice diffusion problem describing the motion of the other particles near a specified cluster with suitable boundary conditions at infinity and at the surface of the cluster. The kinetic coefficients are first found in the limit of zero density, that is when there are very few monomers around the central cluster; we then calculate these coefficients for non-zero densities.

Finally we compare the solution of the Becker-Döring system of equations utilising these coefficients, with experimental results from computer simulations of the lattice gas as described above (Kalos et al., 1978) and with real alloys (Ardell and Nicholson, 1966). We also see to what extent our results agree with the predictions of the theory of Lifshitz and Slyozov (1961), which has been widely used in metallurgy to explain the kinetics of coarsening in quenched alloys.

I.2 The kinetic Ising Model of a lattice gas

Most work on the time evolution of phase transitions in statistical mechanics has been done on dynamical models based on the Ising model (Ising, 1925). The reader is referred to the article, *Towards a rigorous theory of metastability* (Penrose and Lebowitz, 1978), for a review of these models.

The kinetic model relevant to the lattice gas (or binary alloy) is that of Kawasaki (1966, 1972). The simplest dynamical assumption is that the configuration of the lattice gas changes by a random movement to a neighbouring empty site. In binary alloy language, this is interpreted as a random interchange of atoms on neighbouring sites.

Kawasaki's kinetic model of the lattice gas was simulated on the computer (Marro et al. 1975). The lattice was taken to be simple cubic with N sites ($N = 125,000$). The basic dynamic process in the simulation was as follows: a site is picked at random, and then a nearest neighbour is picked at random, and if exactly one of these two sites is full, the particle moves to the other site with a transition probability p_n defined by:

$$p_n = \frac{1}{y^n + 1} \quad (\text{I, 1})$$

where n , positive or negative, is the net decrease or increase respectively in the number of nearest neighbours the particle will have after the proposed move, and y is the Boltzmann factor defined by

$$y = e^{V/kT} \quad (\text{I, 2})$$

where $V > 0$ is the attraction between two particles of the lattice gas which are nearest neighbours, k is Boltzmann's constant, and T is the absolute temperature. Equation (I, 1) satisfies detailed balancing (Glauber, 1963).

In the simulation, the duration Δt_{sim} of one such attempted interchange was defined to be $\frac{1}{N}$ units of time. Therefore, the probability $p(\mathbf{x}, \mathbf{y})$ of moving a particle from a site \mathbf{x} to a neighbouring site \mathbf{y} in time $\frac{1}{N}$, given \mathbf{x} is full and \mathbf{y} is empty can be written as:

$$\begin{aligned} p(\mathbf{x}, \mathbf{y}) = & \\ [\text{Prob (site } \mathbf{x} \text{ is chosen from } N \text{ sites)} \times \text{Prob(choosing nearest neighbour } \mathbf{y}) + & \\ \text{Prob (site } \mathbf{y} \text{ is chosen from } N \text{ sites)} \times \text{Prob(choosing nearest neighbour } \mathbf{x})] & \\ \times \text{transition probability that the interchange between } \mathbf{x} \text{ and } \mathbf{y} \text{ take place} & \\ = \left(\frac{1}{N} \times \frac{1}{6} + \frac{1}{N} \times \frac{1}{6} \right) \times p_n = \frac{p_n}{3} \times \frac{1}{N} = \frac{p_n}{3} \times \Delta t_{sim}, \quad \text{that is} & \end{aligned}$$

$$p(\mathbf{x}, \mathbf{y}) = \frac{p_n}{3} \Delta t_{sim} \quad (\text{I, 3})$$

since $\frac{1}{N}$ is the duration of one attempted interchange in the simulation. The probability that a monomer at site \mathbf{x} goes to a neighbouring site \mathbf{y} is therefore $\frac{p_n}{3}$ per unit time.

Such a model, however, is a simplification of real alloys, where lattice misfit of the two kinds of atoms and resulting elastic distortion has to be taken into account. Besides, exchange in most real alloys take place indirectly via

vacancies (the *hole* mechanism) rather than by the ring mechanism used in the Kawasaki model. The ring mechanism is observed only in Cu-Mo and some pure metals like copper and gold. Marro et al., however noticed that the simulation results did not depend crucially on the number of vacancies.

I.3 Equilibrium properties of the Kawasaki model

Each configuration of the lattice gas can be partitioned into connected subsets which we call *clusters*. A cluster is a collection of occupied sites such that no site is a nearest neighbour of an occupied site outside the cluster, but if a cluster is subdivided into subsets, then at least one member of one subset is the nearest neighbour of a member of another subset. The number per lattice site of clusters consisting of exactly l particles is denoted by c_l . This is also referred to as the concentration of l -clusters.

The equilibrium values of c_l can be found in terms of the partition function Q_l for clusters of size l (Lebowitz and Penrose, 1978). The quantities Q_l are given by

$$Q_l = \sum_{\lambda}^{\prime} y^{n(\lambda)} \quad (\text{I, 4})$$

where y is the Boltzmann factor $e^{V/kT}$ defined in (I, 2), \sum^{\prime} runs over the set of translationally inequivalent clusters λ of size l , and $n(\lambda)$ is the number of pairs of nearest neighbours in cluster λ . The partition functions Q_l are polynomials in the Boltzmann factor y , and have been found by Sykes (1976) for the simple cubic lattice for $1 \leq l \leq 10$:

$$Q_1 = 1$$

$$Q_2 = 3y$$

$$Q_3 = 15y^2$$

$$Q_4 = 83y^3 + 3y^4$$

$$Q_5 = 486y^4 + 48y^5$$

$$Q_6 = 2967y^5 + 496y^6 + 18y^7$$

$$Q_7 = 18748y^6 + 4368y^7 + 378y^8 + 8y^9$$

$$Q_8 = 121725y^7 + 36027y^8 + 4854y^9 + 306y^{10} + y^{12}$$

$$Q_9 = 807381y^8 + 288732y^9 + 51030y^{10} + 5544y^{11} + 159y^{12} + 24y^{13}$$

$$Q_{10} = 5447203y^9 + 2280792y^{10} + 488976y^{11} + 72244y^{12} + 5103y^{13} + 396y^{14} + 24y^{15}$$

The importance of these Q'_l s lies in the fact that the equilibrium value of c_l can be obtained in terms these Q'_l s. For low densities, we have (Penrose and Lebowitz, 1978)

$$c_l = Q_l z^l \quad (\text{I, 5})$$

where z is the fugacity of the system for a given temperature T and density ρ .

Equation (I, 5) has to be modified to hold for higher values of the fugacity z or density ρ . The empirical law corresponding to (I, 5) for higher densities was deduced from computer simulations of a binary alloy (Sur et al., 1977). The results were analysed by Kalos et al. (1978). They found that the distribution of sizes of small clusters at equilibrium and at low supersaturation, when the system appeared to be in a metastable state could be represented by the empirical formulae:

$$c_1 \approx (1 - \rho)^3 w \quad \text{and} \quad c_l \approx (1 - \rho)^4 Q_l w^l, \quad l \geq 2 \quad (\text{I, 6})$$

where ρ is the density in lattice gas language, or fractional concentration of

the minority phase in alloy language. The empirical formula (I, 6) reduces to (I, 5) in the limit of zero density, when $w \rightarrow z$. Equation (I, 6) is very important, and the extent of its validity will be discussed in the next session.

For $l \geq 11$, the coefficients Q_l are obtained from the extrapolation formula for Q_l/Q_{l+1} given by (Penrose et al., 1978):

$$w_l \equiv \frac{Q_l}{Q_{l+1}} = w_s \left(1 + \frac{C}{(l-2)^{1/3}} \right). \quad (\text{I, 7})$$

The physical basis of this equation is that the excess pressure of a spherical droplet of radius r (proportional to $l^{1/3}$) is proportional to $1/r$. The quantity w_s is the saturation value of w in equation (I, 6) and the constant C acts like a surface tension. The presence of $(l-2)$ rather than l in (I, 7) was explained by Frenkel (1946). The reason for this is that for a system of l particles, the total number of internal degrees of freedom is $3(l-2)$ and not $3l$, as it is assumed to be, to a good approximation, in classical thermodynamics. This distinction becomes important only for small l . Equation (I, 7) is related to the capillarity approximation (Abraham, 1974), whereby small clusters are treated as macroscopic drops.

We have performed a least square analysis of (I, 7) for different temperatures for $4 \leq l \leq 9$. We give w_s and C in Table (I, i) for different values of $\frac{V}{kT}$. The accuracy of (I, 7) for $1 \leq l \leq 9$ with these values of w_s and C is always better than 0.2% for the range $0.7 \leq \frac{V}{kT} \leq 2.0$. We also compare three values of w_s for different temperatures with values of w_s observed in the simulations at the coexistence density at these temperatures (Kalos et al., 1978). These are given in italics in Table (I, 1).

Table (I, i). The constants w_s and C in (I, 7) for various temperatures.

$\frac{V}{kT}$	w_s	C
0.7	0.04152	1.044
0.8	0.03624	1.104
0.9	0.03143	1.180
1.0	0.02704	1.275
<i>1.0</i>	<i>(0.03525)</i>	
1.094	0.0235	1.380
<i>1.094</i>	<i>(0.0298)</i>	
1.2	0.01942	1.555
1.3	0.01613	1.764
1.4	0.01315	2.046
1.5	0.01046	2.440
<i>1.5</i>	<i>(0.010526)</i>	<i>(2.415)</i>
1.6	0.00849	3.019
1.7	0.005897	3.932
1.8	0.003989	5.556
1.9	0.002316	9.157
2.0	0.000866	23.450

At $\frac{V}{kT} = 1.5$, the values of w_s differ by only $\frac{1}{2}\%$, but are considerably lower at $\frac{V}{kT} = 1.0$ and 1.094. A possible reason for this is that for these higher temperatures, for given l , there are relatively fewer compact clusters and so the clusters tend to deviate more from the compactness of spherical clusters at higher temperatures. In Fig. (I, ii) and Fig. (I, iii), we plot w_s and C against $\frac{V}{kT}$ for $0.7 \leq \frac{V}{kT} \leq 2.0$.

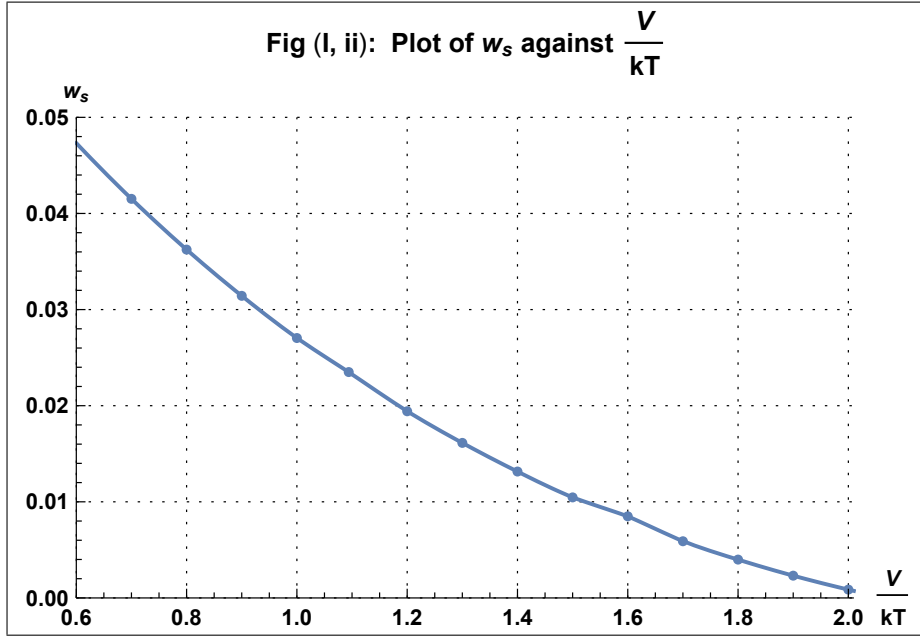


Fig. (I, ii). A graph of w_s against $\frac{V}{kT}$ for the range $0.7 \leq \frac{V}{kT} \leq 2.0$.

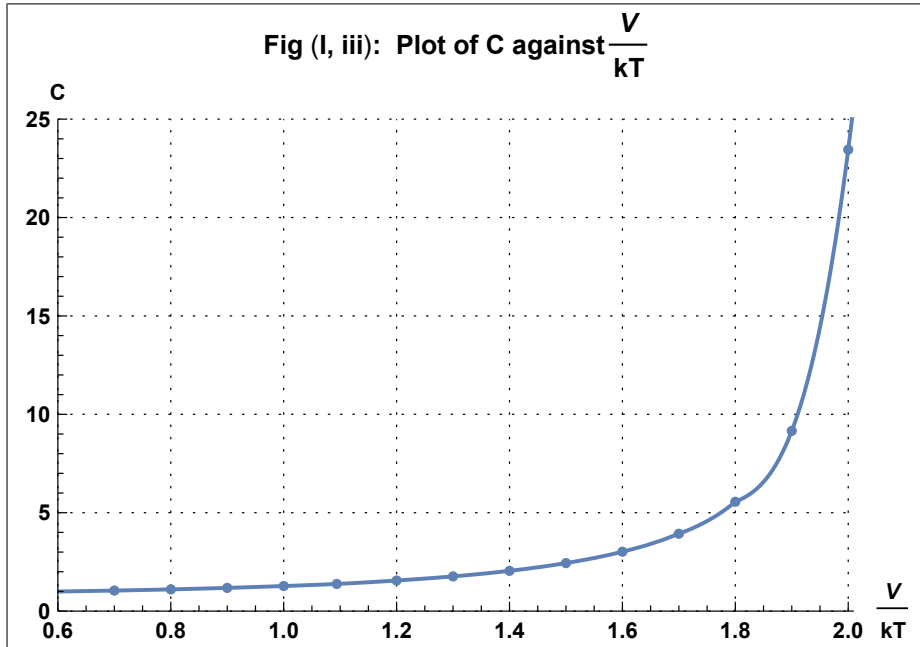


Fig. (I, iii). A graph of C against $\frac{V}{kT}$ for the range $0.7 \leq \frac{V}{kT} \leq 2.0$.

The constants w_s and C occur in formula (I, 7): $w_l \equiv \frac{Q_l}{Q_{l+1}} = w_s \left(1 + \frac{C}{(l-2)^{1/3}} \right)$.

I.4 Validity of the distribution (I, 6) for small clusters under conditions of steady state for various temperatures and densities.

The distribution (I, 6) holds for small clusters under equilibrium conditions (Kalos et al., 1978). To find the parameter w in (I, 6) for a given density ρ and temperature T , we define ρ_L as the total number of particles per site in clusters of size L or less. Assuming (I, 6) is valid,

$$\rho_L = \sum_1^L l c_l = (1 - \rho)^3 w + (1 - \rho)^4 \sum_2^L l Q_l w^l \quad (\text{I, 8})$$

where L is a suitable cutoff, such as 10 or 20, such that clusters less than L are considered ‘small’, and clusters bigger than L are considered ‘big’. The quantity ρ_L signifies the number of particles in the small clusters.

To find the equilibrium distribution of small clusters at infinite temperature, we can put $\rho_L = \rho$ in (I, 8) because c_{L+1} is very small under these conditions. One can then solve for w in (I, 8) and get the distribution of small clusters from (I, 6), with Q_l evaluated at $T = \infty$, or $y = 1$. We compare c_l predicted by the w -formula (I, 6) with the concentrations c_l of small clusters obtained from a simulation (Marro, 1975) with the particles distributed at random on the lattice, corresponding to infinite temperature. In Table (I, ii) we give this comparison for $\rho = 0.075$ using a cutoff value of $L = 10$. We can see that the agreement is quite good. This method works for densities ρ less than about 10%.

Table (I, ii). Comparison of simulation concentrations c_l with c_l as obtained from solving for w in (I, 8). $\rho = 0.075$, $T = \infty$.

l	$125,000 \times c_l$	
	Simulation	Solving (I,9)
1	5790	5866
2	965	965
3	310	286
4	88	97
5	35	36
6	21	14
7	11	6
8	4	2
9	1	1
10	0	0
> 10	1	0

The equation (I, 6) can also be shown to hold under approximately steady state conditions, if one considers w to be a parameter which decreases slowly with time while nucleation is taking place until it reaches w_s at equilibrium. Thus given ρ_L, ρ and T , one can solve for w from (I, 8), and use (I, 6) to give us the steady state distribution for small clusters. This is given in Table (I, iii) for $T = 0.59T_c$ ($y = 4.482$), $w_s = 0.010526$, and $\rho = 0.10$, which is $\gg 0.01046$, the coexistence density at this temperature.

In this table, we compare the predictions of the w -formula (I, 7) with the distribution of small clusters from a simulation by Marro (1976). We

compare them for various times. The parameter w was obtained by finding ρ_{10} from the simulation, and then solving (I, 8) with $L = 10$. The agreement again is quite good over the range $1.4 \leq \frac{w}{w_s} \leq 2$, implying that (I, 6) is valid even for quasi-equilibrium conditions.

In Table (I, iii), we also give the predictions of a set of differential equations by Becker-Döring, using (I, 6) for its steady state properties, and described in Chapter II, for the evolution of c_l with time. We give c_l for $l = 1$ to 10 in the differential equations, for a value of time when the value of c_1 is approximately the same as that in the w -formula (I, 6). The differential equations' distribution is quite near to the w -formula and to the simulation distribution, and it predicts ρ_{10} accurately.

Equation (I, 7) can be used to relate w , which is a measure of the supersaturation, to a characteristic cluster size, l^* , which we define by

$$w = w_s \left(1 + \frac{C}{(l^* - 2)^{1/3}} \right). \quad (\text{I, 9})$$

When l^* is defined in this way, it can be shown that (Penrose et al., 1978) that l^* is a critical size, such that clusters larger than l^* grow at the expense of those less than l^* , which tend to shrink. While nucleation is taking place, w decreases slowly to w_s , and l^* increases by (I, 9). The basic theory in the theory of coarsening (Lifshitz and Slyozov, 1961, and Wagner, 1961) is that l^* increases linearly with time during the coarsening of quenched alloys.

The quantity l^* , or w , characterises the distribution of the small clusters via Equations (I, 9) and (I, 6). We have shown in this section that the important formula (I, 6) holds not only for equilibrium, but also under conditions which are approximately steady state. It holds for temperatures T above and below T_c , and for densities ρ as high as 0.10.

t_{sim}	$\frac{w}{w_s}$	l^*		c_1	c_2	c_3	c_4	c_5	c_6	c_7	c_8	c_9	c_{10}	ρ_{10}
75.7	2.016	15.4	sim	2134	546	248	145	97	69	53	44	34	29	6764
			$w_{Eq(6)}$	1934	497	237	144	100	75	60	50	44	39	6771
			de	1923	497	241	152	110	85	69	59	51	45	7172
550.9	1.701	42.9	sim	1621	368	139	71	39	27	18	14	9	9	3818
			$w_{Eq(6)}$	1631	353	142	73	43	27	18	13	9	7	3813
			de	1631	354	142	74	44	29	20	14	11	9	3896
1105.7	1.621	60.8	sim	1545	333	123	59	32	18	13	9	6	5	3358
			$w_{Eq(6)}$	1554	321	123	60	34	20	13	9	6	4	3352
			de	1555	322	123	61	34	21	14	10	7	5	3399
2358.4	1.506	110.5	sim	1465	282	100	42	23	12	8	4	3	2	2813
			$w_{Eq(6)}$	1445	277	98	45	23	13	8	5	3	2	2809
			de	1443	277	98	45	23	13	8	5	3	2	2807
4118.2	1.429	180.2	sim	1397	260	83	33	16	8	5	3	2	1	2508
			$w_{Eq(6)}$	1371	250	84	36	18	10	5	3	2	1	2504
			de	1371	250	84	36	18	10	5	3	2	1	2504
5570.5	1.431	177.9	sim	1420	266	77	32	16	9	4	3	2	1	2515
			$w_{Eq(6)}$	1373	250	84	37	18	10	5	3	2	1	2510
			de	1373	250	84	37	18	10	5	3	2	2	2510

Table (I, iii). Steady state small cluster distribution at $T = 0.59T_c$, $\rho = 0.10$.

I.5 Fundamental equations of the Lifshitz-Slyozov theory.

In a supersaturated solution, diffusion effects may bring about the formation of grains of the new phase. Two stages of this process may be distinguished. In the first, concentration fluctuations produce nuclei of the new phase which grow directly from the supersaturated medium. The second stage may be considered to begin when the grains thus formed have reached an appreciable size and the degree of supersaturation is small. The rate of formation of the larger droplets is most often controlled (Greenwood, 1969; Ardell, 1969) by the rate at which the solute diffuses between particles. The second stage is often called coarsening or Ostwald ripening.

To obtain the fundamental equation of Lifshitz and Slyozov, we solve the diffusion equation for the monomer concentration

$$\frac{\partial c(\mathbf{r}, t)}{\partial t} = D\nabla^2 c(\mathbf{r}, t)$$

given a spherical cluster of radius R at the origin. D is the diffusion constant of monomers. Assuming steady state and using spherical symmetry, this equation reduces to $\frac{\partial^2}{\partial r^2}(rc) = 0$, that is

$$c(r) = A + \frac{B}{r} \tag{I, 10}$$

where A and B are constants determined by two boundary conditions. As $r \rightarrow \infty$, $c(r)$ tends to the overall monomer concentration c_1 , and so

$$A = c_1.$$

Kelvin's equation now gives $c(R)$, the monomer concentration at the surface of the cluster, as

$$c(R) = c_{1eq} + \frac{\alpha}{R}$$

where c_{1eq} is the equilibrium concentration of monomers, and α is a positive constant. This equation holds for small supersaturations $\Delta \equiv c_1 - c_{1eq} \ll 1$. With these boundary conditions,

$$B = \alpha - R\Delta,$$

and so equation (I, 10) then gives

$$c(r) = c_1 + \frac{\alpha - R\Delta}{r} \quad (\text{I, 11})$$

The rate at which monomers flow towards the central cluster per unit area is given by $j = D \frac{\partial c}{\partial r} \Big|_{r=R}$. When this is multiplied by the surface area of the cluster, it is equal to the rate of increase of the volume of the cluster:

$$4\pi r^2 D \frac{\partial c}{\partial r} \Big|_{r=R} = \frac{d}{dt} \left(\frac{4}{3} \pi R^3 \right).$$

Substituting $c(r)$ from equation (I, 11), we obtain

$$\frac{dR}{dt} = \frac{D}{R} \left(\Delta - \frac{\alpha}{R} \right). \quad (\text{I, 12})$$

Thus for every value Δ of the supersaturation, there exists a critical radius $R_c = \frac{\alpha}{\Delta}$ such that a cluster of this size is in equilibrium with the solution. If $R > R_c$, the grain grows, whilst if $R < R_c$ it dissolves. This is the basic mechanism for coarsening. Both Δ and R_c themselves vary with time.

Assuming a spherical cluster, if we define its volume to be $l = \frac{4}{3} \pi R^3$, and define $\bar{l} = \frac{4}{3} \pi R_c^3$ as the critical size, we can write equation (I, 12) as

$$\frac{dl}{dt} = 4\pi D \alpha \left[\left(\frac{l}{\bar{l}} \right)^{1/3} - 1 \right]. \quad (\text{I, 13})$$

This formula is the basis for the Lifshitz-Slyozov theory. From it we can deduce that particles of size greater than \bar{l} , tend to grow at the expense

of particles of size less than \bar{l} which tend to disappear. The critical size \bar{l} is predicted to grow linearly with time in the case of diffusion controlled growth. It has been shown (Penrose et al., 1978), that for large l , the equations of Becker-Döring (1935) can be reduced to an equation similar to (I, 13) with $\bar{l} = l^*$, defined in equation (I, 9). We will set up the Becker-Döring equations in the next chapter, and we will compare their predictions with those of Lifshitz and Slyozov in Chapter VII.

Chapter II: The Becker-Döring equations

It is the purpose of this Chapter to set up a system of differential equations of the Becker-Döring type (Becker-Döring, 1935) to predict the kinetics of the growth of clusters in the Kawasaki model.

The basic assumption of the Becker-Döring theory is that a droplet or cluster of one phase can increase or decrease in size by at most one particle at a time. So the Becker-Döring model neglects processes like the coagulation of two large clusters to form an even larger one, or its inverse, the breaking up of a large cluster into two large parts. Rough estimates, however, indicate that processes involving more than one large cluster are relatively unimportant for sufficiently small times and for low densities ($\rho = 0.10$) of the minority phase (Penrose et al., 1978). Coalescence effects have been studied by Smoluchowski (1916) in connection with the formation of droplets, and also by Binder (1974, 1976) and by Mirolid and Binder (1977).

We will follow closely the paper *Growth of Clusters in a First-Order Phase Transition* by Penrose et al. (1978), in the formulation of the Becker-Döring equations in this chapter.

II.1 The Kinetic Equations

We define c_l as the number of clusters of size l per site of the lattice. If the only processes considered are the absorption and emission of a monomer by a cluster of arbitrary size, we can write the Becker-Döring equations as

$$\frac{dc_l}{dt} = J_{l-1} - J_l, \quad l \geq 2 \quad (\text{II, 1})$$

where J_l is the net rate of conversion per site of l -particle clusters into $(l+1)$ -

particle clusters, and is given by

$$J_l = a_l c_l c_1 - b_{l+1} c_{l+1}, \quad l \geq 1 \quad (\text{II, 2})$$

Here a_l and b_{l+1} are kinetic coefficients: a_l describes the rate at which l -particle clusters absorb monomers, and b_{l+1} is a coefficient describing the rate at which $(l + 1)$ -particle clusters emit monomers. To complete the system of equations we also need one for c_1 . The condition determining c_1 is the conservation of matter, which can be written as

$$\sum l c_l = \rho = \text{constant} \quad (\text{II, 3})$$

where ρ is the total number of particles divided by the total number of lattice sites. We call ρ the density, which is a constant independent of time.

The coefficients a_l and b_{l+1} in (II, 2) are related through the fact that by a detailed balancing argument, $J_l = 0$ at equilibrium. If the density is small enough for the equilibrium state to have only one phase, it is reasonable to assume that the cluster concentration at equilibrium, c_l^{eq} , are given approximately by equation (I, 6) for all l :

$$c_1 \approx (1 - \rho)^3 w \quad \text{and} \quad c_l \approx (1 - \rho)^4 Q_l w^l, \quad l \geq 2 \quad (\text{I, 6})$$

where Q_l is the partition function for l -sized clusters on the simple cubic lattice. Substituting (I, 6) into equation (II, 2), and setting $J_l = 0$, we obtain for the ratio b_{l+1}/a_l at density ρ , a formula depending weakly on the density through the factor $(1 - \rho)^3$:

$$\frac{b_{l+1}}{a_l} = \frac{c_1^{eq} c_l^{eq}}{c_{l+1}^{eq}} = \begin{cases} w_1 (1 - \rho)^2 & \text{for } l = 1 \\ w_l (1 - \rho)^3 & \text{for } l \geq 2 \end{cases} \quad (\text{II, 4})$$

where w_l is defined by

$$w_l = \frac{Q_l}{Q_{l+1}} \quad (\text{II, 5})$$

The asymptotic nature of w_l has already been discussed in equation (I, 7).

If we let $\rho \rightarrow 0$ in (II, 4), we obtain

$$b_{l+1}(0) = a_l(0)w_l \quad (\text{II, 6})$$

where $b_{l+1}(0)$ and $a_l(0)$ are the values of b_{l+1} and a_l in the limit of zero density.

Equation (II, 4) shows the dependence of the ratio b_{l+1}/a_l on density. In Chapter V, we will show that a_l can be written as

$$a_l = \mu(l^*)a_l(0) \quad (\text{II, 7})$$

where $\mu(l^*)$ gives the variation of a_l with l^* , or equivalently with the size distribution of the small clusters, these being the most mobile.

In Chapter III, we will describe a method of calculating $a_l(0)$ and we will derive an asymptotic formula of the form $a_l(0) \propto l^{1/3}$, i.e. that a_l increases as the radius of an l -cluster approximately in the case of diffusion-controlled growth (Penrose et al., 1978; Lifshitz and Slyozov, 1961). The equations (II, 4), (II, 6) and (II, 7) imply that the variation with density of b_{l+1} is given by

$$b_{l+1} = \mu(l^*)b_{l+1}(0) \times \begin{cases} (1 - \rho)^2 & \text{for } l = 1 \\ (1 - \rho)^3 & \text{for } l \geq 2 \end{cases} \quad (\text{II, 8})$$

where $b_{l+1}(0)$ is the value of b_{l+1} in the limit of zero density.

The factor $(1 - \rho)^3$ in (II, 8) represents the reduction in probability of evaporation of a monomer from an $(l + 1)$ -particle cluster caused by the

possibility that a monomer cannot by definition form on any site next to a site that is already occupied. In (II, 8) we assumed for simplicity that (II, 4) is also valid at higher densities for which the equilibrium has two phases, even though the size distribution formula (I, 6) is not valid for large l , either in the equilibrium state or even in the quasi-stationary state with a time dependent w (Penrose et al., 1978).

For numerical purposes, one has to take a finite system of equations in (II, 1). This is done by letting $c_l = 0$ for $l \geq L$. This L is different from the L in equation (I, 8). We then define the time derivative of c_L by

$$\frac{dc_L}{dt} = J_{L-1} \quad (\text{II, 9})$$

Provided L is big enough, the solution does not depend on the actual value of L . We took L to be 800. The choice of L will be discussed in more detail in Chapter V.

Equations based on the Becker-Döring theory were used by others including Courtney (1962), Abraham (1969), and Bauer et al. (1978). Their differential equations were considerably different from ours. The coefficient a_l was taken to be proportional to $l^{2/3}$ for surface controlled growth. In this work, in Chapters III and IV, we will take a_l proportional to $l^{1/3}$ for diffusion controlled growth, which is the more common mechanism of growth in the coarsening of quenched alloys. Another important distinction is that in our system of equations, we have conservation of mass, which is not assumed in these three cited works. Also c_1 , the concentration of monomers, is assumed to be constant with time in the papers by Courtney and Abraham, whereas in our system, c_1 decreases monotonically with time for the initial conditions described in Section (V,1).

These three authors also used very small values for L , namely 110, 110 and 25. By comparison, we have to take $L \approx 800$ to describe what happens in the simulations (Marro, 1975), since there was a considerable number of clusters of size 600 in the simulation for the later times.

II.2 Existence of a Phase Transition for $\rho < \rho_s$ and $T < T_c$

When in equation (I, 8) we let $L \rightarrow \infty$, we obtain an infinite series for the density in terms of w . The function $\rho(w)$ is the number of particles in the ‘vapour phase’ for a given value of w . The radius of convergence of the series for $\rho(w)$ is given by $w_s = \lim_{l \rightarrow \infty} (Q_l/Q_{l+1})$ from (I, 7). For $T < T_c$, the value $\rho(w_s) = \rho_s$, the critical density, which is finite (Fisher, 1967). For $\rho \leq \rho_s$, one can find a value of w in $(0, w_s]$ so that

$$\rho(w) = \rho \tag{II, 10}$$

In this case, therefore, no new phase is nucleated. For $\rho > \rho_s$, however, no such w can be found since the density in the vapour phase cannot exceed ρ_s . Therefore the quantity $\rho - \rho_s$ is interpreted as the density of the nucleated phase. The quantity ρ_s is the saturated vapour pressure in lattice gas language, or the equilibrium concentration of one metal in a binary alloy.

For $T > T_c$, however, Fisher’s theory would require $C \rightarrow 0$ in (I, 7) as $T \rightarrow T_c$ from above. This is not confirmed by our data in Table (I, i), where for $V/kT_c = 0.89$, C is about 1.18. This suggests that (I, 7) is not accurate for large l for temperatures T near to or larger than T_c .

II.3 The free energy

The system of Becker-Döring equations has a free energy whose derivative with respect to time is always negative. We define the free energy per site f by (Penrose, unpublished)

$$\frac{-f}{kT} = c_1 \left[1 + \log \frac{(1-\rho)^3}{c_1} \right] + \sum_{l=2}^{\infty} c_l \log \left[1 + \frac{(1-\rho)^4 Q_l}{c_l} \right] \quad (\text{II, 11})$$

Differentiating with respect to t , using (II, 1) and (II, 3) for $\frac{dc_l}{dt}$, we have

$$\frac{d}{dt} \left(\frac{-f}{kT} \right) = - \left(J_1 - \sum_{l=1}^{\infty} J_l \right) \log \left[\frac{(1-\rho)^3}{c_1} \right] + \sum_{l=2}^{\infty} (J_{l-1} - J_l) \log \left[\frac{(1-\rho)^4 Q_l}{c_l} \right]$$

We now group the terms with coefficients J_l together and the expression is equal to

$$= J_1 \log \left[\frac{c_1^2}{(1-\rho)^6} \frac{(1-\rho)^4 Q_2}{c_2} \right] + \sum_2^{\infty} J_l \log \left[\frac{c_1}{(1-\rho)^3} \frac{c_l}{Q_l} \frac{Q_{l+1}}{c_{l+1}} \right]$$

Then using (II, 4) for all $l \geq 1$, and using (II, 2) for the definition of J_l , we can express the above expression as

$$\frac{d}{dt} \left(\frac{-f}{kT} \right) = \sum_{l=1}^{\infty} J_l \log \left[1 + \frac{J_l}{b_{l+1} c_{l+1}} \right] \geq 0 \quad (\text{II, 12})$$

The term on the right hand side is always positive whatever the value of J_l since $b_{l+1} c_{l+1} \geq 0$. This means that the free energy is monotonically decreasing for all time whatever the initial conditions.

One can also find the equilibrium distribution of clusters by minimising the free energy subject to the condition that $\sum_1^{\infty} l c_l = \rho$ using Lagrangian multipliers. This gives the same concentrations at equilibrium as given by the distribution (I, 6), and the same relation for ρ_L or ρ in terms of w as in equation (I, 8). Therefore this corroborates the presence of nucleation for $\rho > \rho_s$ as explained in the previous section.

Chapter III: The Kinetic Coefficients $a_l(0)$ in the Limit of Zero Density.

In this Chapter, we will calculate the coefficients $a_l(0)$ for $l = 1$ to 6. Assuming a concentration c_1 of monomers, and c_l of clusters of size l , the quantity $a_l c_l c_1$ is the rate (Becker and Döring, 1935) at which clusters of size l absorb monomers to become clusters of size $l + 1$. Thus a_l is the rate at which clusters of size l absorb monomers to become clusters of size $l + 1$, per unit concentration of l -clusters c_l , and per unit monomer concentration c_1 . The coefficients $a_l(0)$ are then defined as the value of a_l when the density $\rho \rightarrow 0$.

We now give some definitions which we will use throughout this chapter:

- \mathbf{e}_i , $i = 1$ to 6 are the six unit vectors $(1, 0, 0)$, $(-1, 0, 0)$, etc.;
- S = the infinite cubic lattice;
- λ = an equivalence class of translationally equivalent clusters in S ;
- C = set of points in S which are occupied by a given cluster in λ . The origin belongs to C ;
- $N_1(C)$ = set of all nearest neighbours of C not themselves in C ;
- $N_2(C)$ = set of all the nearest neighbours of N_1 not themselves in C or $N_1(C)$;
- B = a closed cubic boundary with faces perpendicular to the three coordinate axes of the lattice S . The boundary B completely encloses C, N_1, N_2 and is disjoint from them.

By these definitions, C, N_1, N_2, B are all disjoint and all subsets of S .

III.1 Microscopic Formulation.

In this section, we formulate the problem of finding $a_l(0)$. Given a class of translationally equivalent clusters λ of size l , we define c_λ to be the concentration of clusters in λ . A cluster in λ can be transformed to a cluster of size $l + 1$ by absorbing a monomer at a lattice site in N_1 . Conversely a cluster of size $l + 1$ occupying the lattice sites of λ and any one site of N_1 , can be converted to a cluster in λ by emitting the particle at N_1 . The union of the equivalence classes of such $(l + 1)$ -clusters is $\{C \cup \mathbf{x} : C \in \lambda \text{ and } \mathbf{x} \in N_1(C)\}$, denoted by λ^+ for brevity. We also denote by c_{λ^+} the total concentration of such $(l + 1)$ -clusters on S which are in λ^+ . Therefore λ^+ can contain clusters of different shape and orientation.

We now define $J_{\lambda\lambda^+}$ to be the net probability per unit time that the clusters in S isomorphic to λ absorb monomers to become some $(l + 1)$ -cluster in λ^+ . Following Becker and Döring (1935) we can write $J_{\lambda\lambda^+}$ as

$$J_{\lambda\lambda^+} = a_{\lambda\lambda^+}c_1c_\lambda - b_{\lambda^+\lambda}c_{\lambda^+} \quad (\text{III, 1})$$

where $a_{\lambda\lambda^+}$ is the probability per unit time that the clusters in λ absorb a monomer to form an $(l + 1)$ -cluster per unit c_1 and per unit c_λ . Then $b_{\lambda^+\lambda}$ is the probability per unit time, per unit c_{λ^+} that any cluster in λ^+ breaks up into a monomer and an l -cluster in λ . This equation is analogous to equation (II, 2) in our formulation of the Becker-Döring equations. We can then divide (III, 1) by c_λ :

$$\frac{J_{\lambda\lambda^+}}{c_\lambda} = a_{\lambda\lambda^+}c_1 - b_{\lambda^+\lambda}\frac{c_{\lambda^+}}{c_\lambda} \quad (\text{III, 2})$$

This gives the net probability per unit time that the given cluster C in λ becomes an $(l + 1)$ -cluster. We assume that the cluster C is at the origin.

The size distribution of clusters on the lattice S can be assumed to be a canonical Gibbs distribution given by (I, 5) in the limit of zero density. A simple generalisation of (I, 5) can be made to obtain c_λ and $c_{\lambda+}$ under the conditions of steady state. Let $n(\lambda)$ be the number of pairs of nearest neighbours in the cluster C in λ , and $n(C \cup \mathbf{x})$ be the number of pairs of nearest neighbours in the $(l + 1)$ -cluster formed by adding a monomer at a site $\mathbf{x} \in N_1$. Then the steady state values of c_λ and $c_{\lambda+}$ are given by

$$c_\lambda = y^{n(\lambda)} c_1^l \quad \text{and} \quad c_{\lambda+} = \sum y^{n(C \cup \mathbf{x})} c_1^{l+1} \quad (\text{III, 3})$$

where y is the Boltzmann factor, $e^{V/kT}$, and where \sum is only over translationally inequivalent clusters in λ^+ . The quantity c_1 is obtained from the conservation of mass condition, $\sum l c_l = \rho$, as explained in (II, 3). The density is assumed to be arbitrarily small, so our analysis is done in the limit of zero density.

For any $\mathbf{x} \in S - C$, that is outside the central cluster, we define the steady state conditional probability $f(\mathbf{x})$ by:

$$f(\mathbf{x}) \equiv \text{prob}\{\text{site } \mathbf{x} \text{ is occupied by a monomer given that sites in } C \text{ are full}\}.$$

When \mathbf{x} is an immediate neighbour of the central cluster C , that is $\mathbf{x} \in N_1$, $f(\mathbf{x})$ is related to the probability that an $(l + 1)$ -cluster is present; otherwise $f(\mathbf{x})$ is related to the probability that there is a monomer in the vicinity of the cluster C .

The probability $f(\mathbf{x})$ is related to $f(\mathbf{x} + \mathbf{e}_i)$, that is f evaluated at a nearest neighbour of \mathbf{x} , via the transition probabilities $p(\mathbf{x}, \mathbf{x} + \mathbf{e}_i)$ which we defined in equations (I, 1), (I, 2) and (I, 3). We will now get a difference equation for $f(\mathbf{x})$ with suitable boundary conditions, and $a_{\lambda\lambda+}$ can then be obtained in terms of $f(\mathbf{x})$.

In the low density limit, we can consider only reactions between a monomer and the given cluster C at the origin, and ignore all other reactions, say between the monomers themselves. If we also neglect the possibility of a cluster λ breaking up, we obtain from the Kawasaki dynamical assumption (Kawasaki, 1966) the condition

$$\frac{df(\mathbf{x})}{dt} = \sum_{i=1}^6 [f(\mathbf{x} + \mathbf{e}_i)p(\mathbf{x} + \mathbf{e}_i, \mathbf{x}) - f(\mathbf{x})p(\mathbf{x}, \mathbf{x} + \mathbf{e}_i)] \quad \text{for } \mathbf{x} \in S - (C \cup N_1) \quad (\text{III, 4})$$

where the sum is over the neighbours of \mathbf{x} .

Provided that the cluster size distribution changes slowly enough with time, an assumption which we will examine later, we can put $df/dt = 0$ in this equation. We then obtain the steady state condition

$$\sum_{i=1}^6 [f(\mathbf{x} + \mathbf{e}_i)p(\mathbf{x} + \mathbf{e}_i, \mathbf{x}) - f(\mathbf{x})p(\mathbf{x}, \mathbf{x} + \mathbf{e}_i)] = 0 \quad \text{for } \mathbf{x} \in S - (C \cup N_1) \quad (\text{III, 5})$$

Far away from cluster C , $p(\mathbf{x}, \mathbf{y})$ is equal to $p_0/3$, and the difference equation (III, 5) reduces to the finite difference analogue of Laplace's equation:

$$\sum_{i=1}^6 [f(\mathbf{x} + \mathbf{e}_i) - f(\mathbf{x})] = 0 \quad \text{for } \mathbf{x} \in S - (C \cup N_1 \cup N_2) \quad (\text{III, 6})$$

For the second nearest neighbouring sites, $\mathbf{x} \in N_2$, however, the more general equation (III, 5) must be used, since some of the possible transitions change the energy.

One can then relate $J_{\lambda\lambda+}/c_\lambda$ to the function f and the transition probabilities. The cluster C can only become an $(l+1)$ -cluster in one move by monomers moving from N_2 to N_1 , the set of nearest neighbours of C . The net rate $J_{\lambda\lambda+}/c_\lambda$ at which cluster C becomes an $(l+1)$ -cluster is therefore

given by

$$\frac{J_{\lambda\lambda^+}}{c_\lambda} = \sum_{n_2 \in N_2, n_1 \in N_1} [p(\mathbf{n}_2, \mathbf{n}_1)f(\mathbf{n}_2) - p(\mathbf{n}_1, \mathbf{n}_2)f(\mathbf{n}_1)] \quad (\text{III, 7})$$

This equation will be used in the next section to specify numerically the boundary conditions for the difference equation (III, 5).

III.2 Boundary Conditions.

The boundary conditions for the difference equation (III, 5) describe what happens at infinity and at the sites $\mathbf{x} \in N_1$, that is the sites adjacent to the cluster λ . At infinity, assuming widely separated parts of the system to be statistically independent, we have

$$f(\mathbf{x}) \rightarrow c_1 \text{ as } \mathbf{x} \rightarrow \infty \quad (\text{III, 8})$$

For adjacent sites, $\mathbf{x} \in N_1$, the relevant condition describes the fact that if $\mathbf{x} \in N_1$, then we have an $(l + 1)$ -cluster. In fact, remembering the definition of λ^+ and c_{λ^+} , we have

$$\begin{aligned} c_{\lambda^+} &= \text{prob}\{\text{there is a cluster } \lambda^+ \text{ of size } l + 1 \text{ at the origin}\} \\ &= \sum_{\mathbf{x} \in N_1} \text{prob}\{\text{there is an } l\text{-cluster } \lambda \text{ at the origin}\} \\ &\quad \times \text{prob}\{\text{site } \mathbf{x} \text{ is full} \mid \text{there is a cluster } \lambda \text{ at the origin}\} \\ &= \sum_{\mathbf{x} \in N_1} c_\lambda f(\mathbf{x}) \end{aligned}$$

where the sum runs over all sites $\mathbf{x} \in N_1$. This can be written as

$$\frac{c_{\lambda^+}}{c_\lambda} = \sum_{\mathbf{x} \in N_1} f(\mathbf{x}) \quad (\text{III, 9})$$

To complete equation (III, 9), we need to know the $f(\mathbf{x})$ individually. We can assume for simplicity that the concentration of the $(l + 1)$ -clusters of various

shapes are at the same ratio as at equilibrium. So $f(\mathbf{x})$ can be assumed to satisfy a Gibbs distribution over N_1 :

$$f(\mathbf{x}) = \text{constant} \times y^{n(C \cup \mathbf{x})} \quad \text{for } \mathbf{x} \in N_1 \quad (\text{III, 10})$$

where $y \equiv e^{V/kT}$ and $n(C \cup \mathbf{x})$ is the number of pairs of nearest neighbours in the $(l + 1)$ -cluster $C \cup \mathbf{x}$. Equation (III, 10) holds at equilibrium, and we will discuss its validity under steady state conditions later on in this section.

The difference equation (III, 5) together with boundary conditions (III, 8), (III, 9) and (III, 10) gives a system of linear equations which can be shown to have a unique solution (Isaacson and Keller, 1966). By the superposition principle, this solution depends linearly on the parameters c_1 and $\frac{c_{\lambda^+}}{c_\lambda}$. The part of the solution which is proportional to c_1 can be found by solving the difference equation under the conditions

$$f(\mathbf{x}) \rightarrow 1 \quad \text{as } \mathbf{x} \rightarrow \infty, \quad f(\mathbf{x}) = 0 \quad \text{for } \mathbf{x} \in N_1 \quad (\text{III, 11})$$

The part of the solution which is proportional to $\frac{c_{\lambda^+}}{c_\lambda}$ can be found by solving the difference equation under the conditions

$$f(\mathbf{x}) \rightarrow 0 \quad \text{as } \mathbf{x} \rightarrow \infty, \quad f(\mathbf{x}) = \frac{y^{n(C \cup \mathbf{x})}}{\sum_{x \in N_1} y^{n(C \cup \mathbf{x})}} \quad \text{for } \mathbf{x} \in N_1 \quad (\text{III, 12})$$

In fact only one of these problems need be solved, because by detailed balancing, $J_{\lambda\lambda^+} = 0$ at equilibrium, which implies that $b_{\lambda+\lambda} = a_{\lambda\lambda^+} \frac{c_1 c_\lambda}{c_{\lambda^+}}$, with c_λ and c_{λ^+} given by (III, 3). We now show how to obtain $a_{\lambda\lambda^+}$ from problem (III, 11). In our numerical work, we only solved (III, 11).

Once the solution of the difference equation (III, 5) with boundary conditions (III, 8) and (III, 11) is known, we can calculate $J_{\lambda\lambda^+}/c_\lambda$. In (III, 7), this was shown to be equal to the net rate of flow of monomers from N_2 to

N_1 , that is from the second nearest neighbours to the nearest neighbours of the central cluster C . By conservation of matter, the flow of clusters from N_2 to N_1 has to be equal to the total monomer flow towards C at a large distance from C . This flow is equal to the sum over any closed surface, which encloses the central cluster and does not pass through any of the lattice sites, of all probability flows

$$p(\mathbf{x}, \mathbf{x} + \mathbf{e}_i)f(\mathbf{x} + \mathbf{e}_i) - p(\mathbf{x} + \mathbf{e}_i, \mathbf{x})f(\mathbf{x}) \quad (\text{III, 13})$$

along bonds which cross the surface, using a sign convention in which an inward flow counts as positive. By (III, 5) and the finite difference analogue of the divergence theorem, the quantity so defined is the same for all such surfaces, so we may calculate it using a large sphere. At large distances from cluster C , our difference equation (III, 5) becomes approximately Laplace's equation (III, 6). So the probability flow along a bond in the \mathbf{x} direction is given by $-\left(\frac{p_0}{3}\right)\frac{\partial f}{\partial x}$, since $p(\mathbf{x}, \mathbf{y}) = \frac{p_0}{3}$ for \mathbf{x} far from cluster C , from equation (I, 3). Consequently, the total flow across a surface S is given approximately by a surface integral

$$\frac{J_{\lambda\lambda^+}}{c_\lambda} = \left(\frac{p_0}{3}\right) \int_S \frac{\partial f}{\partial n} dS \quad (\text{III, 14})$$

where $\frac{\partial}{\partial n}$ denotes the outward normal derivative. At large distances, the solution of the difference equation (III, 5) with boundary condition (III, 8) has the same asymptotic form as that of Laplace's equation namely

$$f(\mathbf{x}) = c_1 - \frac{K}{r} + O\left(\frac{1}{r^2}\right) \quad (\text{III, 15})$$

where K is independent of \mathbf{x} , but depends linearly on c_1 and $\frac{c_{\lambda^+}}{c_\lambda}$, and r is the Euclidean distance of the position vector \mathbf{x} to the centre of gravity of the cluster C .

We can assume that S is the surface of a large sphere with radius R and centre the origin. Then substituting (III, 15) into (III, 14) using spherical coordinates, the integral in (III, 14) becomes equal to $4\pi r^2 \times \frac{\partial f}{\partial r} = 4\pi K$. We therefore have $\frac{J_{\lambda\lambda^+}}{c_\lambda} = 4\pi \left(\frac{p_0}{3}\right) K$, which when combined with (III, 7) gives us

$$\frac{J_{\lambda\lambda^+}}{c_\lambda} = 4\pi \left(\frac{p_0}{3}\right) K = \sum_{n_2 \in N_2, n_1 \in N_1} [p(\mathbf{n}_2, \mathbf{n}_1)f(\mathbf{n}_2) - p(\mathbf{n}_1, \mathbf{n}_2)f(\mathbf{n}_1)] \quad (\text{III, 16})$$

We solved the difference equation (III, 5) under boundary conditions (III, 11). Since these boundary conditions are equivalent to formally putting $c_1 = 1$ and $c_{\lambda^+}/c_\lambda = 0$ in (III, 2), we then obtain $a_{\lambda\lambda^+}$ as being equal to any of the three quantities in (III, 16). Remembering that in (III, 11), $f(\mathbf{n}_1) = 0$ for all $\mathbf{n}_1 \in N_1$, we can write for K and $a_{\lambda\lambda^+}$

$$a_{\lambda\lambda^+} = 4\pi \left(\frac{p_0}{3}\right) K = \sum_{n_2 \in N_2, n_1 \in N_1} p(\mathbf{n}_2, \mathbf{n}_1)f(\mathbf{n}_2) \quad (\text{III, 17})$$

This equation gives $a_{\lambda\lambda^+}$ and K in terms of the probabilities $f(\mathbf{x})$.

III.3 Calculation of the Kinetic Coefficients $a_l(0)$.

To solve the difference equation (III, 5) with boundary conditions (III, 11), we take a finite boundary B which completely contains the cluster C , N_1 and N_2 . For \mathbf{x} on this boundary, we take $f(\mathbf{x})$ to satisfy (III, 15) to first order in $\frac{1}{r}$.

$$f(\mathbf{x}) = 1 - \frac{K}{r} \quad \mathbf{x} \in B \quad (\text{III, 18})$$

This equation strictly speaking holds only when the boundary B recedes to infinity. In the case of $l = 1$ or 2 , however, we found that when B is a cube of side 8, 9 or 10, and using (III, 18) as boundary condition, a_l is the same to 0.1% for these three differently sized boundaries. Therefore we have

omitted higher order terms like $1/r^2$ from the boundary condition (III, 18) for $\mathbf{x} \in B$. The constant K can be expressed numerically in terms of $f(\mathbf{x})$ using (III, 17). One can then solve the difference equation for $f(\mathbf{x})$ by successive over relaxation (S.O.R.). We then obtain $a_{\lambda\lambda+}$ from (III, 17).

So far we have obtained $a_{\lambda\lambda+}$, the probability that a given l -cluster becomes an $(l+1)$ -cluster. In our set of Becker-Döring equations however, we have the average kinetic coefficient a_l for clusters of size l . This is found by adding (III, 1) over all translationally inequivalent clusters λ of size l . Ignoring the $b_{\lambda+\lambda}$ term in this case, we have

$$J_l = \sum_{\lambda} J_{\lambda\lambda+} = \sum_{\lambda} a_{\lambda\lambda+c_1} c_{\lambda} = \frac{\sum_{\lambda} a_{\lambda\lambda+c_1} c_{\lambda}}{\sum_{\lambda} c_{\lambda}} \times \sum_{\lambda} c_{\lambda} c_1 = \frac{\sum_{\lambda} a_{\lambda\lambda+c_1} c_{\lambda}}{\sum_{\lambda} c_{\lambda}} \times c_l c_1 \equiv a_l c_l c_1$$

since $\sum_{\lambda} c_{\lambda} = c_l$, the total concentration of l -clusters. Comparing the coefficients of $c_l c_1$ in this equation with the definition (III, 2) of $J_{\lambda\lambda+}$, we have

$$a_l = \frac{\sum_{\lambda} a_{\lambda\lambda+c_1} c_{\lambda}}{\sum_{\lambda} c_{\lambda}} \quad (\text{III, 19})$$

To simplify matters, we can assume that the l -clusters of different shapes are in the same ratio as at equilibrium. This is a reasonable assumption for small l , because in the simulation, the non-equilibrium distribution of the size of the small clusters was found to be very close to an equilibrium distribution. This will therefore be probably true also of their shapes. Besides, the kinetic coefficient for a cluster of a given size varies by at most 20% with a change in shape for sizes $l \leq 6$. Therefore assuming we have a canonical ensemble of l -clusters at all times, c_{λ} is proportional to $y^{n(\lambda)}$, where $y \equiv e^{V/kT}$, and $n(\lambda)$ is the number of pairs of nearest neighbours in cluster λ . The mean value

$a_l(0)$ of $a_{\lambda\lambda+}$ for clusters λ of size l in the limit of zero density is therefore:

$$a_l(0) = \frac{\sum_{\lambda} a_{\lambda\lambda+} y^{n(\lambda)}}{\sum_{\lambda} y^{n(\lambda)}} \quad (\text{III, 20})$$

where λ runs over all the translationally inequivalent clusters of size l .

In the first column of Table (III, i), we list the coefficients $a_l(0)$, $1 \leq l \leq 6$, calculated from the canonical average (III, 20) with simulation parameters $V/kT = 1.5$, and transition probabilities $p(\mathbf{x}, \mathbf{y}) = \frac{p_i}{3}$, given by (I, 1) and (I, 3). In the second column of Table (III, i), we also give the result of a regression equation from (III, 24). In the third column, we give the result of a Green's function calculation for the cases $l = 1, 2$, done in Chapter IV. All estimates are quite close to one another.

To see the effect of different averaging on the value of $a_l(0)$, for given l , we also took a_l to be the arithmetic mean of the relevant $a_{\lambda\lambda+}$, and the resulting value agreed to better than 1% with the canonical average (III, 20).

Table (III, i). The kinetic coefficients in the limit of zero density, $a_l(0)$, for simulation parameters $\frac{V}{kT} = 1.5$ and $p_0 = \frac{1}{2}$. Transition probabilities are $p(\mathbf{x}, \mathbf{y}) = \frac{p_i}{3}$, with p_i given in (I, 1) and (I, 2).

$a_l(0)$			
l	Canonical Average (III, 20); S.O.R.	Regression (III, 24) $a_l(0) = \frac{1}{6}([874 + 1888l])^{1/3}$	Green's Function (IV,17) and (IV, 29)
1	2.29	2.34	2.29
2	2.81	2.78	2.80
3	3.17	3.12	
4	3.34	3.39	
5	3.63	3.63	
6	3.78	3.84	

In Table (III, ii), we also give values for $a_l(0)$, $1 \leq l \leq 6$, for values of V/kT in the range $-2.2 \leq V/kT \leq 2.2$. The range when $V/kT < 0$ corresponds to the situation when $p_0 > p_{-1}$ by equations (I, 1) and (I, 2). This situation can occur when both types of particles in a binary alloy are large compared to the lattice in which they are embedded, but in this case Equation (I, 1) does not hold.

Table (III, ii). Table of $a_l(0)$, $1 \leq l \leq 6$, the kinetic coefficients in the limit of zero density, for parameters γ in the range $-0.8 \leq \gamma \leq 0.8$. Constants M and N in the equation (III, 24), $\frac{a_l(0)}{D} = (M + Nl)^{1/3}$, are obtained by least squares for each temperature. $D = \frac{p_0}{3} = \frac{1}{6}$ is the diffusion constant for monomers.

$a_l(0)$								
$\gamma \equiv \frac{p_{-1}}{p_0} - 1$	$l = 1$	2	3	4	5	6	M	N
-0.8	0.758	1.010	1.165	1.251	1.412	1.493	-35	125
-0.6	1.221	1.583	1.833	1.944	2.171	2.283	-38	435
-0.4	1.536	1.957	2.240	2.387	2.653	2.778	37	771
-0.2	1.764	2.217	2.534	2.699	2.976	3.118	169	1072
0.0	1.937	2.415	2.750	2.924	3.208	3.360	341	1324
0.2	2.077	2.567	2.922	3.086	3.383	3.533	558	1519
0.4	2.187	2.691	3.046	3.223	3.509	3.663	799	1663
0.6	2.279	2.792	3.149	3.325	3.609	3.761	1040	1776
0.8	2.359	2.876	3.233	3.405	3.671	3.826	1341	1837

III.4 Comparison of $a_l(0)$ with the diffusion theory of a spherical cluster.

We now relate the coefficient $a_l(0)$ found in the previous section with the prediction of classical diffusion theory for a spherical cluster. If we assume a large cluster of size l to be spherical, we can then relate $a_l(0)$ to the diffusion constant D of monomers and the radius R_l of the cluster

$$a_l(0) = 4\pi DR_l \quad (\text{III, 21})$$

This formula holds for large l . In the derivation of (III, 21), (Chandrasekhar, 1954), (Penrose and Lebowitz, 1978), it is assumed that all the small clusters are monomers.

The diffusion constant D for monomers can be easily obtained from equation (I, 3). This equation implies that in the limit of zero density, a monomer has a probability of $\frac{p_0}{3} = \frac{1}{6}$ per unit time of moving to each neighbouring site. Since there are six possible directions, the mean square displacement Δx^2 of a monomer per unit time $= \frac{p_0}{3} \times 6 = 1$. Einstein's relation then gives

$$D = \frac{\Delta x^2}{6\Delta t} = \frac{p_0/3 \times 6}{6} = \frac{p_0}{3} = \frac{1}{6} \quad (\text{III, 22})$$

This is twice the estimated value of D in Penrose et al., which is incorrect.

To get $a_l(0)$ for a spherical cluster, we therefore substitute (III, 22) into (III, 21). Assuming the cluster to be a sphere of volume l , we obtain

$$a_l(0) = 4\pi \times \frac{1}{6} \times \left(\frac{3l}{4\pi}\right)^{1/3} \approx 1.3l^{1/3} \quad (\text{III, 23})$$

which is again twice the estimated value in this reference.

In the spirit of (III, 21), we expect that $a_l(0)^3$ should be linear in l for large l . However, we found that for small l also, this approximate formula holds:

$$a_l(0) \approx D(M + Nl)^{1/3} \quad (\text{III, 24})$$

where $D = \frac{p_0}{3} = \frac{1}{6}$ is the diffusion constant for monomers. The parameters M and N depend on the ratios p_i/p_0 but not on l . For $1 \leq l \leq 6$ and $V/kT = 1.5$, the parameters are obtained graphically as

$$M = 874 \quad N = 1888 \quad (\text{III, 25})$$

In the second column of Table (III, i), we calculate $a_l(0)$ using (III, 24) and (III, 25). These values agree to about 2% with those in the first column of the same table, which were calculated using the canonical average (III, 20).

The equation (III, 24) holds for a wide range of temperatures, as can be seen from Table (III, ii) and Fig. (III, i). In this table, we give values of $a_l(0)$ for various values of γ in the range $-0.8 \leq \gamma \leq 0.8$, which correspond to the range $-2.2 \leq V/kT \leq 2.2$. In the last two columns, we give values of M and N for each temperature using least squares. In Fig. (III, i), we plot the values in this table in the form $a_l(0)^3$ against l , and for each temperature, we obtain a straight line with a small intercept, as predicted by (III, 24). The accuracy of (III, 24) is always better than 2% over this range of temperature. As already pointed out earlier, $V/kT \leq 0$ implies the fact that $p_{-1} < p_0$.

We are now in a position to compare the prediction (III, 23) for a spherical cluster with the empirical formula (III, 24). For large l , one can neglect M and we can write $a_l(0) = D(Nl)^{1/3}$ with $D = 1/6$. For the simulation value $V/kT = 1.5$, we have $N = 1888$ from (III, 25), and so

$$a_l(0) \approx 2.06l^{1/3} \quad (\text{III, 26})$$

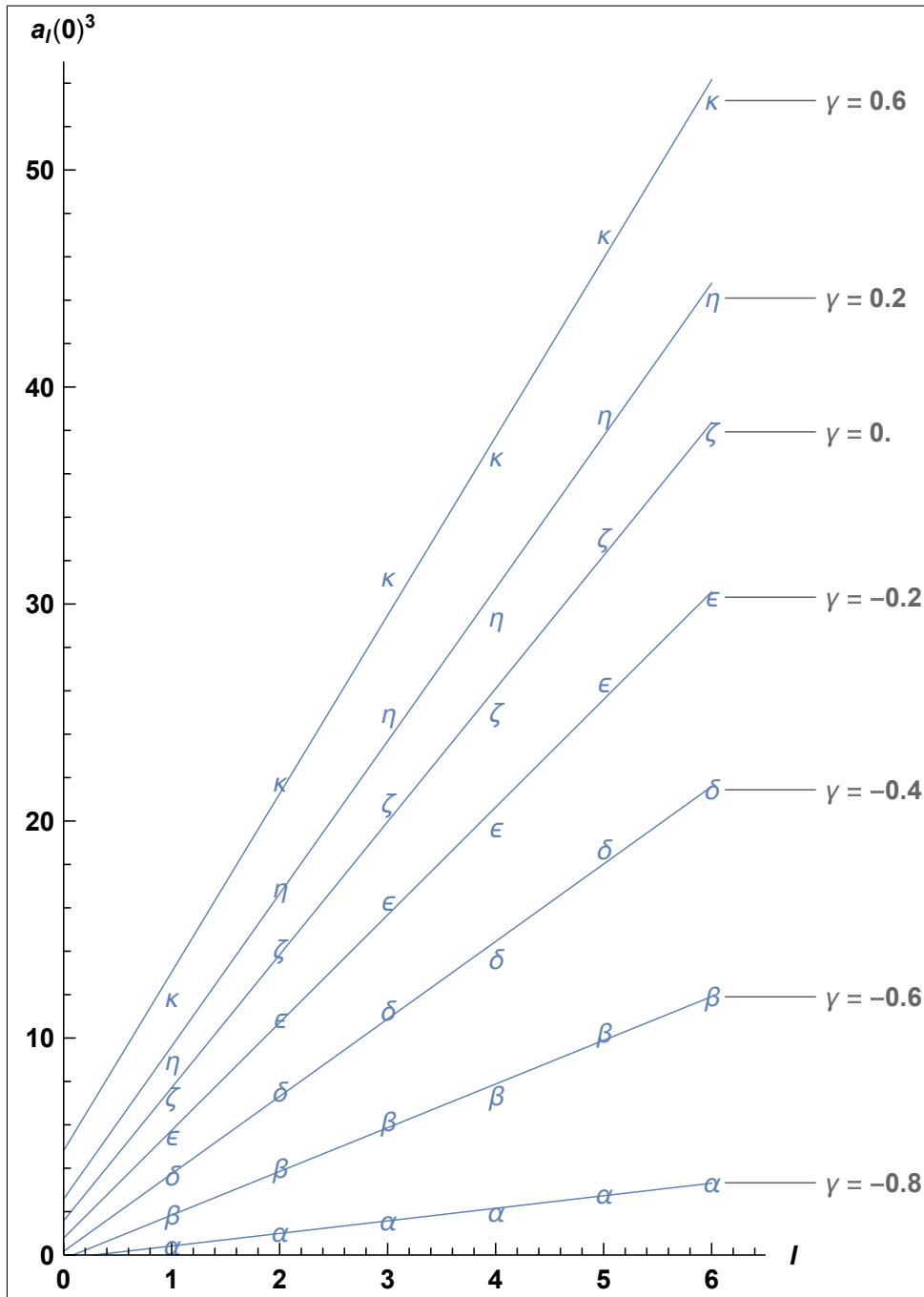


Fig. (III, i). Graphs of $a_l(0)^3$ against l for the range $-0.8 \leq \gamma \leq 0.8$. The points lie on a straight line with a small intercept, for each value of γ , as predicted by (III, 24). Please note that $\gamma \equiv \frac{p-1}{p_0} - 1$.

The asymptotic form (III, 26) for the kinetic coefficients $a_l(0)$ for clusters of size l on a simple cubic lattice is considerably larger than the prediction (III, 23) for a spherical cluster.

This is partly due to a temperature effect, whereby $a_l(0)$ increases with an increase in temperature, or equivalently an increase in p_{-1} . This can be seen in Table (III, ii) for the range $-2.2 \leq V/kT \leq 2.2$, and also in Fig. (III, i). It can be noticed that the estimates (III, 22) and (III, 23) based on diffusion theory for a spherical cluster depend only on p_0 , but do not depend on p_{-1} . To show how $a_l(0)$ in Table (III, ii) increases with p_{-1} for fixed p_0 , we plot the quantity $p_0/a_l(0)$ against p_0/p_{-1} for fixed l in Fig. (III, ii). We do this for $l = 1$ to 6 for the range $0.2 \leq p_{-1}/p_0 \leq 2$. For each l , we obtain a straight line. These straight lines meet approximately on the line $p_0/p_{-1} = -1$, and their slopes depend on l . In fact we can write the empirical formula

$$\frac{p_0}{a_l(0)} = f(l) \left(1 + \frac{p_0}{p_{-1}} \right) + 0.06 \quad (\text{III, 27})$$

This formula is accurate to better than 1% over the range considered. The equation (III, 27) shows an increase of $a_l(0)$ with p_{-1} . In fact, $\frac{1}{a_l(0)}$ is linear in $\frac{1}{p_{-1}}$ for fixed p_0 and fixed l .

Another reason for the discrepancy between (III, 26) and (III, 23) is the fact that the more compact a cluster λ is, the smaller is the value $a_{\lambda\lambda+}$. This is readily seen in Table (III, iii), where we give the values $a_{\lambda\lambda+}$ for translationally inequivalent clusters of size 3 and 4. We can take the number of nearest neighbouring sites of a cluster λ , or equivalently the number of sites in N_1 , to be a measure of the compactness of λ .

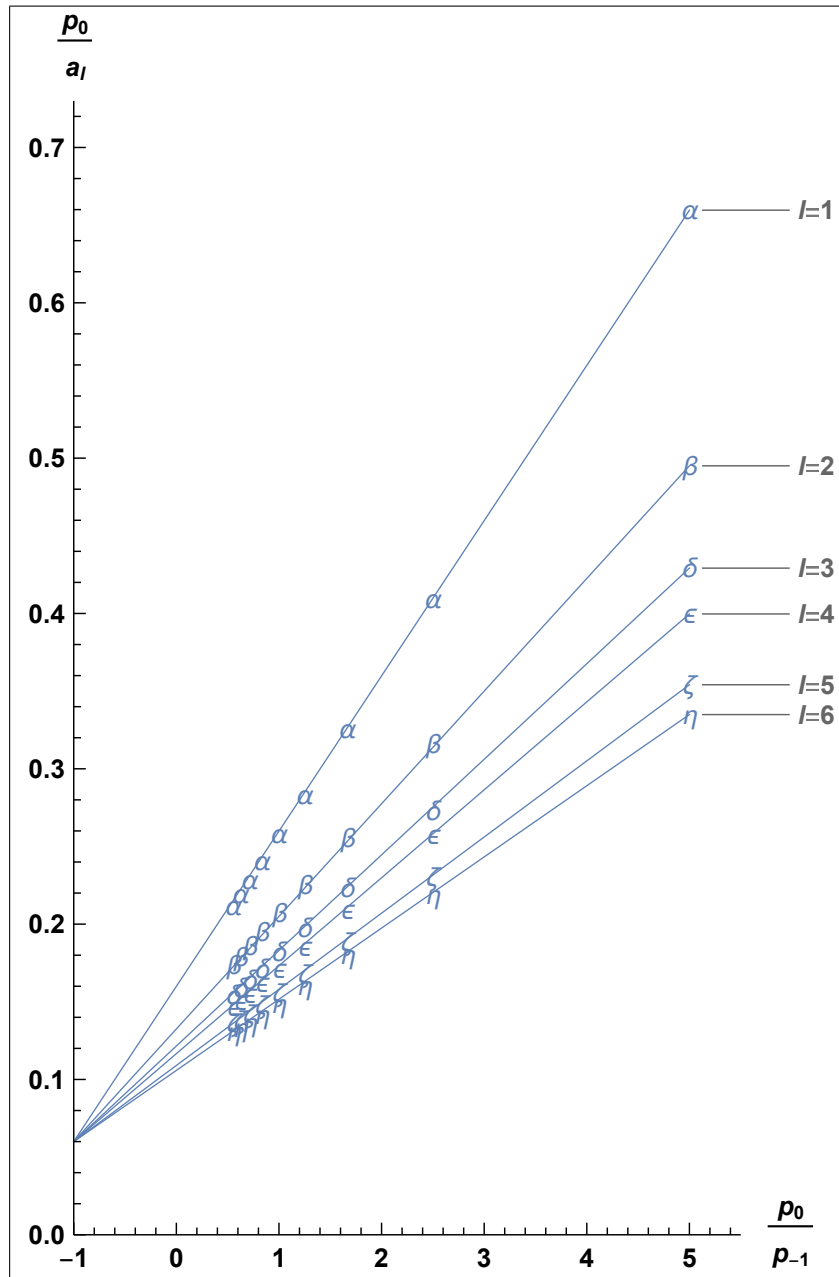



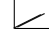

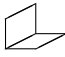


Fig. (III, ii). Graphs of $\frac{p_0}{a_l(0)}$ against $\frac{p_0}{p_{-1}}$ for $1 \leq l \leq 6$ over the range $0.2 \leq \frac{p_{-1}}{p_0} \leq 2$. The graphs for each integer l are all straight lines meeting on the line $\frac{p_0}{p_{-1}} = -1$, at $\frac{p_0}{a_l} \approx 0.06$.

		$a_{\lambda\lambda^+}$												
		3-clusters						4-clusters						
γ		G. Avg. $a_3(0)$ (III,20)						G. Avg. $a_4(0)$ (III,20)						
		—	└	└└	└└└	└└└└	—	└	└└	└└└	└└└└	└└└└└	└└└└└└	└└└└└└└
-0.8	1.25	1.15	1.17	1.44	1.39	1.28	1.29	1.22	1.17	1.08	1.28	1.28	1.17	1.08
-0.6	1.91	1.79	1.81	2.19	2.11	1.99	1.97	1.91	1.83	1.73	1.99	1.97	1.83	1.73
-0.4	2.33	2.22	2.24	2.65	2.56	2.46	2.40	2.36	2.27	2.18	2.46	2.40	2.27	2.18
-0.2	2.62	2.51	2.53	2.96	2.86	2.78	2.69	2.69	2.57	2.50	2.78	2.69	2.57	2.50
0.0	2.83	2.73	2.75	3.20	3.09	3.02	2.91	2.92	2.79	2.73	3.02	2.91	2.79	2.73
0.2	3.00	2.90	2.92	3.38	3.25	3.19	3.07	3.10	2.95	2.90	3.19	3.07	2.95	2.90
0.4	3.13	3.02	3.04	3.52	3.39	3.33	3.20	3.23	3.08	3.02	3.33	3.20	3.08	3.02
0.6	3.23	3.13	3.15	3.64	3.49	3.43	3.31	3.33	3.18	3.12	3.43	3.31	3.18	3.12
0.8	3.32	3.21	3.23	3.74	3.58	3.51	3.40	3.42	3.26	3.20	3.51	3.40	3.26	3.20

Table (III, iii). Values of $a_{\lambda\lambda^+}$ for translationally inequivalent clusters λ of sizes $l = 3, 4$, for values of γ in the range $-0.8 \leq \gamma \equiv \frac{p-1}{p_0} - 1 \leq 0.8$. We also give $a_3(0)$ and $a_4(0)$ calculated from the Gibbs average (III, 20) of the individual $a_{\lambda\lambda^+}$.

In Table (III, iii), the clusters for a given l are arranged from left to right in increasing level of compactness. It can be observed that the more compact a cluster is, the smaller $a_{\lambda\lambda^+}$ is:

- The straight cluster of size 3, , has a value $a_{\lambda\lambda^+}$ which is at least 3% higher than that for the bent cluster, , for most temperatures.
- For clusters of size 4, $a_{\lambda\lambda^+}$ for the straight cluster, , is about 14% higher than that for the most compact 4-cluster, .
- Clusters of intermediate compactness have intermediate values of $a_{\lambda\lambda^+}$. This can be seen for the 4-clusters in Table (III, iii). A slight deviation to this rule occurs for the square 4-cluster, , which has four bonds, in contrast to the other 4-clusters which have just three bonds.
- For $l = 6$, $a_{\lambda\lambda^+}$ for the straight cluster is 4.12, whilst $a_{\lambda\lambda^+}$ for  is 3.34 at $\gamma = 0.2$, a discrepancy of about 20%.

Throughout this chapter, we have assumed steady state diffusion. This is noticed in some real alloys. Thus, for example, Pedder (1978) reports that the coarsening of the cadmium oxide phase in silver-cadmium alloys is well modelled by a steady state diffusion theory, in which the diffusion of cadmium atoms to the larger cadmium clusters determines the rate of coarsening. In the simulation also, the concentration of the small clusters varies little with time, so that we can justify our assumption of a steady state in the equations (III, 5) and (III, 6). In the numerical solution of the the Becker-Döring equations, to be discussed in Chapter V, J_l/c_l is found to be less than 0.001 for the small clusters, and 0.01 for the larger clusters.

Chapter IV: Calculation of $a_1(0)$ and $a_2(0)$ in terms of $\gamma \equiv \frac{p-1}{p_0} - 1$, using the Green's function $G(\mathbf{r})$.

IV.1 The Green's function $G(\mathbf{r})$.

In this chapter, we will check the S.O.R. calculation for $a_l(0)$ in the previous chapter by finding a_1 and a_2 in terms of the parameter $\gamma \equiv \frac{p-1}{p_0} - 1$ using Green's function $G(\mathbf{r})$ of the finite difference Laplacian. The coefficients a_1 and a_2 will be obtained as quotients of two polynomials in γ . We again assume a low density.

As in Chapter III, we have to solve equation (III, 5) under boundary conditions such as (III, 11) in the presence of cluster C at the origin of coordinates. For sites \mathbf{x} far from cluster C , the difference equation (III, 5) reduces to the finite difference analogue of Laplace's equation, (III, 6). We therefore introduce Green's function $G(\mathbf{r})$ for the finite difference Laplacian, which can be expressed using the difference operator Δ , defined by

$$\Delta G(\mathbf{r}) = \sum_{i=1}^6 [G(\mathbf{r} + \mathbf{e}_i) - G(\mathbf{r})] \quad (\text{IV, 1})$$

where the sum is over the six nearest neighbours $\mathbf{r} + \mathbf{e}_i$ of \mathbf{r} . We can then define $G(\mathbf{r})$ as

$$\begin{cases} \Delta G(\mathbf{0}) & = & 4\pi & \mathbf{r} = \mathbf{0} \\ \Delta G(\mathbf{r}) & = & 0 & \mathbf{r} \neq \mathbf{0} \\ G(\mathbf{r}) & = & \frac{1}{r} & \text{for large } \mathbf{r} \end{cases} \quad (\text{IV, 2})$$

where r is the Pythagorean length of the vector \mathbf{r} . Since $G(\mathbf{r})$ depends only on r , $G(\mathbf{r})$ is symmetrical about the origin, and if $\mathbf{r} = (x, y, z)$, then $G(x, y, z) = G(-x, y, z) = G(y, -x, -z) = \text{etc.}$ Besides, equations (IV, 2)

define a unique G , because if there were two G 's satisfying (IV, 2), the difference $d(\mathbf{r})$ will satisfy $\Delta d(\mathbf{r}) = 0$ for all \mathbf{r} using the linearity of the operator Δ , and also $d(\mathbf{r}) = 0$ for large \mathbf{r} . These two conditions imply that $d(\mathbf{r}) = 0$ everywhere, and hence $G(\mathbf{r})$ is unique. (Isaacson and Keller, 1966).

We found $G(\mathbf{r})$ numerically using equation (IV, 2) and the boundary condition $G(\mathbf{r}) = 1/r$ for $\mathbf{r} \in B$, where B is a big boundary which contains the origin. We used an SOR method to solve for G for different cubes of edges 18, 20, 22, and we found that the solution does not depend on the size of the boundary used. In the program to do this, we used the symmetry properties of $G(\mathbf{r})$. The values of $G(\mathbf{r})$ for small r are shown in Table (IV, i).

IV.2 Calculation of $a_1(0)$ in terms of γ .

To find $a_1(0)$ we consider a monomer C situated at the origin of coordinates of the simple cubic lattice S . See Fig. (IV, i). The monomer is denoted by \bullet in this figure. The set N_1 of nearest neighbours of the cluster C consists of the six unit vectors \mathbf{e}_i , $i = 1$ to 6, where \mathbf{e}_i are the unit vectors $(1, 0, 0)$, $(-1, 0, 0)$, etc. These are denoted by \bullet in Fig. (IV, i), where we give only an x - y section through the origin for clarity. The set N_2 of the second nearest neighbours of the monomer C consists of 18 lattice sites, which can be divided into two symmetries a and b , with degeneracies 12 and 6 respectively:

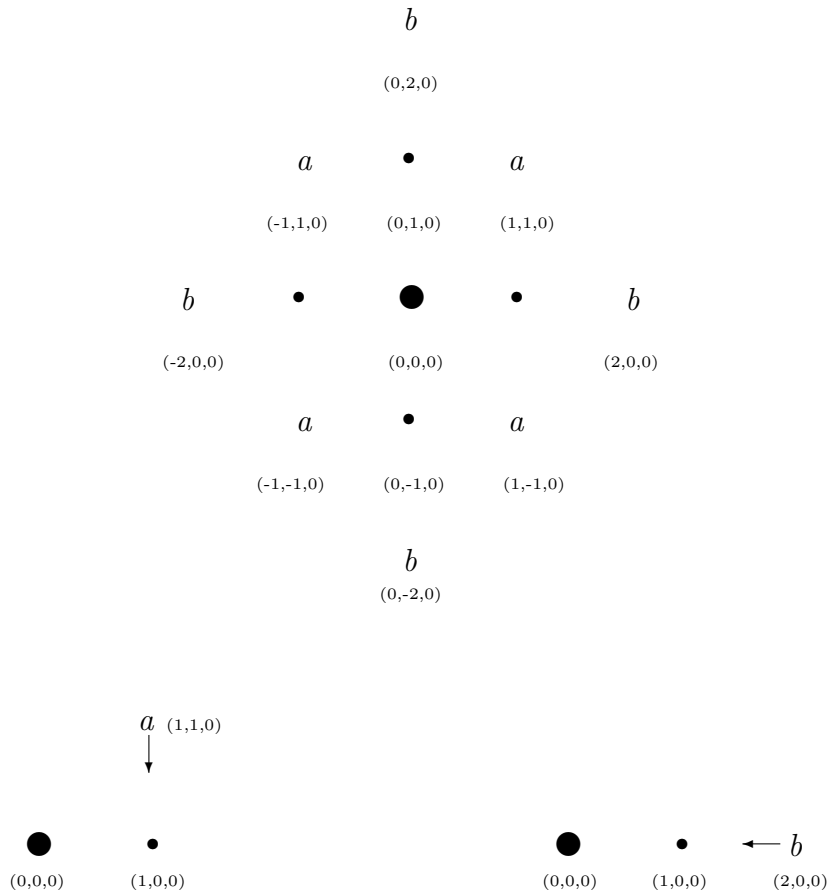
- a comprises the 12 sites at $\mathbf{r}_a = (\pm 1, \pm 1, 0), (0, \pm 1, \pm 1), (\pm 1, 0, \pm 1)$;
- b comprises the 6 sites at $\mathbf{r}_b = (\pm 2, 0, 0), (0, \pm 2, 0)$ and $(0, 0, \pm 2)$.

The twelve sites marked a have the same symmetry relative to the origin, as do the six sites marked b . These symmetries are shown separately in the lower part of Fig. (IV, i).

Table (IV, i). Table of Green's function $G(\mathbf{r})$ and the functions $H^i(\mathbf{r})$, $i = 1, 2$, for $a_1(0)$ from (IV, 5), and the functions $G^i(\mathbf{r})$, $i = 1$ to 4, for $a_2(0)$ from (IV, 22), for relevant values of \mathbf{r} .

	Green's f.	$a_1(0)$		$a_2(0)$			
\mathbf{r}	$G(\mathbf{r})$	$H^1(\mathbf{r})$	$H^2(\mathbf{r})$	$G^1(\mathbf{r})$	$G^2(\mathbf{r})$	$G^3(\mathbf{r})$	$G^4(\mathbf{r})$
(0,0,0)	3.1760						
(1,0,0)	1.0810	8.3204	3.2331				
(1,1,0)	0.6935	8.9867	2.8316	0.7722	4.3228	4.1480	5.2562
(1,1,1)	0.5476	6.9381	2.5485	0.7035	3.7506	3.7274	6.9194
(2,0,0)	0.5389	5.6632	4.8409	1.3364	5.6088	3.2160	3.7968
(2,1,0)	0.4515	5.4153	2.7124	0.9387	6.3290	3.2036	3.7506
(1,2,0)	0.4515	5.4153	2.7124	0.6298	3.2036	6.1199	3.7274
(2,1,1)	0.4016						
(2,2,0)	0.3525						
(2,2,1)	0.3287						
(2,2,2)	0.2846						
(3,0,0)	0.3461	3.9944	2.3924	3.3781	3.7548	2.5192	2.8140
(3,1,0)	0.3207						
(3,1,1)	0.3019						
(3,2,0)	0.2773						
(4,0,0)	0.2549						
(4,1,0)	0.2452						
(5,0,0)	0.2022						

Fig. (IV, i). The top diagram shows a monomer \bullet at the origin. For clarity, we show only the x - y plane. The sites marked \bullet are the nearest neighbours of the central cluster \bullet , and are the six sites at $(\pm 1, 0, 0)$, $(0, \pm 1, 0)$, $(0, 0, \pm 1)$. N_1 is the set of nearest neighbours comprising these six sites. The set of second nearest neighbours, N_2 , consists of 18 sites marked a and b signifying the two symmetries, which are shown separately in the bottom two diagrams. There are 12 sites marked a , situated at positions $\mathbf{r}_a = (\pm 1, \pm 1, 0)$, $(0, \pm 1, \pm 1)$, $(\pm 1, 0, \pm 1)$. The other 6 sites marked b are at positions $\mathbf{r}_b = (\pm 2, 0, 0)$, $(0, \pm 2, 0)$, $(0, 0, \pm 2)$.



End of Fig. (IV, i)

The function $f(\mathbf{r})$ for the monomer case is by definition the probability that site \mathbf{r} is occupied by a monomer given there is a monomer at the origin. Then $f(\mathbf{r})$ has to satisfy the difference equation (III, 5) as in Chapter III. As in (III, 8), the boundary condition for large \mathbf{r} is $f(\mathbf{r}) \rightarrow c_1$. For nearest neighbour sites such as $(1,0,0)$, that is $\mathbf{r} \in N_1$, $f(\mathbf{r})$ can be taken to be zero as in (III, 11), because by (III, 9), f_{100} is proportional to c_2/c_1 , rather than c_1 . For this problem therefore, we can take $f(\mathbf{r})$ to satisfy the boundary conditions

$$\begin{aligned} f(\mathbf{r}) &\rightarrow c_1 & \mathbf{r} &\rightarrow \infty \\ f_{xyz} &= 0 & (x, y, z) &\equiv \mathbf{r} \in N_1 \end{aligned}$$

with $f(\mathbf{r})$ being linear in c_1 as in (III, 11). (Here we used the notation that if $\mathbf{r} = (x, y, z)$, then we denote $f(\mathbf{r})$ as f_{xyz}).

Since $f(\mathbf{r})$ satisfies Laplace's finite difference equation (III, 6) for sites $\mathbf{x} \in S - (C \cup N_1 \cup N_2)$, and since $f(\mathbf{r}) \approx c_1 - K/r$ for large r , as in (III, 18), it can be easily shown using the properties (IV, 2) of $G(\mathbf{r})$, that these properties are automatically satisfied if we write $f(\mathbf{r})$ as

$$f(\mathbf{r}) = c_1 + \sum_{\mathbf{y} \in N_2} G(\mathbf{r} - \mathbf{y})g(\mathbf{y}) + h(\mathbf{r}) \quad (\text{IV, 3})$$

where $h(\mathbf{r}) = 0$ for all $\mathbf{r} \notin N_1$. In (IV, 3), $g(\mathbf{y})$ are unknown coefficients linear in c_1 and c_2/c_1 , and the summation is over the sites \mathbf{y} in N_2 , the set of second nearest neighbours of the central cluster C . The problem of finding $f(\mathbf{r})$ is therefore reduced to finding $g(\mathbf{y})$ for $\mathbf{y} \in N_2$, and $h(\mathbf{r})$ for $\mathbf{r} \in N_1$. Since for $\mathbf{r} \in N_2$, $f(\mathbf{r})$ has to satisfy (III, 5), the quantities $g(\mathbf{y})$ and $h(\mathbf{r})$ are obtained by considering (IV, 3) at the sites $\mathbf{r} \in N_2$. This will be done later on in this section.

In equation (IV, 3), two coefficients $g(\mathbf{y}_1)$ and $g(\mathbf{y}_2)$ are equal if the two vectors \mathbf{y}_1 and \mathbf{y}_2 in N_2 have the same symmetry relative to C , the central cluster. Splitting the sum in (IV, 3) over the two symmetries a and b , we can rewrite (IV, 3) in the form

$$f(\mathbf{r}) = c_1 + g_1 H^1(\mathbf{r}) + g_2 H^2(\mathbf{r}) + h(\mathbf{r}) \quad (\text{IV, 4})$$

where $h(\mathbf{r}) \neq 0 \iff \mathbf{r} \in N_1$, and where $H^1(\mathbf{r}) = \sum_{\mathbf{y} \in a} G(\mathbf{r} - \mathbf{y})$, the sum now being restricted to sites in N_2 having symmetry a , and g_1 is the common value of $g(\mathbf{y})$ for \mathbf{y} in symmetry a . The terms $H^2(\mathbf{r})$ and g_2 are interpreted similarly for symmetry b . The functions $H^1(\mathbf{r})$ and $H^2(\mathbf{r})$ are given explicitly by

$$\left\{ \begin{array}{l} H^1(\mathbf{r}) = \quad G(\mathbf{r} - \overline{110}) + G(\mathbf{r} - \overline{-110}) + G(\mathbf{r} - \overline{-1-10}) + G(\mathbf{r} - \overline{1-10}) \\ \quad + G(\mathbf{r} - \overline{011}) + G(\mathbf{r} - \overline{0-11}) + G(\mathbf{r} - \overline{0-1-1}) + G(\mathbf{r} - \overline{01-1}) \\ \quad + G(\mathbf{r} - \overline{101}) + G(\mathbf{r} - \overline{-101}) + G(\mathbf{r} - \overline{-10-1}) + G(\mathbf{r} - \overline{10-1}) \\ H^2(\mathbf{r}) = \quad G(\mathbf{r} - \overline{200}) + G(\mathbf{r} - \overline{020}) + G(\mathbf{r} - \overline{002}) \\ \quad + G(\mathbf{r} - \overline{-200}) + G(\mathbf{r} - \overline{0-20}) + G(\mathbf{r} - \overline{00-2}) \end{array} \right. \quad (\text{IV, 5})$$

where (x, y, z) is written as \overline{xyz} for brevity. In Table (IV, i), we give the values of $H^1(\mathbf{r})$ and $H^2(\mathbf{r})$ in the third and fourth columns for relevant values of \mathbf{r} using the values $G(\mathbf{r})$ given in the second column of that table.

Using the boundary property $G(\mathbf{r}) = 1/r$ for large r , one can easily relate the constant K defined in (III, 15) to the quantities $g(\mathbf{y})$ in (IV, 3), or the g_i 's in (IV, 4). Comparing the coefficient of $1/r$ in the two equations, we have the relation

$$K = - \sum_{\mathbf{y} \in N_2} g(\mathbf{y}) = -(12g_1 + 6g_2) \quad (\text{IV, 6})$$

where 12 and 6 are the degeneracies of symmetries a and b . Equation (III, 16) then gives us the relation

$$\frac{J_1}{c_1} = -4\pi \left(\frac{p_0}{3}\right) (12g_1 + 6g_2) \quad (\text{IV, 7})$$

Comparing (IV, 7) with (III, 2), since J_1/c_1 , g_1 and g_2 are linear in c_1 , we then get a_1 as the coefficient of c_1 in the right hand side of (IV, 7). We now find g_1 and g_2 in terms of the physical quantities c_1 , c_2 , p_i and $\gamma \equiv \frac{p-1}{p_0} - 1$.

The quantities g_1 and g_2 can be obtained by considering the difference equation (III, 5) on the sites where it differs from the finite difference analogue of Laplace's equation, namely the sites in N_2 , eg. the sites $(1, 1, 0)$ and $(2, 0, 0)$. Writing the difference equation (III, 5) for $(2, 0, 0)$, and dividing by $p_0/3$, we obtain

$$f_{300} + 4f_{210} - 5f_{200} + \left(\frac{p_1}{p_0}f_{100} - \frac{p-1}{p_0}f_{200}\right) = 0 \quad (\text{IV, 8})$$

We then apply the operation Δ in (IV, 1) to the site $(2, 0, 0)$ and subtract this from (IV, 8), thus obtaining

$$\Delta f_{200} = \alpha f_{100} + \gamma f_{200} \quad (\text{IV, 9})$$

where

$$\alpha = 1 - \frac{p_1}{p_0} \quad \text{and} \quad \gamma = \frac{p-1}{p_0} - 1 \quad (\text{IV, 10})$$

One can easily find $\Delta f(\mathbf{r})$ in terms of $\Delta H^1(\mathbf{r})$ and $\Delta H^2(\mathbf{r})$. Using (IV, 5), (IV, 2) and the linearity of Δ , we have

$$\begin{cases} \Delta H^1(1, 1, 0) = \Delta H^2(2, 0, 0) = -4\pi, \text{ etc.} \\ \Delta H^i(\mathbf{r}) = 0 \text{ otherwise} \end{cases} \quad (\text{IV, 11})$$

We then apply the operator Δ to (IV, 4) for the sites $\mathbf{r} = (2, 0, 0)$ and $(1, 1, 0)$.

By the linearity of Δ we obtain

$$\begin{cases} \Delta f_{200} = -4\pi g_2 + h_{100} \\ \Delta f_{110} = -4\pi g_1 + 2h_{100} \end{cases} \quad (\text{IV, 12})$$

Eliminating Δf_{200} between (IV, 12) and (IV, 9), we obtain the relation

$$-4\pi g_2 + h_{100} = \alpha f_{100} + \gamma f_{200} \quad (\text{IV, 13})$$

Doing a similar analysis for f_{110} we obtain the analogue of (IV, 13) as

$$-4\pi g_1 + 2h_{100} = 2\alpha f_{100} + 2\gamma f_{110} \quad (\text{IV, 14})$$

We can then use the fact that $f_{100} = 0$, and the equation (IV, 4) for $\mathbf{r} = (1, 0, 0)$, $(1, 1, 0)$ and $(2, 0, 0)$ to eliminate h_{100} , f_{110} and f_{200} from (IV, 13) and (IV, 14) to obtain two simultaneous equations for g_1 and g_2 in terms of c_1, c_2, γ and α only. Doing this procedure on equation (IV, 13) and on [(IV, 14) - 2×(IV, 13)], we obtain:

$$\begin{cases} g_2[-4\pi - H_{100}^2 - \gamma H_{200}^2] + g_1[-H_{100}^1 - \gamma H_{200}^1] = c_1(1 + \gamma) \\ g_2[8\pi - 2\gamma(H_{110}^2 - H_{200}^2)] - g_1[4\pi + 2\gamma(H_{110}^1 - H_{200}^1)] = 0 \end{cases}$$

On substituting the values of H_{xyz}^i from Table (IV, i), we then obtain

$$\begin{cases} g_2[-15.7995 - 4.8409\gamma] + g_1[-8.3204 - 5.6632\gamma] = c_1(1 + \gamma) \equiv c_1 \frac{p-1}{p_0} \\ g_2[25.1328 + 4.0184\gamma] + g_1[-12.5664 - 6.6470\gamma] = 0 \end{cases}$$

Solving for g_1 and g_2 we then obtain these formulae:

$$\begin{cases} g_1 = \frac{-(25.1328 + 4.0184\gamma)}{407.658 + 341.619\gamma + 54.9345\gamma^2} \frac{p-1}{p_0} c_1 \\ g_2 = \frac{-(12.5664 + 6.647\gamma)}{407.658 + 341.619\gamma + 54.9345\gamma^2} \frac{p-1}{p_0} c_1 \end{cases} \quad (\text{IV, 15})$$

Substituting these equations into (IV, 7) for J_1/c_1 , we obtain the equation:

$$\frac{J_1}{c_1} = \frac{3.874(1 + 0.234\gamma)}{1 + 0.838\gamma + 0.1348\gamma^2} p_{-1}c_1 \quad (\text{IV, 16})$$

The coefficient of c_1 in this equation then gives us $a_1(0)$, the diffusion constant of monomers in the limit of zero density:

$$a_1(0) = \frac{3.874(1 + 0.234\gamma)}{1 + 0.838\gamma + 0.1348\gamma^2} p_{-1} \quad (\text{IV, 17})$$

In this equation, $a_1(0)$ is expressed as the product of p_{-1} and the ratio of two polynomials in $\gamma \equiv \frac{p_{-1}}{p_0} - 1$.

To check (IV, 17), we can calculate $\frac{\partial c_2}{\partial t}$, and $a_1(0)$ is the coefficient of c_1^2 in this formula. Considering the various ways in which a particle can move to or from $(1, 0, 0)$ in one move, and remembering that by symmetry $f_{110} = f_{1-10} = f_{101} = \text{etc}$, and that $p(\mathbf{x}, \mathbf{y}) = \frac{p_i}{3}$, we have

$$\frac{\partial c_2}{\partial t} = c_1 \times \frac{\partial f_{100}}{\partial t} = c_1 \times 6 \left[\frac{p_{-1}}{3}(f_{200} + 4f_{110}) - 5\frac{p_{+1}}{3}f_{100} \right] \quad (\text{IV, 18})$$

where the factor 6 occurs because a monomer has 6 neighbouring sites in which a dimer can form. Then substituting (IV, 4) into (IV, 18), we obtain for $f_{100} = 0 = c_2$,


$$\frac{\partial c_2}{\partial t} = p_{-1}c_1[10c_1 + 2(H_{200}^1 + 4H_{110}^1)g_1 + 2(H_{200}^2 + 4H_{110}^2)g_2]$$

On using the values of H^i from Table (IV, i),

$$\frac{\partial c_2}{\partial t} = p_{-1}c_1[10c_1 + 2(41.610g_1 + 16.167g_2)] \quad (\text{IV, 19})$$

Substituting (IV, 15) for g_1 and g_2 , and using (II, 1) and (II, 2) with $c_2 = c_3 = 0$, we again arrive at equation (IV, 16), and hence the same value for $a_1(0)$ as in (IV, 17). This also serves as a numerical check for $a_1(0)$.

IV.3 Calculation of $a_2(0)$ in terms of γ .

To find $a_2(0)$ we have to solve (III, 5) for $f(\mathbf{r})$, but this time we have a dimer as the central cluster. We assume the dimer is situated at $(0, 0, 0)$ and $(1, 0, 0)$. See Fig. (IV, ii). The dimer is denoted by .

N_1 is the set of nearest neighbours of the dimer, and contains 10 sites, denoted by \bullet . The set of second nearest neighbours N_2 contains 26 sites in all, and they fall under four separate symmetries relative to the central dimer. These four symmetries are shown separately in Fig. (IV, ii), and are denoted by A, B, C and D. The first symmetry, A, contains two sites $(-2, 0, 0)$ and $(3, 0, 0)$. This is the axial symmetry. The other symmetries, B, C, D, each contain 8 sites. Vectors such as $(2, 1, 0)$, $(1, 2, 0)$ and $(0, 1, 1)$ belong respectively to these three symmetries.

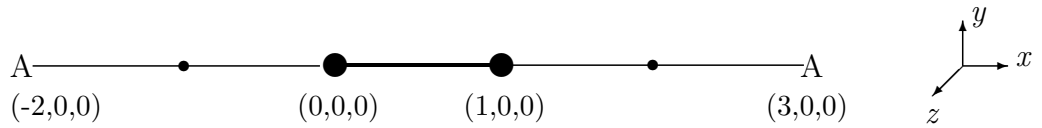
The function $f(\mathbf{r})$ which satisfies (III, 5) for the dimer case has to satisfy certain boundary conditions which are different from the monomer case. For large r , the boundary condition is unchanged, so $f(\mathbf{r}) \rightarrow c_1$ as $r \rightarrow \infty$. For $\mathbf{r} \in N_1$, however, $f(\mathbf{r})$ is proportional to c_3/c_2 , and in a way similar to (III, 11), we can formally require $f(\mathbf{r}) = 0$ for $\mathbf{r} \in N_1$. The boundary conditions then are

$$f(\mathbf{r}) \rightarrow c_1 \text{ as } r \rightarrow \infty; \quad f(\mathbf{r}) = 0 \text{ for } \mathbf{r} \in N_1 \quad (\text{IV, 20})$$

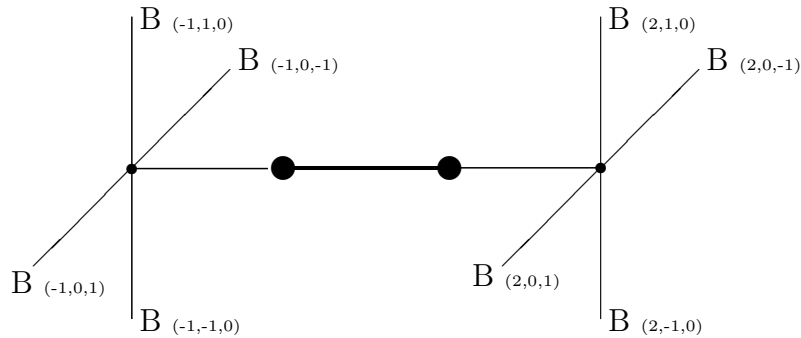
The function $f(\mathbf{r})$ is then linear in c_1 .

As in the monomer case, $f(\mathbf{r})$ has to satisfy certain symmetry properties in the dimer case. It is easy to observe from the first diagram in Fig. (IV, ii) that symmetry about the plane $x = 1/2$, and symmetry about the x -axis lead to the equations $f(x + 1, y, z) = f(-x, y, z) \quad \forall x > 0$, and $f(x, y, z) = f(x, -y, z) = f(x, z, y) = \dots$

Fig. (IV, ii). Illustration showing a dimer at $(0,0,0)$ and $(0,0,1)$. This is represented by $\bullet\text{---}\bullet$, whilst the nearest neighbours are represented by \cdot . The second nearest neighbours are denoted by A, B, C, D, relating to the four different symmetries with respect to the central dimer. There are 26 second nearest neighbours, 2 in A, and 8 in each of B, C and D.

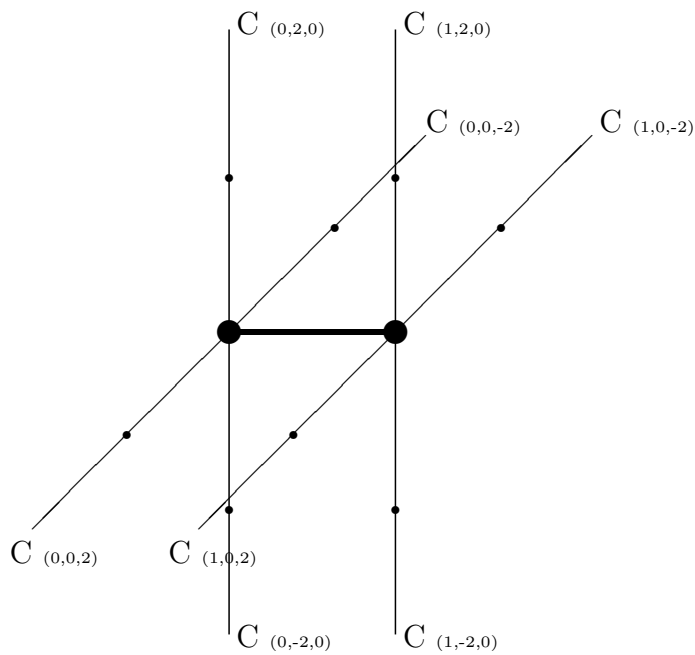


1st symmetry: degeneracy = 2; sites A at $(-2,0,0)$ and $(3,0,0)$.

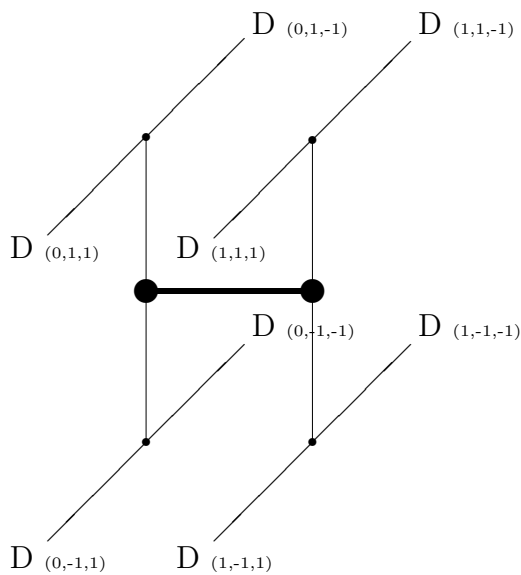


2nd symmetry: degeneracy = 8; sites B at $(-1$ or $2, \pm 1, 0)$ and $(-1$ or $2, 0, \pm 1)$.

Please turn over for symmetries C and D.



3rd symmetry: degeneracy = 8; sites C at (0 or 1, ± 2 , 0) and (0 or 1, 0, ± 2).



4th symmetry: degeneracy = 8; sites D at (0 or 1, ± 1 , ± 1)

End of Fig. (IV, ii).

To solve for $f(\mathbf{r})$ in the dimer case, we can write analogously to (IV, 3) and (IV, 4) the formula

$$f(\mathbf{r}) = c_1 + \sum_{i=1}^4 g_i G^i(\mathbf{r}) + h(\mathbf{r}) \quad (\text{IV, 21})$$

where the summation is over the four symmetries of the sites in N_2 , g_i depend on c_1 , c_3/c_2 , p_i but are independent of r , and $h(\mathbf{r}) \neq 0 \iff \mathbf{r} \in N_1$, that is if \mathbf{r} is a nearest neighbour of the central dimer. The quantities $G^i(\mathbf{r})$ are linear combinations of $\sum_{\mathbf{n} \in N_2}^i G(\mathbf{r} - \mathbf{n})$ where the sum \sum_i is over the vectors $\mathbf{n} \in N_2$ having the same symmetry i . Symmetries A, B, C, D in Fig. (IV, ii) are here represented by symmetries 1 to 4 respectively. Explicitly, the $G^i(\mathbf{r})$ for the four symmetries $i = 1$ to 4 are given by

$$\left\{ \begin{array}{l} G^1(\mathbf{r}) = G(\mathbf{r} - \overline{300}) + G(\mathbf{r} - \overline{200}) \\ G^2(\mathbf{r}) = G(\mathbf{r} - \overline{210}) + G(\mathbf{r} - \overline{201}) + G(\mathbf{r} - \overline{20\overline{1}}) + G(\mathbf{r} - \overline{2\overline{10}}) \\ \quad + G(\mathbf{r} - \overline{110}) + G(\mathbf{r} - \overline{101}) + G(\mathbf{r} - \overline{10\overline{1}}) + G(\mathbf{r} - \overline{1\overline{10}}) \\ G^3(\mathbf{r}) = G(\mathbf{r} - \overline{020}) + G(\mathbf{r} - \overline{0\overline{20}}) + G(\mathbf{r} - \overline{002}) + G(\mathbf{r} - \overline{00\overline{2}}) \\ \quad + G(\mathbf{r} - \overline{120}) + G(\mathbf{r} - \overline{1\overline{20}}) + G(\mathbf{r} - \overline{102}) + G(\mathbf{r} - \overline{10\overline{2}}) \\ G^4(\mathbf{r}) = G(\mathbf{r} - \overline{011}) + G(\mathbf{r} - \overline{01\overline{1}}) + G(\mathbf{r} - \overline{0\overline{11}}) + G(\mathbf{r} - \overline{0\overline{1\overline{1}}}) \\ \quad + G(\mathbf{r} - \overline{111}) + G(\mathbf{r} - \overline{11\overline{1}}) + G(\mathbf{r} - \overline{1\overline{11}}) + G(\mathbf{r} - \overline{1\overline{1\overline{1}}}) \end{array} \right. \quad (\text{IV, 22})$$

The $G^i(\mathbf{r})$ are given in Table (IV, i) for relevant values of \mathbf{r} . It is easy to show using the definition of G and G^i , and the linearity of the operation Δ , that

$$\left\{ \begin{array}{l} \Delta G_{300}^1 = \Delta G_{210}^2 = \Delta G_{120}^3 = \Delta G_{111}^4 = -4\pi \\ \Delta G^i(\mathbf{r}) = 0 \text{ if } \mathbf{r} \notin \text{symmetry } i \end{array} \right. \quad (\text{IV, 23})$$

Using the boundary property $G(\mathbf{r}) = 1/r$ for large r , one can easily relate the constant K in (III, 15) to the quantities g_i in (IV, 21). In the same way as in the derivation of (IV, 6), we can write

$$\frac{J_2}{c_2} = -4\pi \left(\frac{p_0}{3} \right) (2g_1 + 8g_2 + 8g_3 + 8g_4) \quad (\text{IV, 24})$$

In this equation, the coefficient of g_i is the degeneracy of each symmetry, (refer to Fig. (IV, ii)), and $\frac{p_0}{3}$ is the value of $p(\mathbf{x}, \mathbf{y})$ far from the central dimer in the limit of zero density. The coefficients g_i are linear in c_1 , and so $a_2(0)$ is obtained as the coefficient of c_1 in the right hand side of (IV, 24).

To find g_i , we proceed as we did for $a_1(0)$. We write the equation (III, 5) for the sites P in N_2 . From this we then subtract the corresponding identity for $\Delta f(\mathbf{r})$ given by (IV, 1). Using (IV, 23) and the linearity of Δ , we arrive at the equations

$$\Delta f_{300} = -4\pi g_1 + h_{200} = \alpha f_{200} + \gamma f_{300} \quad (\text{a})$$

$$\Delta f_{210} = -4\pi g_2 + h_{110} + h_{200} = \alpha(f_{100} + f_{200}) + 2\gamma f_{210} \quad (\text{b})$$

$$\Delta f_{120} = -4\pi g_3 + h_{110} = \alpha f_{110} + \gamma f_{120} \quad (\text{c})$$

$$\Delta f_{111} = -4\pi g_4 + 2h_{110} = 2\alpha f_{110} + 2\gamma f_{111} \quad (\text{d})$$

The quantities h_{200} and h_{110} can be eliminated by using equations (IV, 21) and the second boundary condition in (IV, 20) for sites \mathbf{r} in N_1 . We then have

$$f_{110} = c_1 + \sum_1^4 g_i G_{110}^i + h_{110} = 0 \quad (\text{e})$$

$$f_{200} = c_1 + \sum_1^4 g_i G_{200}^i + h_{200} = 0 \quad (\text{f})$$

In the simultaneous equations (a) - (d), we can eliminate f_r and h_r using (IV, 21), (e) and (f). The coefficients of g_i will then depend only on c_1, γ, α and the g^i 's. Having done these eliminations and substitutions, we take linear

combinations as follows for simplicity:

$$\begin{aligned}
(c) - (d)/2 : \quad & -2\pi(2g_3 - g_4) = \gamma \sum_1^4 g_i (G_{120}^i - G_{111}^i) \\
(a) - (b) + (c) : \quad & -4\pi(g_1 - g_2 + g_3) = \gamma \sum_1^4 g_i (G_{300}^i - 2G_{210}^i + G_{120}^i) \\
(a) - (c) : \quad & -4\pi(g_1 - g_3) = \sum_1^4 g_i [(G_{200}^i - G_{110}^i) + \gamma(G_{300}^i - G_{120}^i)] \\
(a) : \quad & -4\pi g_1 - (1 + \gamma)c_1 = \sum_1^4 g_i (G_{200}^i + \gamma G_{300}^i) \quad (\text{IV, 25})
\end{aligned}$$

When we substitute the values $G^i(r)$ from Table (IV, i) into (IV, 25) and write the equations in matrix form, we have

$$\begin{pmatrix} -0.0737\gamma & -0.5470\gamma & 4\pi + 2.3925\gamma & -2\pi - 3.1920\gamma \\ 4\pi + 2.1305\gamma & -4\pi - 5.6996\gamma & 4\pi + 2.2319\gamma & -0.9598\gamma \\ 13.1311 + 2.7483\gamma & 1.2860 + 0.5512\gamma & -13.4984 - 3.6007\gamma & -1.4594 - 0.9134\gamma \\ 13.9028 + 3.3781\gamma & 5.6088 + 3.7548\gamma & 3.2160 + 2.5192\gamma & 3.7968 + 2.8140\gamma \end{pmatrix} \begin{pmatrix} g_1 \\ g_2 \\ g_3 \\ g_4 \end{pmatrix} = \begin{pmatrix} 0 \\ 0 \\ 0 \\ A \end{pmatrix}$$

$$\text{with } A = -c_1(1 + \gamma) \equiv -c_1 p_{-1}/p_0. \quad (\text{IV, 26})$$

The g_i 's are then found by Cramer's rule in terms of the parameter γ . Denoting the Cramer determinant by det , we have for det and g_i the equations

$$\begin{aligned}
det &= 42000.3(1 + 1.547\gamma + 0.835\gamma^2 + 0.188\gamma^3 + 0.015\gamma^4) \\
det \times g_1 &= (1194.71 + 1494.13\gamma + 587.192\gamma^2 + 72.2967\gamma^3)A \\
det \times g_2 &= (2333.04 + 2004.45\gamma + 524.851\gamma^2 + 42.816\gamma^3)A \quad (\text{IV, 27}) \\
det \times g_3 &= (1138.33 + 1337.66\gamma + 488.425\gamma^2 + 53.7929\gamma^3)A \\
det \times g_4 &= (2276.66 + 1735.05\gamma + 412.727\gamma^2 + 31.329\gamma^3)A
\end{aligned}$$

We can then use (IV, 24) and (IV, 27) to give us J_2/c_2 in terms of γ and c_1 :

$$\frac{J_2}{c_2} = \frac{4.824(1 + 0.901\gamma + 0.260\gamma^2 + 0.024\gamma^3)}{(1 + 1.547\gamma + 0.835\gamma^2 + 0.188\gamma^3 + 0.015\gamma^4)} p_{-1} c_1 \quad (\text{IV, 28})$$

where again the detailed balance condition is satisfied. The coefficient of c_1 is $a_2(0)$ which is then given by:

$$a_2(0) = \frac{4.824(1 + 0.901\gamma + 0.260\gamma^2 + 0.024\gamma^3)}{(1 + 1.547\gamma + 0.835\gamma^2 + 0.188\gamma^3 + 0.015\gamma^4)^{p-1}} \quad (\text{IV, 29})$$

We can check (IV, 29) by calculating $\frac{\partial c_3}{\partial t}$, and $a_2(0)$ is then the coefficient of $c_1 c_2$ in this formula. We can again assume that the ratios of the concentration of various 3-sized clusters of different shapes and orientation are the same as at equilibrium. Since given a dimer at $(0, 0, 0)$ and at $(1, 0, 0)$, a cluster of size 3 can be formed by absorbing a monomer at one of the 8 sites isomorphic to $(1, 1, 0)$ or at one of the two sites $(2, 0, 0)$ or $(-1, 0, 0)$, we can write

$$c_3 = c_2(8f_{110} + 2f_{200})$$

We can then find the derivative of c_3 with respect to time by considering how a monomer can go to or move from $(1, 1, 0)$ and $(2, 0, 0)$. We use the symmetry of f in the dimer case, the form for $f(\mathbf{r})$ given in (IV, 21), and the fact that $p(\mathbf{x}, \mathbf{y}) = p_i/3$ to obtain:

$$\begin{aligned} \frac{\partial c_3}{\partial t} &= 8c_2 \left[\frac{p-1}{3}(2f_{111} + f_{120} + f_{210}) - \frac{p_1}{3} 4f_{110} \right] \\ &\quad + 2c_2 \left[\frac{p-1}{3}(f_{300} + 4f_{210}) - \frac{p_1}{3} 5f_{200} \right] \\ &= p_{-1}c_2 \left[\frac{42}{3}c_1 + \frac{2}{3} \sum_1^4 (8G_{111}^i + 8G_{210}^i + 4G_{120}^i + G_{300}^i) g_i \right] \\ &\quad + \text{terms proportional to } p_1 \text{ or } c_3 \\ &= p_{-1}c_2 \left[14c_1 + \frac{2}{3}(19.035g_1 + 97.206g_2 + 82.447g_3 + 103.084g_4) \right] \end{aligned}$$

where we have substituted the relevant value of $G^i(\mathbf{r})$ from Table (IV, i). From (IV, 27), we can substitute for g_i into the above expression for $\frac{\partial c_3}{\partial t}$,

and we obtain the same formula as (IV, 28). This therefore gives the same expression for $a_2(0)$ as (IV, 29).

We can now check numerically $a_1(0)$ and $a_2(0)$ given by (IV, 17) and (IV, 29) with the corresponding numerical values obtained from the canonical average (III, 20). This is done in Table (IV, ii) for $-0.8 \leq \gamma \leq 3$. It can be noticed that the accuracy is better than 1% in all cases over this range of the parameter γ . This serves as a numerical check for $a_1(0)$ and $a_2(0)$.

It can be noticed from (IV, 17) and (IV, 29) that $a_1(0)$ and $a_2(0)$ depend only on p_0 and p_{-1} and do not depend on p_1 . Physically the reason for this is that a_l depends on the rate at which monomers diffuse towards the central cluster at large distances from the origin: this rate is proportional to p_0 . Also, a_l depends on p_{-1} which is a measure of the attraction between the central cluster and a monomer. Conversely, a_l does not depend on p_1 , because this is a measure of the rate at which clusters break up. It can also be seen in the mathematical analysis for $\frac{\partial c_{l+1}}{\partial t}$ in this chapter that p_1 always multiplies $f(\mathbf{r})$ for $\mathbf{r} \in N_1$, which is proportional to $\frac{c_{\lambda+}}{c_\lambda}$ rather than c_1 , and so $a_l(0)$, the coefficient of c_1 in this quantity, does not depend on p_1 .

Table (IV, ii). The kinetic coefficients in the limit of zero density, $a_1(0)$ and $a_2(0)$, calculated by the Green's function method are compared to the S.O.R estimates obtained in the previous chapter. A closed formula for $a_1(0)$ and $a_2(0)$ are given in equations (IV, 17) and (IV, 29).

$\gamma = \frac{p-1}{p_0} - 1$	$a_1(0)$		$a_2(0)$	
	Green (IV, 17)	S.O.R. (III, 20)	Green (IV, 29)	S.O.R. (III, 20)
-0.8	0.76	0.76	1.01	1.01
-0.6	1.22	1.22	1.58	1.58
-0.4	1.53	1.54	1.95	1.96
-0.2	1.76	1.76	2.22	2.22
0.0	1.94	1.94	2.41	2.42
0.2	2.07	2.08	2.56	2.57
0.4	2.19	2.19	2.69	2.69
0.6	2.28	2.28	2.79	2.79
0.8	2.36	2.36	2.87	2.88
1.0	2.42	2.43	2.94	2.95
1.2	2.48	2.48	3.00	3.01
1.4	2.53	2.54	3.05	3.06
1.6	2.58	2.58	3.10	3.11
1.8	2.62	2.62	3.14	3.15
2.0	2.65	2.66	3.18	3.19
2.2	2.69	2.69	3.21	3.23
2.4	2.72	2.72	3.24	3.26
2.6	2.74	2.75	3.27	3.29
2.8	2.77	2.77	3.30	3.31
3.0	2.79	2.80	3.32	3.34

Chapter V: Comparison of the Differential Equations with the Simulation of a Quenched Alloy at the same value of l^* .

In this chapter, we compare the numerical solution of the Becker-Döring system of differential equations described in Chapter II with concentrations of various sized clusters in the simulation of a quenched alloy. This simulation was described in Sur et al. (1977) and in Penrose et al. (1978).

V.1 Numerical Computation of the Differential Equations

The system of differential equations used is that given in equations (II,1), (II, 2) and (II, 3). We take $a_l(0)$ for $l \geq 7$ to be given by the extrapolation formula

$$a_l(0) = \frac{1}{6}(874 + 1888l)^{1/3}$$

which is given in (III, 24) and (III, 25). For the partition functions Q_l for $l \geq 11$, we use equation (I, 7) with $w_s = 0.010526$ and $C = 2.415$. The quantities $b_l(0)$ are then given by the equations (II, 8). The parameter $\mu(l^*)$ in (II, 7) and (II, 8), which describes the variation of a_l and b_l when the density is non-zero, is taken equal to 1, for numerical convenience. The factor $\mu(l^*)$ will be estimated empirically in the next section, and will be found theoretically in the next chapter.

The initial concentrations in the differential equations were taken to be the equilibrium distribution at infinite temperature as in the simulation. These initial values are shown for density $\rho = 0.075$ in Table (I, ii). Since the lattice gas in the simulation was quenched to $T = 0.59T_c$, where T_c is the critical temperature, the coefficients $a_l(0)$, $b_l(0)$ and Q_l in our differen-

tial equations are all evaluated at this temperature, which is equivalent to $\frac{V}{kT} = 1.5$, or $y = 4.482$. In the differential equations as in the simulation therefore, the temperature changes instantaneously from $T = \infty$ at time zero to $T = 0.59T_c$ thereafter, and the temperature is held constant at this value.

For numerical integration, we used a Runge-Kutta procedure. We took a system of equations with maximum cluster size $L = 800$, that is $c_l = 0$ for $l > 800$. Equation (II, 9) gives the differential equation satisfied by c_L , the concentration of clusters of maximum size L . $L = 800$ was considered to be sufficiently large, since in the simulation, the biggest cluster contained about 600 particles over the time range considered. We then computed the solution of the differential equations for $\rho = 0.075$ for $L = 800$ and $L = 1600$, and found that c_{600} differed by not more than 10% over the same time interval as will be considered in this chapter. Besides, the number of clusters larger than 600 was at most only 1% of the total number of clusters larger than 20 for this interval of time. For our computer runs we therefore settled on $L = 800$. We solved the differential equations for the three densities $\rho = 0.05, 0.075$ and 0.10 , all at temperatures $T = 0.59T_c$.

V.2 Empirical Estimate of $\mu(l^*)$

The differential equations were computed with $\mu(l^*) = 1$ in (II, 7) and (II, 8). We take equation (I, 9) to be our definition of l^* with $w_s = 0.010527$ and $C = 2.415$ for $\frac{V}{kT} = 1.5$, and with $w = \frac{c_1}{(1-\rho)^3}$ from (I, 6). We denote l^* in the simulation and in the differential equations by l_{sim}^* and l_{de}^* . We will compare the simulation at time t with the differential equations at time t_{de} , where

$$l_{sim}^*(t) = l_{de}^*(t_{de}) \tag{V, 1}$$

that is we will compare them when the value of l^* is the same in both.

Since the w -formula (I, 6) was used in the detailed balance condition (II, 4) for b_{l+1}/a_l , and since J_l/c_l in (II, 2) is very small except for the earliest times, we expect that l^* , or w , determines via (I, 6) the distribution of clusters in the differential equations also. This is borne out by Table (I, iii), where for each value of l^* , we give the corresponding distribution predicted by the differential equations at this value of l^* , for $\rho = 0.10$ and $T = 0.59T_c$. For l_{de}^* , we took w to be $c_1/(1 - \rho)^3$ in (I, 9). From Table (I, iii), we see that $\rho_{10} = \sum_1^{10} l c_l$ for the differential equations and from the w -formula (I, 6) agree to about 1% after $t = 1000$. Our method of comparison at the same l^* based on (V, 1) will therefore ensure that the comparison is made when the total number of particles in the small clusters, and hence also in the large clusters, is the same in both the differential equations and in the simulation. Besides, l^* is expected to be linear in t_{de} (Penrose et al., 1978), so it is as good a variable as time as an independent variable for this problem.

The importance of (V, 1) lies also in the fact that we can obtain an empirical value for $\mu(l^*)$ by finding the relation between the simulation time t and t_{de} . Indeed since $\mu(l^*) = 1$ in the differential equation, we can write the Becker-Döring equations in Section (II, 1) as

$$\frac{d\mathbf{c}}{dt} = \mu(l^*)f(\mathbf{c}) \quad \text{and} \quad \frac{d\mathbf{c}}{dt_{de}} = f(\mathbf{c})$$

where $\mathbf{c} = (c_1, c_2, \dots)$ and $f(\mathbf{c})$ is independent of $\mu(l^*)$. From these two equations, therefore

$$\frac{dt_{de}}{dt} = \mu(l^*) \quad \text{or} \quad t = \int_0^{t_{de}} \frac{dt_{de}}{\mu(l^*)} \quad (\text{V, 2})$$

Equation (V, 2) gives us the relation between t , t_{de} and $\mu(l^*)$. In Fig. (V, i), we plot t_{de} against t for the three densities $\rho = 0.05, 0.075, 0.10$. The pairs of

values t and t_{de} for given l^* increased approximately linearly over the range $20 \leq l^* \leq 200$ for these densities. As seen in Fig. (V, i), the graphs of t_{de} against t are approximately linear except for the earlier times ($t < 1000$) for the lower densities.

$$t_{de} = \mu(l^*)(t + t_0) \quad (\text{V}, 3)$$

where

$$\begin{aligned} \mu(l^*) &= 2.89, \quad t_0 = 0 && \text{for } \rho = 0.05; \\ \mu(l^*) &= 3.30, \quad t_0 = 400 && \text{for } \rho = 0.075; \\ \mu(l^*) &= 3.23, \quad t_0 = 800 && \text{for } \rho = 0.10. \end{aligned}$$

Thus, except for the earlier times the slope, $\mu(l^*)$, is approximately constant over the time range considered and is approximately equal to 3.0 for these densities. The equations also have an intercept which increases with density. This intercept signifies that l^* increases very rapidly with time initially over a period $t \cong t_0$, from $l^* \cong 2$ to a certain value, $l^* \cong 30$, and then increases more slowly after that. In the next chapter, we will calculate $\mu(l^*)$, and the quantities l_{de}^* and l_{sim}^* will then be compared together as a function of time.

V.3 Comparison of the concentrations of large clusters in the Becker-Döring equations and the simulation at the same value of l^* .

We now compare c_l for $l \geq 20$ in the differential equations and the simulation at the same value of l^* as explained in the previous section. We do this for densities $\rho = 0.05, 0.075$ and 0.10 . We drew histograms for the simulation concentrations at various values of l^* in the available range $0 \leq l^* \leq 210$, which is equivalent to the simulation time range $0 \leq t \leq 6000$ for these three densities.

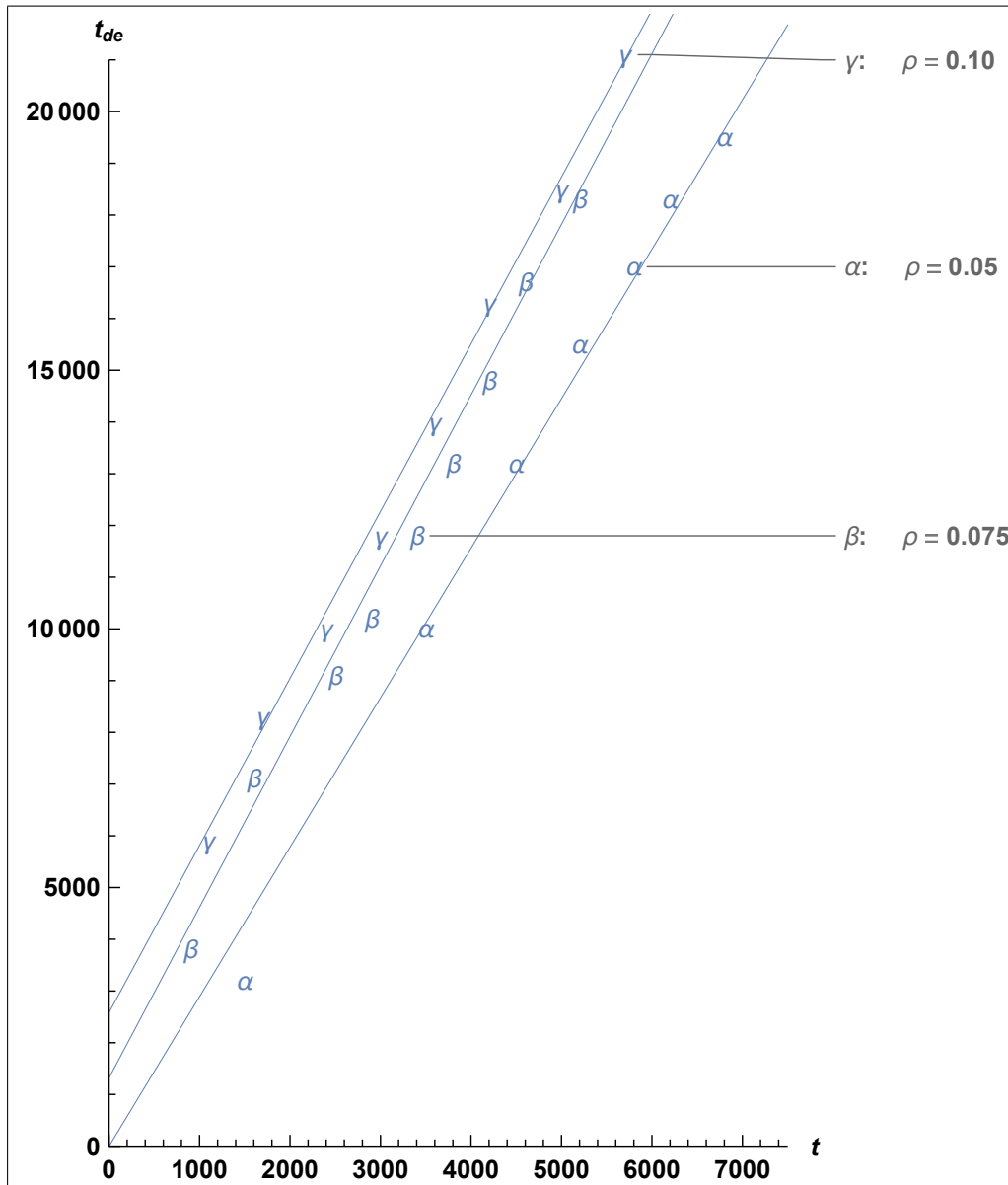


Fig. (V, i). Graph of t_{de} , the time in the Becker-Döring equations with coefficient $a_l(0)$, against simulation time t ($\equiv t_{sim}$), when the value of l^* is the same in the simulation and the Becker-Döring equations. The slope of this graph gives an empirical estimate of $\mu(l^*)$, which is seen to be practically constant for $t > 1000$. Plots for $\rho = 0.05, 0.075$ and 0.10 are presented.

To find c_l for the simulation, we define g_l as the total number of clusters of size l or larger:

$$g_l = \sum_l^{\infty} c_l \quad (\text{V}, 4)$$

Then we take c_l in the histograms for the simulation concentrations to be defined by

$$c_{l+\frac{1}{2}(h-1)} = \frac{g_l - g_{l+h}}{h} \quad (\text{V}, 5)$$

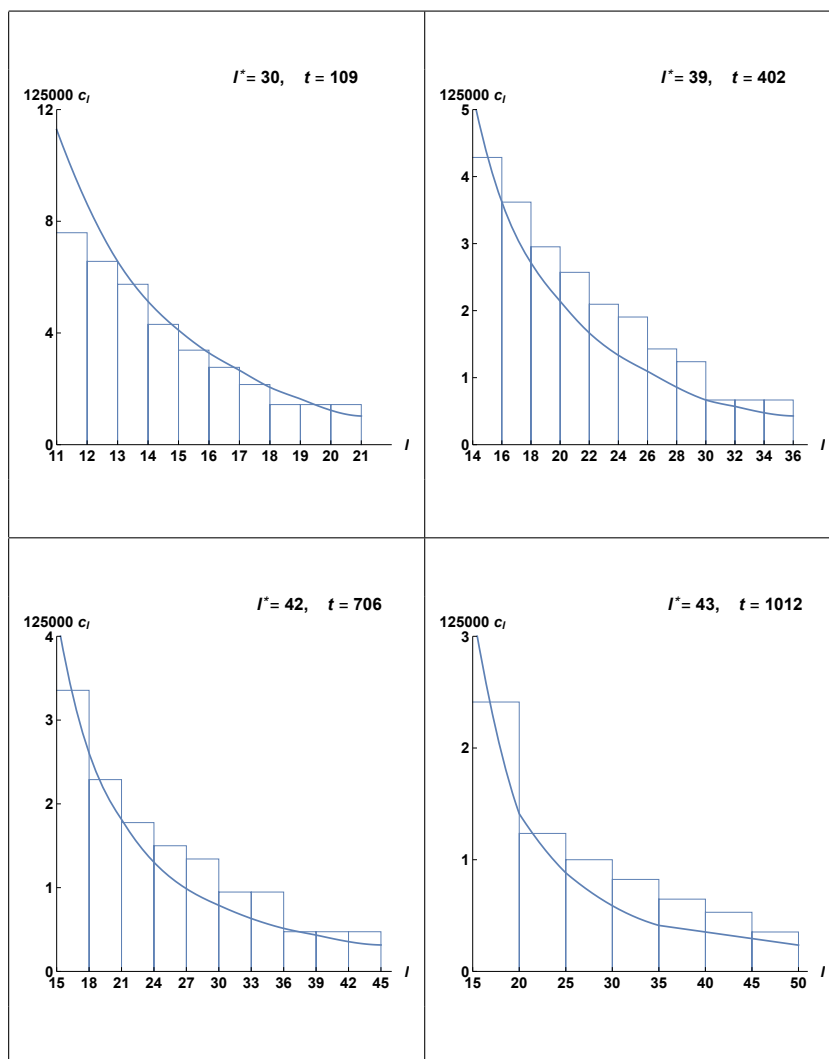
where h is chosen to be the least value so that c_l does not fluctuate too rapidly with l . In fact we found that h is about $\frac{1}{2}l^*$.

The histograms for the simulation concentrations c_l for $l \geq 20$ are given in Fig. (V, ii) for the three densities $\rho = 0.05, 0.075$ and 0.10 respectively. In each diagram, we also give the concentrations c_l predicted by the Becker-Döring equations at the same value of l^* as in the simulation.

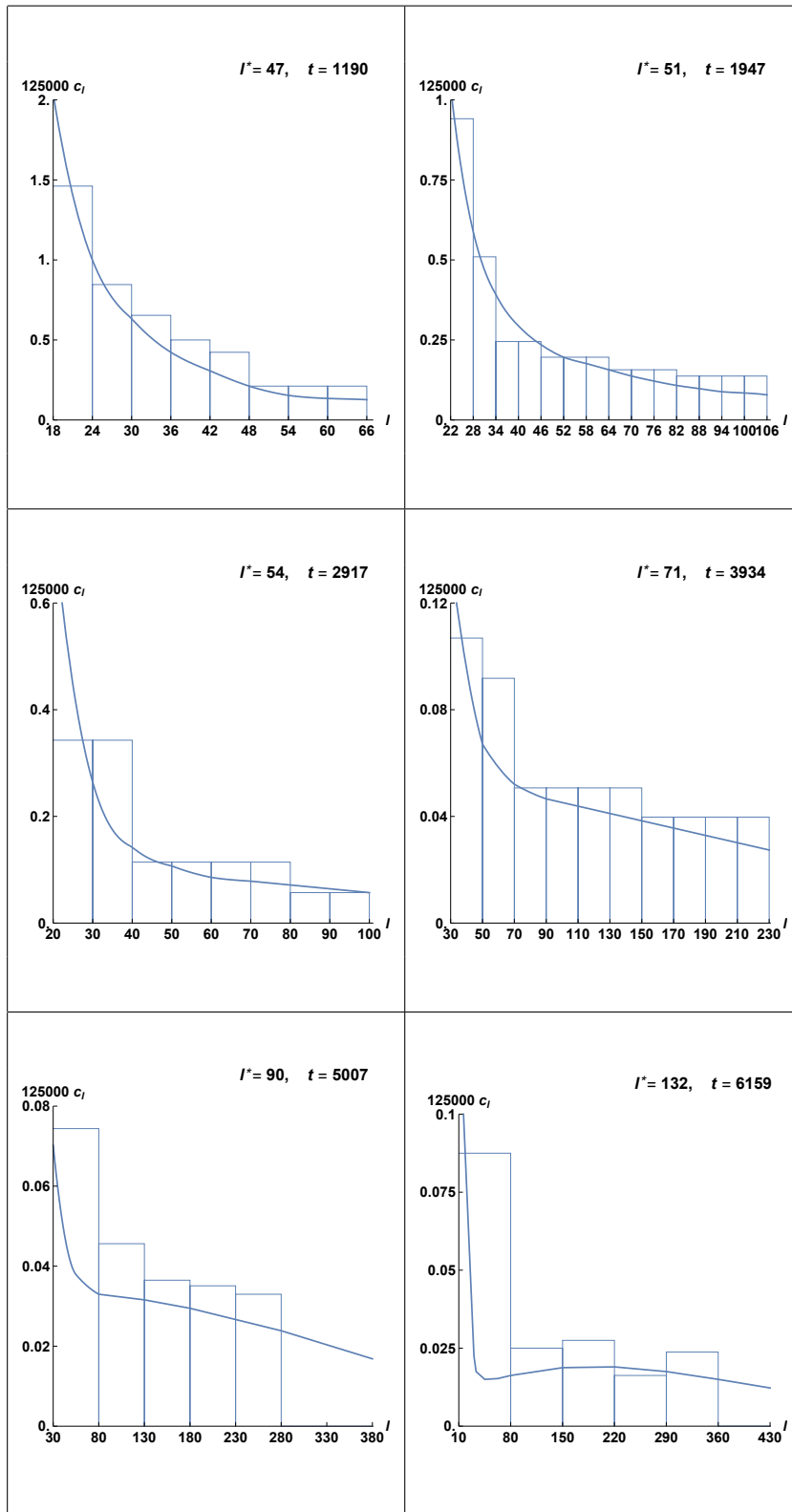
Both the histograms and the solution of the differential equations are monotonic decreasing with l for earlier simulation times $0 \leq t \leq 1000$, or equivalently for $l^* \leq 40$. For these earlier times, for densities $\rho = 0.075$ and 0.10 , the differential equations are quite close to the histogram (to $\approx 10\%$), as can be seen by inspecting the relevant diagrams in Fig. (V, ii). Gradually, however, a point of inflection appears at about $t = 1800$ for density $\rho = 0.075$, and at about $t = 1000$ for $\rho = 0.10$. Near this point of inflection eventually, a small maximum and minimum start appearing at about $t = 2800$ and $t = 1800$ for densities 0.075 and 0.10 respectively. The minimum and maximum become more pronounced with time, signifying the separation of the particles into two phases. The differential equations are quite successful in predicting the times, or rather the value of l^* , at which the point of inflection first appears in the simulation.

Fig (V, ii). Comparison of c_l for $l \geq 20$ for the simulation and the Becker-Döring equations for $0 \leq t \leq 7000$. Plots for densities $\rho = 0.05, 0.075$ and 0.10 .

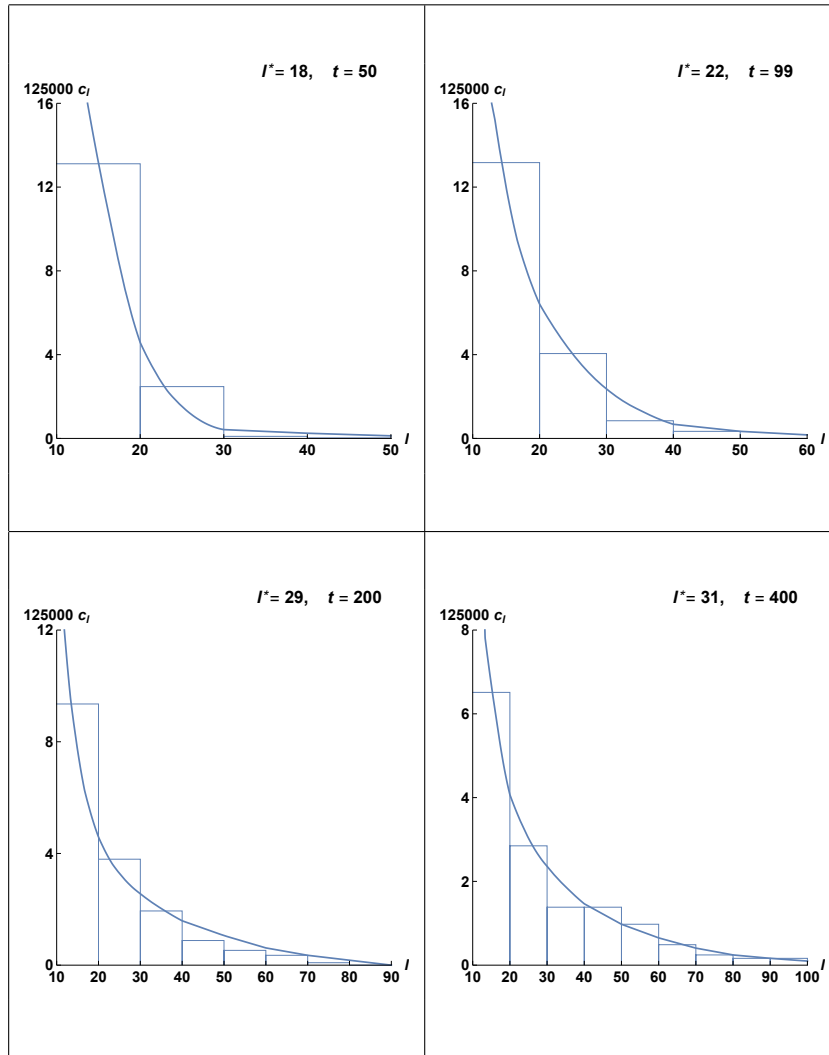
Density $\rho = 0.05$.



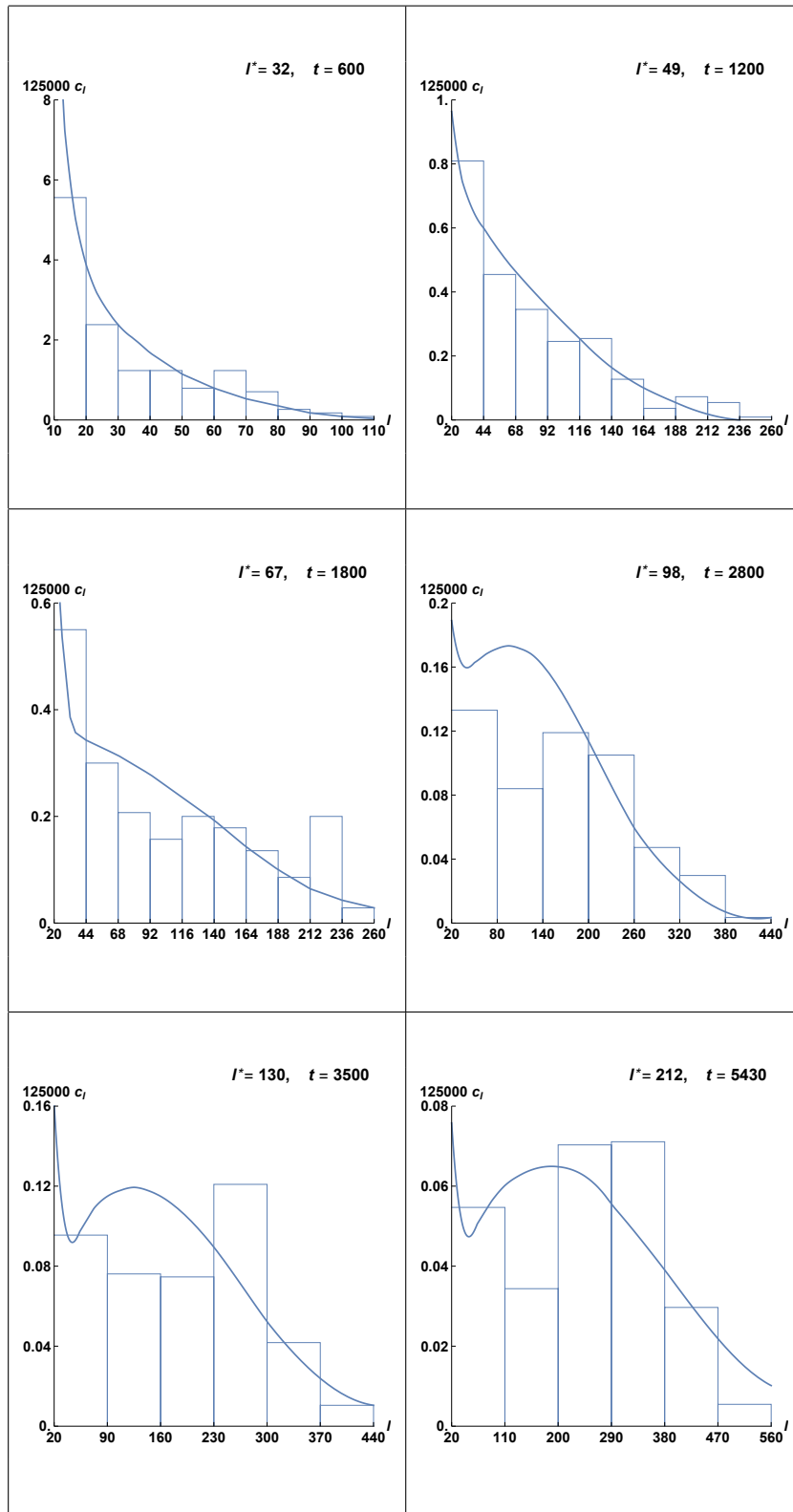
Plots for $\rho = 0.05$ continued overleaf ...



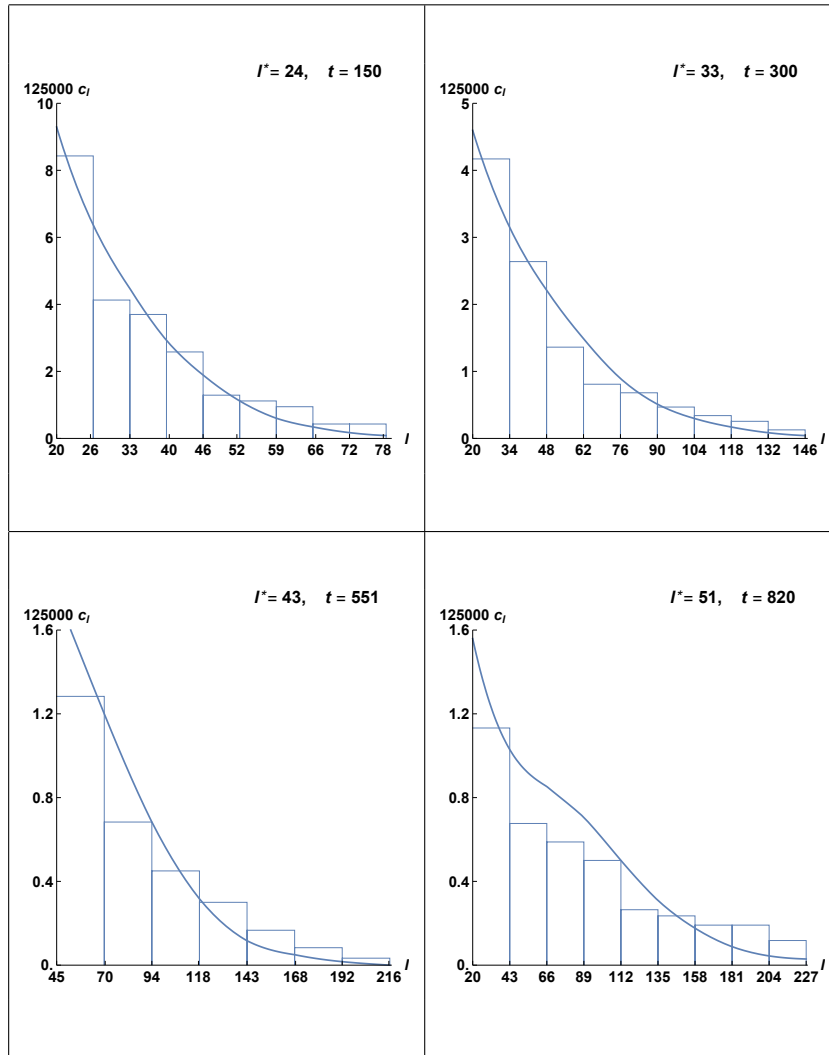
Density $\rho = 0.075$.



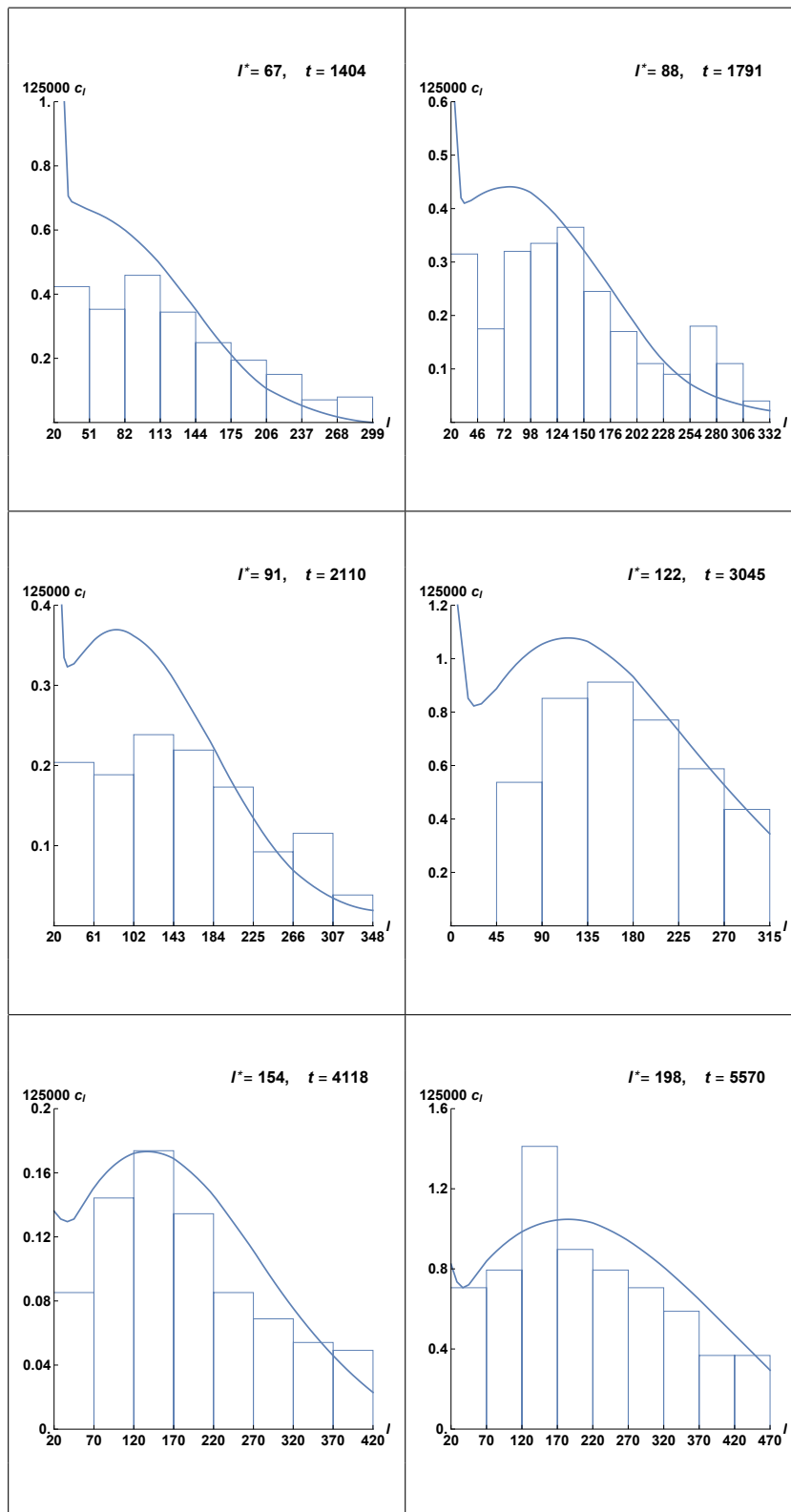
Plots for $\rho = 0.075$ continued overleaf ...



Density $\rho = 0.10$.



Plots for $\rho = 0.10$ continued overleaf ...



For $\rho = 0.05$, the differential equations generally underestimate c_l during the time range $0 \leq t \leq 6000$. The maximum and minimum do not materialise in this time range. However, the broad point of inflexion observed in the simulation after $t = 5000$, is successfully predicted by the differential equations, although they predict the c_l 's to be slightly lower than those observed in the simulation.

It is interesting to see how well the differential equations predict the position of the local maximum and minimum in the c_l - l histograms and the concentrations at these two points. In Table (V, i), we give l_{max} and l_{min} , which we define as that value of l for which c_l is the local maximum and minimum respectively. We also give $c_{l_{max}}$ and $c_{l_{min}}$, which are the concentrations of the local maximum and minimum respectively. We compare these quantities for the simulation and the differential equations at the same l^* , for densities $\rho = 0.075$ and 0.10 . For the simulation, we give the range of values of l for which c_l is a local maximum or minimum in the histogram.

On inspecting Table (V, i), we find that when the maximum and minimum first appear, the differential equations tend to underestimate l_{max} and l_{min} , and overestimate $c_{l_{max}}$ and $c_{l_{min}}$. In the case of $\rho = 0.10$, the differential equations are more accurate for later times, when the maxima and minima are more pronounced. For $\rho = 0.10$, the quantities l_{max} and l_{min} all lie within the corresponding range for the simulation at these later times. Towards the end of the time range considered ($t \cong 5000$), the differential equation concentrations at the maximum and minimum, $c_{l_{max}}$ and $c_{l_{min}}$, are accurate to about 5% for $\rho = 0.10$, and to about 18% for $\rho = 0.075$. One can also notice that l_{max} increases with time, and is roughly equal to l^* in the differential equations and the simulation.

Table (V, i). Position of local maxima and minima in the c_l - l curve, l_{max} and l_{min} , and concentrations at these two points, $c_{l_{max}}$ and $c_{l_{min}}$, for differential equations and simulation. These quantities are compared when l^* is the same in both the simulation and the differential equations. The symbol t stands for the time in the simulation. Densities $\rho = 0.075, 0.10$.

$\rho = 0.075$						
l^*	t		l_{min}	$c_{l_{min}}$	l_{max}	$c_{l_{max}}$
98	2800	simulation	80-140	0.086	140-200	0.123
		de same l^*	42	0.163	97	0.178
130	3500	simulation	90-235	0.075	235-305	0.119
		de same l^*	34	0.092	130	0.121
212	5430	simulation	110-200	0.034	200-390	0.068
		de same l^*	31	0.040	200	0.062

$\rho = 0.10$						
l^*	t		l_{min}	$c_{l_{min}}$	l_{max}	$c_{l_{max}}$
90	1949	simulation	20-103	0.260	103-145	0.30
		de same l^*	33	0.40	82	0.44
91	2110	simulation	20-100	0.20	101-142	0.25
		de same l^*	32	0.33	84	0.38
122	3045	simulation	20-90	0.11	90-180	0.18
		de same l^*	29	0.17	130	0.22
154	4118	simulation	20-70	0.09	120-170	0.175
		de same l^*	32	0.12	145	0.18
198	5570	simulation	20-70	0.07	120-220	0.12
		de same l^*	32	0.07	190	0.11

For $\rho = 0.10$, l_{min} is approximately constant ($l_{min} \cong 30$) for the differential equations over the whole time range. It always lies within the corresponding range of l_{min} in the simulation and becomes more accurate for the later times. This is not the case for $\rho = 0.075$. For this density, l_{min} decreases with time in the differential equations, whereas in the simulation, $l_{min} \cong l^*$ and increases with time. This increase in l_{min} with time is probably only a transient feature in the simulation. Histograms for real alloys (Ardell and Nicholson, 1966) do not predict such a local minimum for c_l for asymptotic times. The concentrations c_l from the differential equations will be compared with histograms of real alloys in Chapter VII.

For $l > l_{max}$, c_l is monotonic decreasing in l in the differential equations. This is true also in the simulation when the maxima and minima are more pronounced, that is after $t \cong 2200$ for $\rho = 0.10$, and after $t \cong 2800$ for $\rho = 0.075$. In this region again, the c_l - l curve is quite near to the histogram. We will discuss the large clusters in more detail in Chapter VII.

Chapter VI: Calculation of $\mu(l^*)$:

Comparison of l_{sim}^* and l_{de}^* at the same value of simulation time t .

In the previous chapters we compared the concentration c_l predicted by the simulation and the differential equations when the value of l^* is the same in both, that is, when equation (V, 1) holds. To complete the comparison, therefore, we have to compare $l_{sim}^*(t)$ and $l_{de}^*(t)$ as functions of t , the simulation time. Since $\mu(l^*)$ was put equal to 1 in the differential equations, l_{de}^* was given in terms of t_{de} in (V, 1). To find l_{de}^* in terms of t , rather than t_{de} , we use (V, 2), which relates t to t_{de} and $\mu(l^*)$. We therefore turn our attention to calculate $\mu(l^*)$.

The quantity $\mu(l^*)$ was defined in (II, 7) as $\mu(l^*) = a_l/a_l(0)$, namely as the ratio of the coefficient a_l when the supersaturation is w , to $a_l(0)$, the value of a_l in the limit of zero density. The quantities l^* , w , and the concentrations c_l of the small clusters are related by (I, 6) and (I, 9). To find $\mu(l^*)$, for any l^* , we use (III, 17), where we interpret $p_0/3$ to be the diffusion constant in the limit of zero density, as shown in (III, 22). Taking an average such as (III, 20) over all translationally inequivalent clusters λ of size l , we can write (III, 17) for any density as $a_l = 4\pi D(l^*)K_l$, where K_l is the average of K for clusters of size l . Since K , defined in (III, 15), and hence K_l , is independent of density, we have $a_l/a_l(0) = D(l^*)/D = 6D(l^*)$, using (III, 22). Therefore

$$\mu(l^*) = 6D(l^*) \tag{VI, 1}$$

The quantity $\mu(l^*)$ has been obtained analytically (Penrose, unpublished) on the Bethe lattice, a lattice with constant coordination number q but with no polygons. On the Bethe lattice, the equilibrium or steady state concentrations of the small clusters, which determine l^* , and $D(l^*)$, can be found

exactly in terms of a certain parameter ξ . Besides we will show that for low densities, the equilibrium properties of the lattice gas on the Bethe lattice with coordination number $q = 6$ are practically identical quantitatively to the properties of the lattice gas on the simple cubic lattice. The steady state concentrations of the small clusters on the two lattices also agree to a considerable extent for low densities. I am most grateful to my supervisor Professor Oliver Penrose, (Penrose, 1979), for showing me most of the results in the next three sections.

VI. 1 Statistical mechanics of a lattice gas on the Bethe lattice

We now consider a lattice gas with fugacity z on a Bethe lattice with coordination number q . In the following for brevity, we denote an empty site by \circ , and an occupied site by \bullet .

Given a large finite Bethe lattice, we can define the following notation:

$\Xi(\circ\text{---}\times)$ is the grand partition function of the lattice gas given that a particular site on the boundary is empty;

$\Xi(\bullet\text{---}\times)$ is the grand partition function given that this site is occupied. Since this particle is on the boundary its coordination number is 1, namely it has only 1 nearest neighbour.

Similarly in $\Xi(\bullet\text{---}\times)$, both sides are given occupied, and so on.

When the fugacity is z , we can define θ to be

$$\theta = \frac{\Xi(\bullet\text{---}\times)}{z \Xi(\circ\text{---}\times)} \quad (\text{VI, 2})$$

Since in $\Xi(\circ\text{---}\times)$, the site adjacent to the left one can only be either full or empty, we can write

$$\begin{aligned}
\Xi(\circ\text{---}\times) &= \Xi(\circ\text{---}\times) + \Xi(\circ\text{---}\times) \\
&= \Xi(\circ\text{---}\times) \left[1 + \frac{\Xi(\circ\text{---}\times)}{\Xi(\circ\text{---}\times)} \right] \\
&= \Xi(\circ\text{---}\times) [1 + z\theta^{q-1}] \tag{VI, 3}
\end{aligned}$$

because the $(q-1)$ branches coming out of the right hand site are statistically independent of each other since we are using the Bethe lattice.

Similarly for $\bullet\text{---}\times$ we can write

$$\begin{aligned}
\Xi(\bullet\text{---}\times) &= \Xi(\bullet\text{---}\times) + \Xi(\bullet\text{---}\times) \\
&= \Xi(\circ\text{---}\times) \left[\frac{\Xi(\bullet\text{---}\times)}{\Xi(\circ\text{---}\times)} + \frac{\Xi(\bullet\text{---}\times)}{\Xi(\circ\text{---}\times)} \right] \\
&= \Xi(\circ\text{---}\times) [z + z^2y\theta^{q-1}] \tag{VI, 4}
\end{aligned}$$

where $y = \exp(V/kT)$ accounts for the fact that there is an attraction V between the two full sites appearing in the term $\Xi(\bullet\text{---}\times)$. If we define parameter ξ to be

$$\xi = z\theta^{q-1} \tag{VI, 5}$$

we can divide (VI, 4) by (VI, 3), and using (VI, 2) and (VI, 5), we obtain the relation

$$\theta = \frac{1 + zy\theta^{q-1}}{1 + z\theta^{q-1}} = \frac{1 + y\xi}{1 + \xi} \tag{VI, 6}$$

We will now relate θ and ξ to the density ρ of the lattice gas on the Bethe lattice. We use the fact that the density is equal to the probability that a given site is full, whereas $(1 - \rho)$ is equal to the probability that it is empty:

$$\frac{\rho}{1 - \rho} = \frac{\Xi(\bullet\text{---}\times)}{\Xi(\circ\text{---}\times)} = z\theta^q = \theta\xi \tag{VI, 7}$$

where the last two equalities follow from (VI, 4) and (VI, 5).

VI. 2 Equilibrium distribution of small clusters on the Bethe lattice.

The equilibrium distribution of small clusters on the Bethe lattice can be calculated exactly in terms of the quantities z , ρ , and ξ introduced in the previous section.

We first find c_1 , the equilibrium or steady state concentration state of monomers.

$$\text{Prob} \{ \text{the origin } O \text{ is empty} \} = 1 - \rho.$$

$$\text{Prob} \{ \text{a neighbouring site } x \text{ is empty} \mid O \text{ is empty} \}$$

$$= \frac{\Xi(\circ \text{---} \times)}{(\Xi(\circ \text{---} \times) + \Xi(\circ \text{---} \bullet))} = \frac{1}{1 + \xi}, \quad \text{using (VI, 3) and (VI, 5). Then}$$

$$\text{Prob} \{ O \text{ and its } q \text{ nearest neighbours are empty, } \begin{array}{c} \circ \\ \circ \text{---} \circ \\ \circ \end{array} \} = (1 - \rho) \left(\frac{1}{1 + \xi} \right)^q.$$

The concentration of monomers at fugacity z is then given (Lebowitz and Penrose, 1977) by

$$c_1 = z(1 - \rho) \left(\frac{1}{1 + \xi} \right)^q \quad (\text{VI, 8})$$

Similarly, one can derive the steady state concentrations c_l of l -clusters on the Bethe lattice with coordination number q . As for the monomer case, we have to find the probability that the sites on the cluster and its nearest neighbours are empty. We denote the set of sites on an l -cluster and its nearest neighbours by S_l . If one increases l by 1, the number of sites in S_{l+1} is $q - 1$ more than in S_l . It can then be easily shown by induction that the probability that S_l is empty is equal to $\frac{1 - \rho}{(1 + \xi)^{(q-1)l+1}}$. This is true for the monomer case when $l = 1$. Assuming it is true for an integer l ,

$$\text{Prob} \{ S_{l+1} \text{ is empty} \}$$

$$\begin{aligned}
&= \text{Prob}\{S_l \text{ is empty}\} \times \text{Prob}\{\text{the } q-1 \text{ extra sites in } S_{l+1} \text{ are empty} \mid S_l \text{ is empty}\} \\
&= \frac{1 - \rho}{(1 + \xi)^{(q-1)l+1}} \times \frac{1}{(1 + \xi)^{q-1}} \\
&= \frac{1 - \rho}{(1 + \xi)^{(q-1)(l+1)+1}}.
\end{aligned}$$

Therefore, this formula is valid for all l .

The concentration c_l of l -clusters at equilibrium or steady state is then given (Penrose and Lebowitz, 1977) by

$$c_l = z^l \times \text{Prob}\{S_l \text{ is empty}\} \times \text{partition function of the } l\text{-clusters},$$

which for the Bethe lattice with coordination number q becomes:

$$c_l = \left(\frac{q(q-1) [(q-1)l-1]!}{(l-1)! [(q-2)l+2]!} y^{l-1} \right) \left(\frac{1-\rho}{1+\xi} \right) \left(\frac{z}{(1+\xi)^{q-1}} \right)^l \quad (\text{VI, 9})$$

The first term in big round brackets is the partition function for the l -clusters on the Bethe lattice: the term involving factorials is (Fisher and Essam, 1961) the number of inequivalent l -clusters on the lattice, and y^{l-1} is the Boltzmann factor for the l -clusters, since these have $l-1$ bonds on the Bethe lattice. The equation (VI, 9) corresponds to the approximate equation (I, 6) for the equilibrium or steady state concentrations c_l on the simple cubic lattice.

We can now calculate the parameters ρ and c_l for $l = 1$ to 10 for the Bethe lattice with $q = 6$, and compare them with the equilibrium parameters of the simple cubic lattice. For coexistence of the two phases, by the theory of the Ising model, the fugacity z satisfies the relation

$$z = y^{-q/2} = y^{-3} \quad (\text{VI, 10})$$

We can then solve for θ using the first relation in (VI, 6), and then find ρ and ξ using (VI, 7), and c_l using (VI, 9). We also define w_s as in (I, 8) by

$$w_s = \frac{c_1}{(1-\rho)^3} \quad (\text{VI, 11})$$

The quantity ρ found in this way is the coexistence density for the Bethe lattice, and is analogous to (I, 8) which is the corresponding expression for the simple cubic lattice. In Table (VI, i), we give ρ , c_l , and w_s for three different temperatures. We also give observed values of ρ , c_l , and w_s in simulations of a lattice gas on a simple cubic lattice (Kalos et al., 1978).

Table (VI, i). Equilibrium parameters for the Bethe lattice with coordination number $q = 6$, for three different temperatures. These are compared with corresponding values from a simulation of a lattice gas on the simple cubic lattice (Kalos et al., 1978).

$\frac{V}{kT}$	1.5		1.0926		0.99438	
	0.011109		0.03771		0.050163	
z	Bethe	s. cubic	Bethe	s. cubic	Bethe	s. cubic
θ	1.0483		1.1275		1.1710	
ξ	0.014064		0.06871		0.11148	
ρ	0.014530	0.0146	0.072	0.075	0.116	0.127
c_1	0.010066	0.010126	0.02349	0.023370	0.023735	0.023002
w_s	0.010519	0.010526	0.0294	0.029837	0.0344	0.035247
c_2	0.001402	0.001382	0.005684	0.005944	0.005745	0.006060
c_3	0.000326	0.000328	0.002292	0.002582	0.002317	0.002673
c_4	0.000096	0.000102	0.001171	0.001388	0.001184	0.001621
c_5	0.000032	0.000035	0.000686	0.000870	0.000694	0.000940
c_6	0.000012	0.000013	0.000440	0.000549	0.000445	0.000716
c_7	0.000005	0.000006	0.000300	0.000395	0.000304	0.000525
c_8	0.000002	0.000002	0.000215	0.000278	0.000217	0.000459
c_9	0.000001	0	0.000159	0.000210	0.000161	0.000336
c_{10}	0	0	0.000122	0.000163	0.000123	0.000294
$\sum_1^{10} c_l$	0.014524	0.014593	0.058959	0.064709	0.059595	0.071932

In Table (VI, i), the predictions of (VI, 8) and (VI,9) are very close to the observed values of c_l on the simple cubic lattice for the lower temperature given by $V/kT = 1.5$. Besides, the sum $\sum_1^{10} l c_l$ agrees to within $\frac{1}{2}\%$ with the corresponding value observed in the simulation. Also since w_s is very well predicted for this temperature, we can define l^* exactly as for the simple cubic lattice, with $w_s = 0.010526$ and $C = 2.415$ in equation (I, 8) for $V/kT = 1.5$.

For the higher temperatures, however, the theory for the Bethe lattice underestimates c_l for $l \geq 2$. This is because in (VI, 9), the last term raised to the l 'th power is $\frac{z}{(1+\xi)^{q-1}} = c_1 \frac{1+\xi}{1-\rho} \approx c_1 \frac{1+\theta\xi}{1-\rho} = \frac{c_1}{(1-\rho)^2}$, whereas the corresponding term in (I, 6) is $w = \frac{c_1}{(1-\rho)^3}$, thus leading to a higher concentration c_l for the simple cubic lattice for the larger values of ρ . The disparity becomes more serious for higher temperatures or densities.

VI. 3 The diffusion constant on the Bethe lattice as a function of ξ .

We consider two adjacent sites α and β on the Bethe lattice with $q = 6$, with respective fugacities z_α and z_β , and local monomer concentrations, c_α and c_β . If $j_{\alpha\beta}$ is the probability per unit time that particles go from α to β , we can write down the definition of the diffusion constants D_z and D_c as

$$j_{\alpha\beta} = D_z(z_\alpha - z_\beta) = D_{c_1}(c_\alpha - c_\beta) \quad (\text{VI, 12})$$

If one lets $z_\alpha \rightarrow z_\beta$, and $c_\alpha \rightarrow c_\beta$ in this equation, we then have that

$$D_c = D_z \frac{dz}{dc_1} \quad (\text{VI, 13})$$

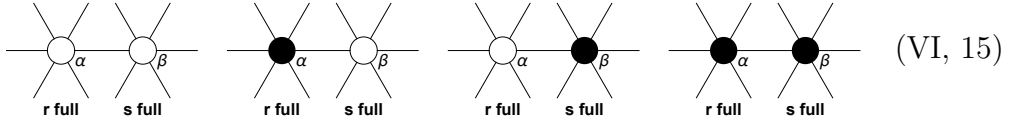
where $\frac{dz}{dc_1}$ is the variation of fugacity z with the concentration of monomers c_1 . The quantity $\frac{dz}{dc_1}$ can be obtained by logarithmic differentiation of ξ , z ,

ρ , θ and c_1 in equations (VI, 8), (VI, 5) and (VI, 6), and (VI, 7). This gives us

$$\frac{dz}{dc_1} = \left(\frac{z}{c_1}\right) \left(\frac{1 + 6\xi - 4y\xi + y\xi^2}{1 - \rho - 4y\xi - 2y\xi\rho - 5y\xi^2 - y\xi^2\rho}\right) \quad (\text{VI, 14})$$

The two equations (VI, 13) and (VI, 14) give us D_c the quantity we are interested in, provided we know D_z . We therefore calculate this quantity.

We take a general case when r neighbours of α and s neighbours of β are occupied and each of α and β can be occupied or unoccupied. These situations can be illustrated by



The probabilities of these cases are respectively in the ratio

$$\xi_\alpha^r \xi_\beta^s : z_\alpha y^r \xi_\alpha^r \xi_\beta^s : z_\beta y^s \xi_\alpha^r \xi_\beta^s : z_\alpha z_\beta y^{r+s+1} \xi_\alpha^r \xi_\beta^s \quad (\text{VI, 16})$$

The transition probabilities per unit time for a particle to go from site α to β or vice-versa for these four cases are given by

$$0, \quad \frac{p_{r-s}}{3}, \quad \frac{p_{s-r}}{3}, \quad 0 \quad (\text{VI, 17})$$

respectively, where

$$p_{r-s} = \frac{1}{1 + y^{r-s}} \quad (\text{VI, 18})$$

using (I, 1), (I, 2) and (I, 3). To find the absolute probabilities of (VI, 15), we add the four probabilities in (VI, 16), for all r and s between 0 and $q - 1 = 5$. It is easy to show, using the binomial theorem, that this normalisation constant is equal to

$$(1 + \xi_\alpha)^{q-1} (1 + \xi_\beta)^{q-1} + z_\alpha (1 + y\xi_\alpha)^{q-1} (1 + \xi_\beta)^{q-1} \\ + z_\beta (1 + \xi_\alpha)^{q-1} (1 + y\xi_\beta)^{q-1} + y z_\alpha z_\beta [(1 + y\xi_\alpha)(1 + y\xi_\beta)]^{q-1}$$

Using (VI, 6) and (VI, 5) on this expression, we obtain the normalisation constant as

$$(1 + \xi_\alpha)^{q-1}(1 + \xi_\beta)^{q-1}(1 + \xi_\alpha + \xi_\beta + y\xi_\alpha\xi_\beta) \quad (\text{VI, 19})$$

The absolute probabilities for the configurations in (VI, 15) are then given by (VI, 16)/(VI, 19). Remembering that there are $\binom{q-1}{r} \times \binom{q-1}{s}$ configurations for each case in (VI, 15), we can express $j_{\alpha\beta}$ using (VI, 16), (VI, 17), and (VI, 19) as

$$j_{\alpha\beta} = \frac{\sum_r \sum_s \binom{q-1}{r} \binom{q-1}{s} \xi_\alpha^r \xi_\beta^s (z_\alpha y^r p_{r-s} - z_\beta y^s p_{s-r})}{(1 + \xi_\alpha)^{q-1}(1 + \xi_\beta)^{q-1}(1 + \xi_\alpha + \xi_\beta + y\xi_\alpha\xi_\beta)} \quad (\text{VI, 20})$$

Since from equation (I, 1), $y^r p_{r-s} = y^s p_{s-r}$, we use the first equality in (VI, 12) and let $\xi_\alpha \rightarrow \xi_\beta$ thus obtaining the diffusion constant D_z as

$$D_z = \frac{\sum_r \sum_s \binom{q-1}{r} \binom{q-1}{s} \xi^{r+s} y^r p_{r-s}}{(1 + \xi)^{2q-2}(1 + 2\xi + y\xi^2)} \quad (\text{VI, 21})$$

For $\frac{V}{kT} = 1.5$, or equivalently $y = 4.4816$, (VI, 21) becomes

$$D_z = \frac{(0.5 + 8.176\xi + 75.07\xi^2 + 386.19\xi^3 + 1441.2\xi^4 + 3508\xi^5)}{3(1 + \xi)^{10}(1 + 2\xi + 4.4816\xi^2)} \quad (\text{VI, 22})$$

which gives D_z as a function of ξ . As $\xi \rightarrow 0$, $D_z \rightarrow \frac{1}{6}$ from (VI, 22), $\rho \rightarrow 0$ from (VI, 5) and (VI, 7), and so $\frac{dz}{dc_1} \rightarrow 1$ using (VI, 8) and (VI, 14). Equation (VI, 13) then implies that

$$D_c \rightarrow \frac{1}{6} \quad \text{as} \quad \xi \rightarrow 0 \quad (\text{VI, 23})$$

which agrees with (III, 22). This also implies that $\mu(l^*) = 6D_c$, as predicted by (VI, 1).

In Table (VI, ii), we give for various values of ξ , the corresponding quantities θ , ρ , z , c_1 , w , $\frac{dz}{dc}$, D_z and $6D_c$, which we calculate from (VI, 6), (VI, 7), (VI, 5), (VI, 8), (VI, 11), (VI, 14), (VI, 22) and (VI, 13) respectively. We also list l^* which can be obtained from c_1 via (I, 9) with $w = \frac{c_1}{(1-\rho)^3}$ where ρ in Table (VI, ii) is interpreted as the total number of small clusters during steady state. We plot $\mu(l^*) \equiv 6D_c$ against l^* in Fig. (VI, i). This graph shows that $\mu(l^*)$ is very large for small l^* , but quickly decreases to about 2 for $l^* \cong 50$. Then $\mu(l^*)$ decreases very slowly to 1 as $l^* \rightarrow \infty$, or equivalently $w \rightarrow w_s$.

Since D_z is always positive, D_c has the same sign as $\frac{dz}{dc_1}$ from (VI, 13). Whenever ξ is such that the denominator of (VI, 14) becomes 0, $\frac{dz}{dc_1}$ and D_c become infinite, and as ξ decreases, these quantities change sign. This is evident from the last two lines in Table (VI, ii) and in Fig. (VI, i). From these we see that D_c is negative for $l^* < 26$, infinite at $l^* \approx 26$, and positive for $l^* > 26$.

This confirms the predictions of Cahn (1961, 1962) that in the early stages of the time evolution of quenched alloys, the diffusion constant is negative for the earliest times when the supersaturation is high or l^* small. This phenomenon was termed spinodal decomposition, and has been observed experimentally for short times in liquid mixtures (Huang et al., 1974) and in alloys such as the B_2O_3 -PbO- Al_2O_3 system (Zarzycki J. and Naudin F., 1969) where the spinodal mechanism gives way to Ostwald ripening or coarsening within a few minutes after the quench. The infinite value of D_c therefore corresponds to a crossover between spinodal decomposition for higher values of ξ , to coarsening for the smaller values, or equivalently from small to large values of l^* .

ξ	θ	ρ	z	c_1	w	l^*	$\frac{dz}{dc}$	D_z	$\mu(l^*) \equiv 6D_c$
0.005	1.01732	0.00506	0.004588	0.04430	0.00450		1.077	0.1704	1.101
0.010	1.03447	0.01024	0.008441	0.00787	0.00812		1.170	0.1744	1.224
0.015	1.05145	0.01553	0.011670	0.01051	0.01101	151271	1.287	0.1786	1.379
0.020	1.06827	0.02092	0.014375	0.01250	0.01332	755.1	1.440	0.1829	1.581
0.025	1.08492	0.02641	0.01663	0.01396	0.01513	170.4	1.651	0.1875	1.858
0.030	1.10141	0.03199	0.01851	0.01501	0.01654	77.5	1.966	0.1922	2.267
0.035	1.11774	0.03765	0.02005	0.01571	0.01762	48.0	2.494	0.1971	2.950
0.040	1.13391	0.04339	0.02134	0.01613	0.01843	35.3	3.589	0.2021	4.352
0.045	1.14993	0.04920	0.02238	0.01634	0.01901	28.9	7.344	0.2073	9.135
0.05	1.16580	0.05508	0.02322	0.01637	0.01941	25.4	-28.5	0.2127	-36.34

Table (VI, ii). Parameters on the Bethe lattice in terms of ξ at steady state at temperature corresponding to $V/kT = 1.5$, or equivalently $y = 4.4816$.

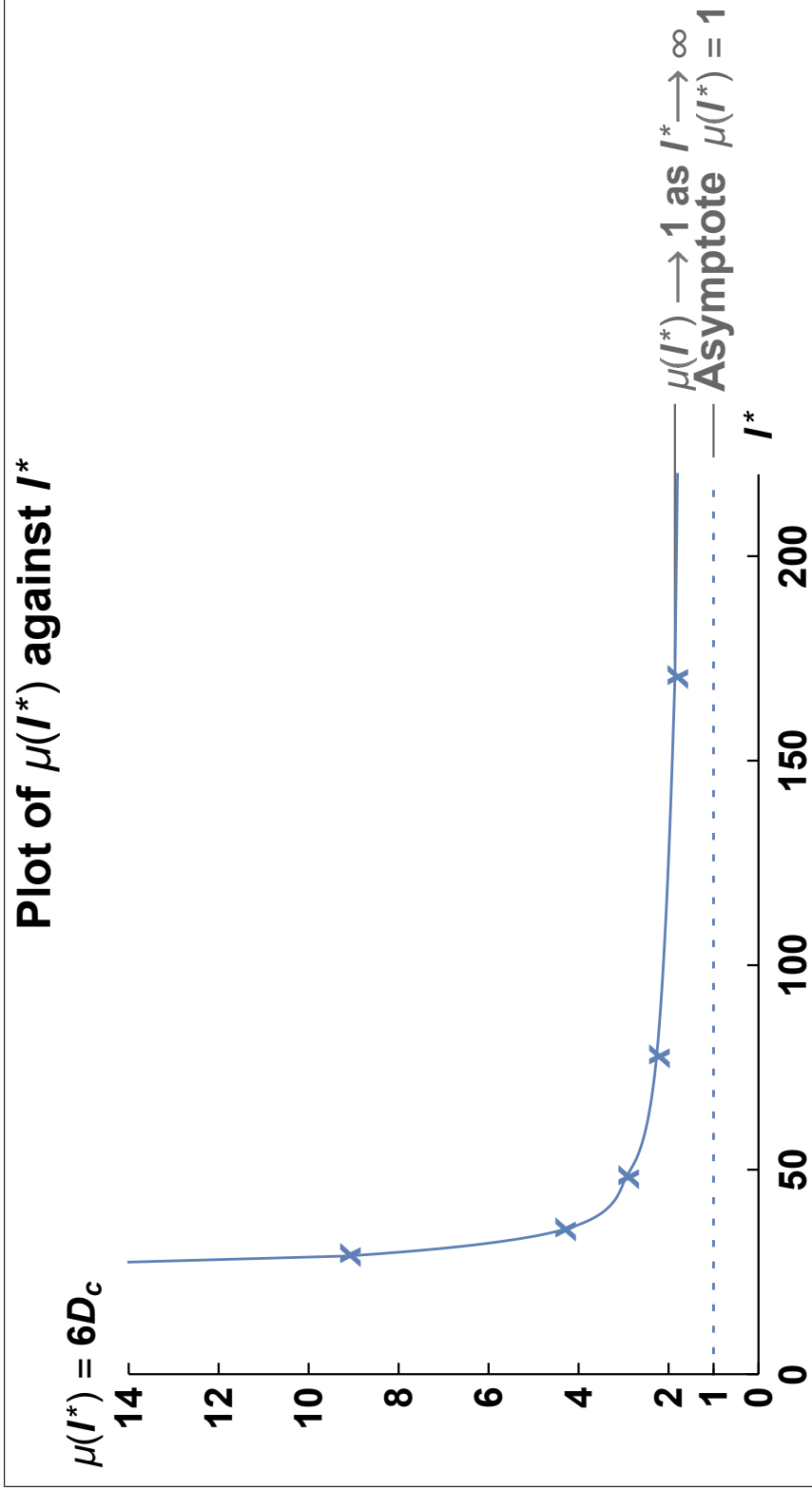


Fig. (VI, i). Graph of $\mu(I^*)$ against I^* . The quantity $\mu(I^*)$ is effectively constant and ≈ 2 in the range $50 \leq I^* \leq 200$.

For large I^* , $\mu(I^*) \rightarrow 1$. In this plot, $V/kT = 1.5$

VI. 4 Comparison of l_{de}^* and l_{sim}^* at the same value of simulation time t .

Since we know $\mu(l^*)$ as a function of c_1 , or equivalently l^* , we can find the simulation time t ($\equiv t_{sim}$) corresponding to the differential equation time t_{de} using equation (V, 2). We plot a graph of $1/(6D_c)$ against t_{de} for the densities $\rho = 0.05, 0.075$ and 0.10 in Fig. (VI, ii). The area bounded by this graph, the ordinate t_{de} , and the t_{de} -axis gives the required simulation time t corresponding to t_{de} . This graph is done by first noting the value of l_{de}^* at t_{de} from the computer solution of the differential equations, l^* being defined by (I, 9) with $w = c_1(1 - \rho)^{-3}$, where ρ is the overall density. We then find the value of $1/(6D_c)$ at $l^* = l_{de}^*$ from Fig. (VI, i). In Table (VI, iii), we give for these three densities t_{de} , $l_{de}^*(t_{de})$, the simulation time t ($\equiv t_{sim}$) corresponding to t_{de} and $l_{sim}^*(t_{sim})$. We then plot these values of l_{de}^* and l_{sim}^* on the same graph against simulation time t . This is done in the figures Fig. (VI, iii), Fig. (VI, iv) and Fig. (VI, v) for densities $\rho = 0.05, 0.075$ and 0.10 respectively.

The integration (V, 2) for the simulation time t was done graphically from Fig. (VI, ii). For negative values, of D_c , we took $1/(6D_c)$ to be zero because D_c is very large when it is negative. Besides, D_c is negative only for a short time initially.

It can be seen for all densities, that l_{de}^* and l_{sim}^* increase very quickly from 2 to about 30 over the simulation time range $0 \leq t \leq 300$. Then l^* increases more slowly after that, and reaches 200 at about $t = 6000$. As we saw in the previous section, this very large increase in l^* initially is due to the fact that the diffusion constant is infinite at $l^* \approx 30$, and then

changes sign and becomes positive for larger values of l^* . We therefore have spinodal decomposition over the (simulation) time range $0 \leq t \leq 300$ for all three densities, and after that there is a crossover to the slower coarsening mechanism with positive D_c .

In the following discussion, t and t_{sim} are synonymous, and both denote the simulation time.

For $\rho = 0.05$, $l_{de}^*(t)$ and $l_{sim}^*(t)$ agree very well with each other over the whole time range considered $0 \leq t \leq 7000$, as can be seen from Table (VI, iii) and Fig. (VI, iii). It can be seen that both $l_{de}^*(t)$ and $l_{sim}^*(t)$ grow slowly at first over the range $300 \leq t \leq 4000$. After that l^* is approximately linear in t for $t \geq 4000$. In fact for this time range we can write for both l^* 's:

$$l^*(t) \cong -81 + 0.035t \quad 4000 \leq t \leq 7000, \quad \rho = 0.05 \quad (\text{VI, 24})$$

Graphs of $l_{de}^*(t)$ and $l_{sim}^*(t)$ against t are also plotted for higher densities: for $\rho = 0.075$ in Fig. (VI, iv), and for $\rho = 0.10$ in Fig. (VI, v). For these higher densities, however, l_{de}^* and l_{sim}^* do not agree so well together. Both l_{de}^* and l_{sim}^* are both approximately linear over practically the whole time range, $300 \leq t \leq 7000$, except for the very initial stages. However the rate of growth of l_{de}^* is smaller than that of l_{sim}^* . In fact we can write:

$$\begin{aligned} l_{sim}^*(t) &\cong 0.038t, & l_{de}^*(t) &\cong 20 + 0.028t \\ \text{for } 300 \leq t \leq 7000, & \text{ for density } \rho = 0.075 & & (\text{VI, 25}) \end{aligned}$$

and similarly

$$\begin{aligned} l_{sim}^*(t) &\cong 30 + 0.030t, & l_{de}^*(t) &\cong 34 + 0.024t \\ \text{for } 300 \leq t \leq 7000, & \text{ for density } \rho = 0.10 & & (\text{VI, 26}) \end{aligned}$$

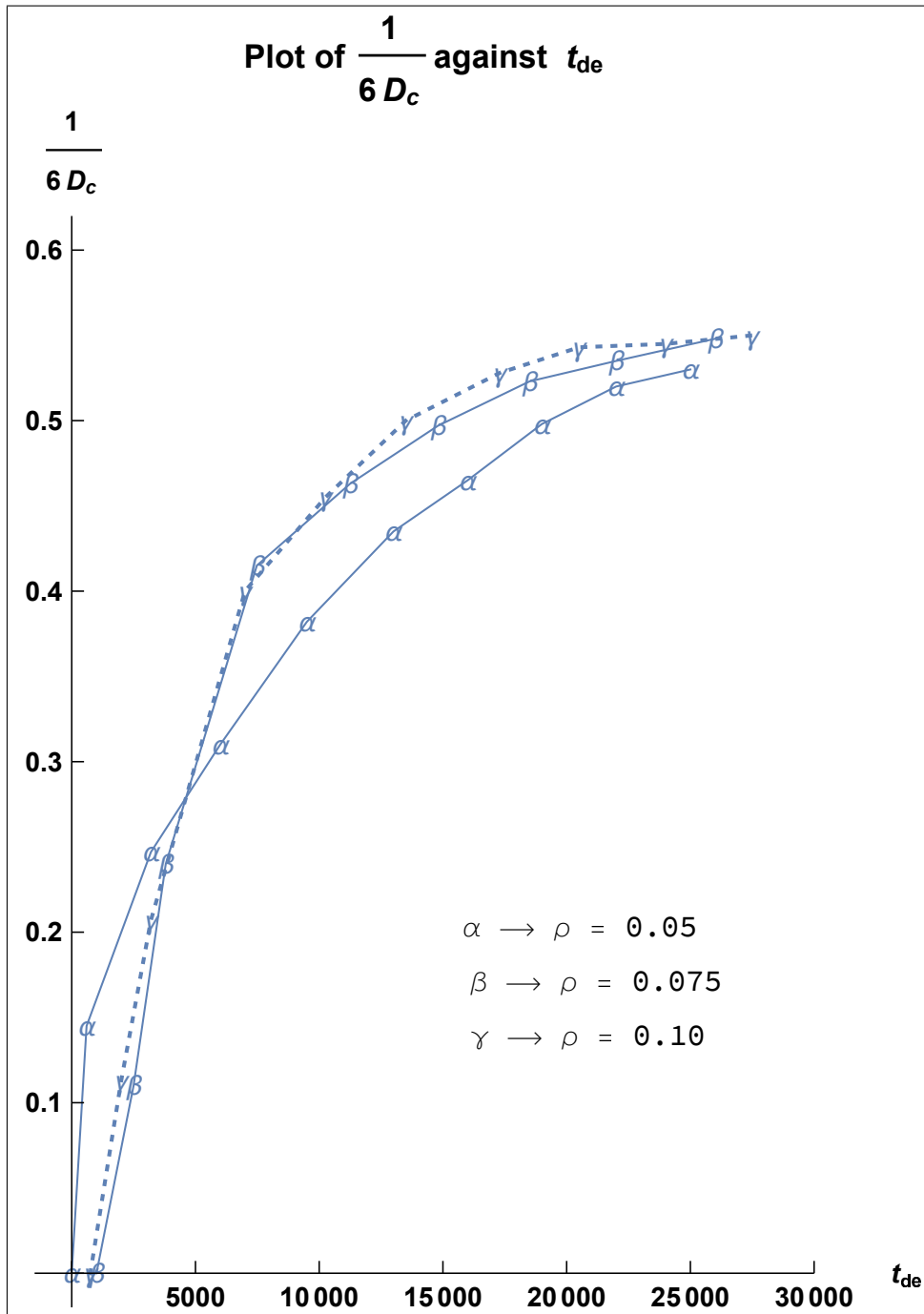


Fig. (VI, ii). Graph of $\frac{1}{6D_c}$ against t_{de} . The area under this graph up to t_{de} gives the simulation time t according to the theory in this chapter. Graphs for densities $\rho = 0.05$ (α), 0.075 (β), 0.10 (γ).

Table (VI, iii). Comparison of l_{de}^* and l_{sim}^* corresponding to the same simulation time t , where $t \equiv t_{sim}$.

ρ	t_{de}	$l_{de}^*(t_{de})$	$t \equiv t_{sim}$	$l_{sim}^*(t_{sim})$
0.05	3150	39	560	43
	6300	47	1440	47
	9500	57	2520	52
	12600	73	3800	68
	15800	104	5200	100
	18900	153	6740	156
0.075	3400	37	290	30
	6800	59	1340	55
	10200	99	2800	98
	13600	144	4430	164
	17100	185	6180	204
0.01	3700	38	315	35
	7400	72	1565	75
	11100	112	3195	124
	14800	146	4985	175
	18500	180	6885	230
	20300	198	7876	235

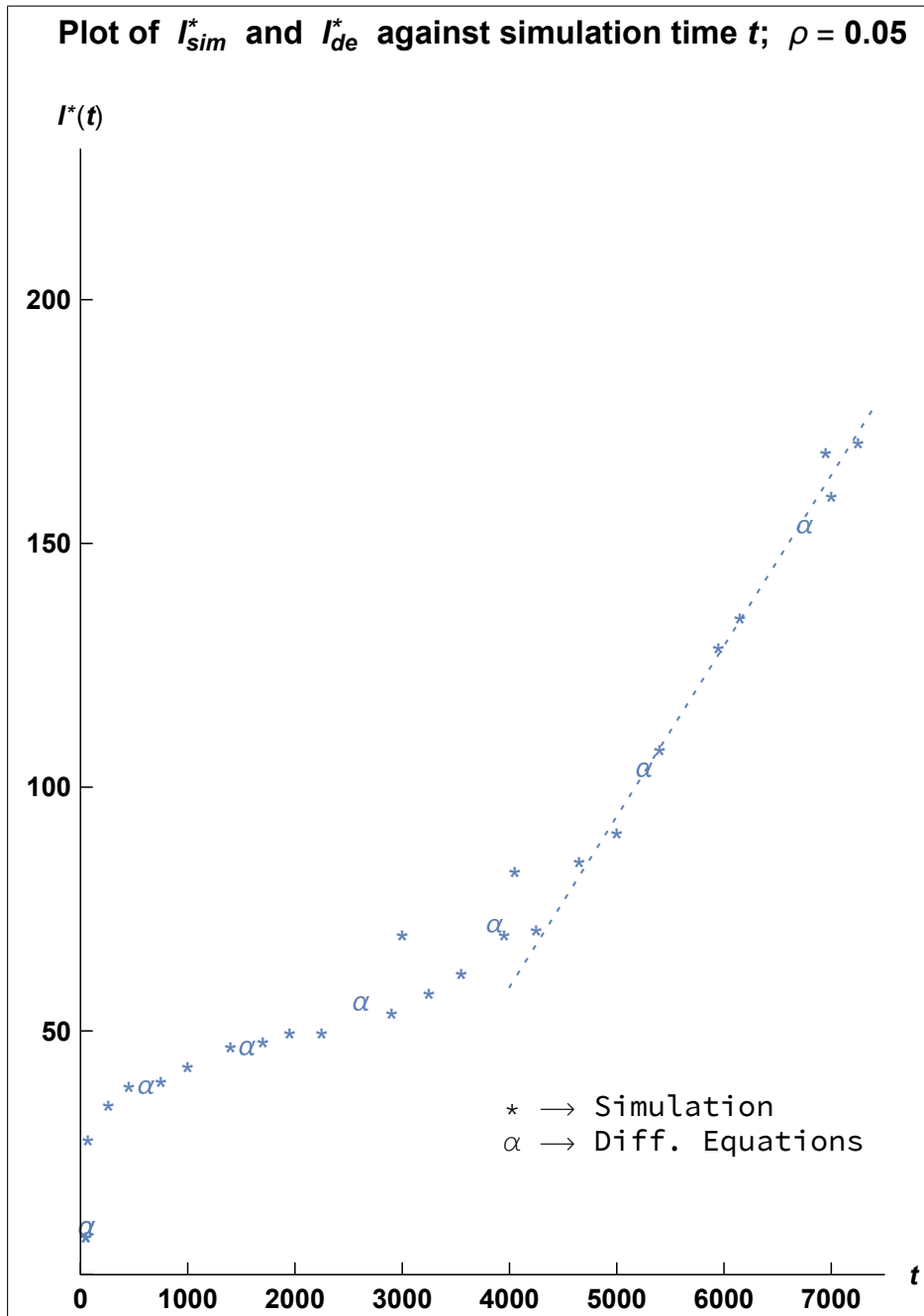


Fig. (VI, iii). Graph of l_{sim}^* and l_{de}^* against simulation time t ($\equiv t_{sim}$) for density $\rho = 0.05$. After $t = 4000$, both l_{sim}^* and l_{de}^* satisfy $l^* \cong 0.035t - 81$.

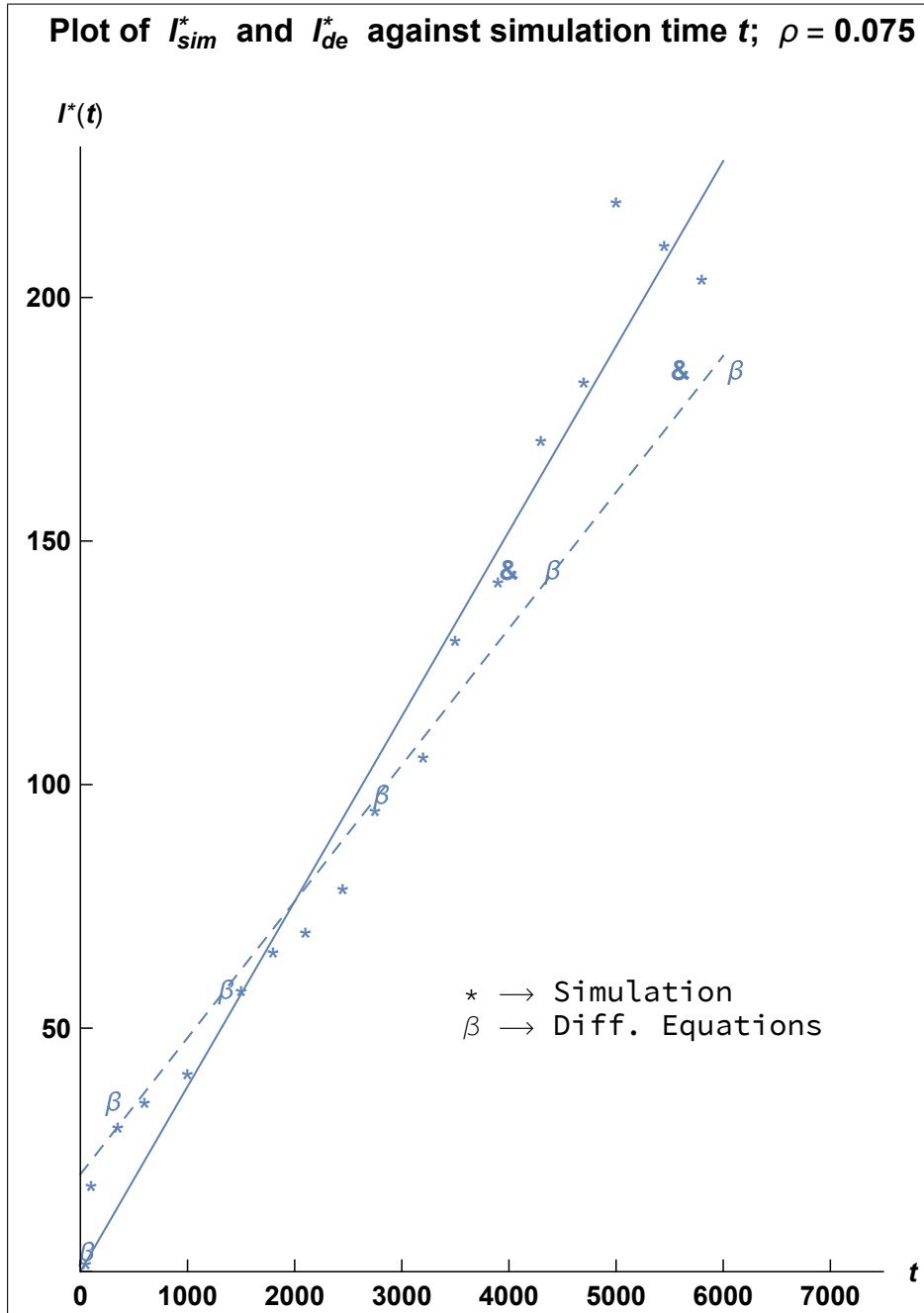


Fig. (VI, iv). Graph of l_{sim}^* and l_{de}^* against simulation time t ($\equiv t_{sim}$) for density $\rho = 0.075$. For $t \geq 0$, $l_{sim}^*(t) \cong 0.038t$ (the full line), whilst $l_{de}^*(t) \approx 20 + 0.028t$ (the dashed line). The two $\&$ points are β points, but using ρ_{20} rather than c_1 to calculate l_{sim}^* and l_{de}^* . (See text).

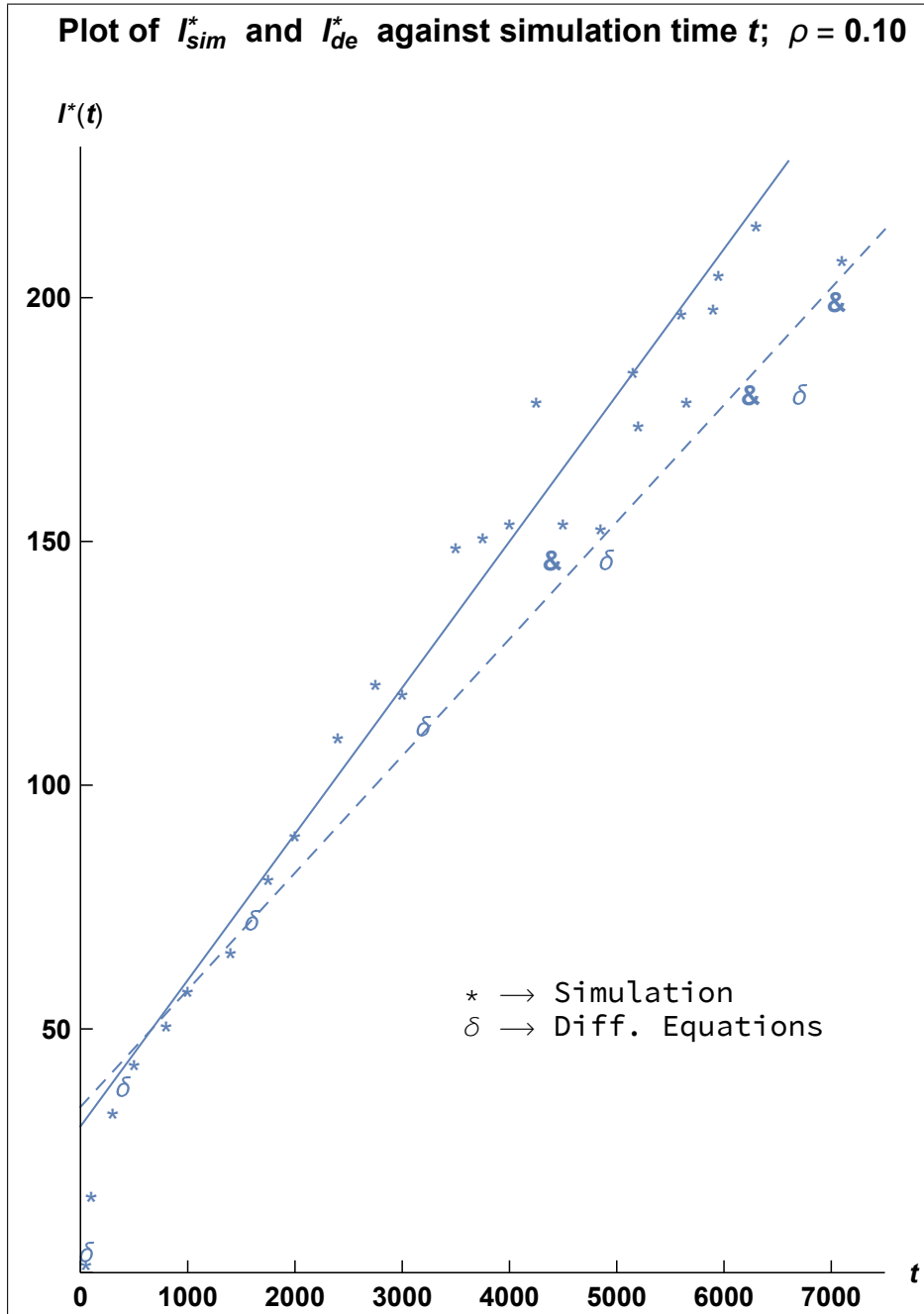


Fig. (VI, v). Graph of l_{sim}^* and l_{de}^* against simulation time t ($\equiv t_{sim}$) for density $\rho = 0.10$. For $t \geq 0$, $l_{sim}^*(t) \approx 30 + 0.030t$ (the full line), whilst $l_{de}^*(t) \approx 34 + 0.024t$ (the dashed line). The three $\&$ points are δ points, but using ρ_{20} rather than c_1 to calculate l_{sim}^* and l_{de}^* . (See text).

In the theory of coarsening, it has been assumed (Lifshitz and Slyozov, 1961) that $l_{de}^*(t_{de})$ should be linear in t_{de} asymptotically. Since t ($\equiv t_{sim}$) is related to t_{de} via $\mu(l^*)$ in (V, 2) and since $\mu(l^*)$ is approximately constant from Fig. (V, i) and Fig. (VI, i) over most of the considered time range, we expect $l^*(t)$ to be linear in t also for large t . The three equations (VI, 24), (VI, 25) and (VI, 26) therefore show that the Lifshitz-Slyozov assumption is valid also at early times.

It can be noticed from Fig. (VI, iv) and Fig. (VI, v) that l_{de}^* underestimates l_{sim}^* for $t \gtrsim 4000$ for the higher densities. A possible reason for the observed discrepancy in l^* is that for fixed c_1 , c_l in the Bethe lattice is $(1 - \rho)^l$ smaller than c_l for the simple cubic lattice, as we pointed out towards the end of Section VI. 3. To take this into account, we used ρ_{20} instead of c_1 for calculating l_{de}^* and l_{sim}^* . We can then consider $6D_c$ as a function of ρ_{20} . Doing this leads to improved values of l_{de}^* for the larger times for $\rho = 0.075$ and 0.10. These values are shown as & in Fig. (VI, iv) and Fig. (VI, v).

One must also recall that the effect of coagulation of large clusters increases the higher the density. It has been estimated (Penrose et al., 1978) that coagulation between large clusters increases the number of particles in the large clusters by about one quarter the number of particles per site in the large clusters. This phenomenon becomes more important for higher densities (Lebowitz et al., 1976).

To obtain an average value of $\mu(l^*)$ as predicted by this theory, we plot t_{de} against $t_{sim}(\equiv t)$ as given in Table (VI, iii). This graph is given in Fig. (VI, vi). From this we see that this curve is approximately linear, and hence $\mu(l^*)$ is approximately constant. Analogously to (V, 3), we can write:

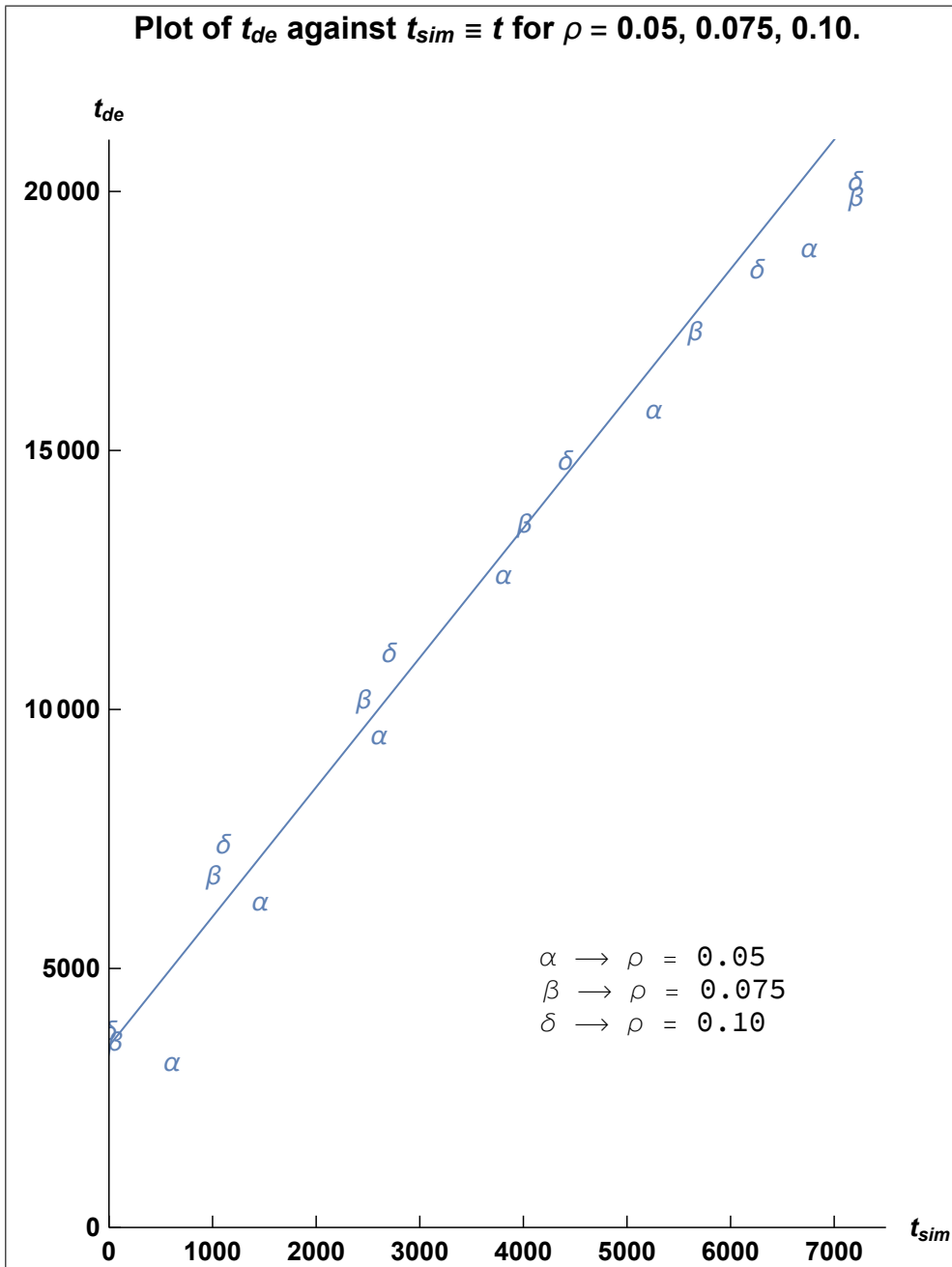


Fig. (VI, vi). Graph of t_{de} against simulation time t_{sim} ($\equiv t$), as predicted by the theory in this chapter, for densities $\rho = 0.05, 0.075$ and 0.10 . All three cases are approximated by the straight line, $t_{de} = \mu(l^*)(t_{sim} + t_0)$, with average slope $\mu(l^*) \cong 2.5$ and $t_0 \cong 1400$. Compare with Fig (V,i) and (V,3).

$$t_{de} = \mu(l^*)(t_{sim} + t_0) \quad (\text{VI, 27})$$

where $\mu(l^*) \cong 2.5$, $t_0 \cong 1400$ for densities $\rho = 0.05, 0.075$ and 0.10 . As in (V, 3), $\mu(l^*)$ is approximately constant over $0 \leq t \leq 7000$. The average slope is smaller and the intercept bigger in this case than in (V, 3). The intercept t_0 arises because of the presence of spinodal decomposition since l^* increases very rapidly in this regime.

The main conclusions we draw from this chapter are the following:

- For $\rho = 0.05$, $l_{de}^*(t)$ and $l_{sim}^*(t)$ are quite close to each other for $0 \leq t \leq 7000$, and are linear in time for $4000 \lesssim t \lesssim 7000$. The growth rates are also very similar on this time range. See equation (VI, 24) and Fig. (VI, iii).
- For the higher densities, $\rho = 0.075$ and 0.10 , the agreement is less satisfactory. $l_{de}^*(t)$ tends to underestimate $l_{sim}^*(t)$ after $t \gtrsim 4000$. Both quantities are approximately linear in time over the whole time range, $0 \leq t \leq 7000$, implying that the Lifshitz-Slyozov coarsening mechanism starts early, soon after spinodal decomposition has taken place. However the rate of growth of $l_{de}^*(t)$ underestimates that of $l_{sim}^*(t)$ by about 30%. See equations (VI, 25), (VI, 26) and Figs. (VI, iv) and (VI, v).
- For each density, $\mu(l^*)$ is approximately constant over the whole time range considered, except perhaps for the earliest times, in the regime of spinodal decomposition.

Chapter VII: Comparison of the Becker-Döring Equations with the Lifshitz-Slyozov Theory and with Real Alloys.

The purpose of this chapter is to compare the predictions of our differential equations with those of the theory of Lifshitz and Slyozov (1961), and with the cluster distribution observed in real alloys such as Ni-Al (Ardell and Nicholson, 1966).

VII. 1 Reduction of the Becker-Döring equations to (I, 13).

It has been shown (Penrose et al, 1978) that the Becker-Döring equations as described in Chapter II, can be reduced to an equation similar to (I, 13), which describes the rate of growth of droplets of size l with time. For large l and t , we can assume that the scale of variation of c_l is l^* , so that $1 - \frac{c_{l-1}}{c_l}$ has the order of magnitude of $1/l^*$. If we assume l^* itself is large, we can approximate the Becker-Döring equations by the partial differential equation (op. cit.)

$$\frac{\partial c(l, t)}{\partial t} = A \frac{\partial}{\partial l} \left[\left(\frac{l}{l^*} \right)^{1/3} - 1 \right] c(l, t) \quad (\text{VII, 1})$$

where A is the coefficient of $\left(\frac{l}{l^*} \right)^{1/3}$ in the quantity $a_l c_l c_1$. Here we use (II, 7) and the asymptotic formulae (III, 24) and (III, 25) to substitute for $a_l(0)$, and write c_1 in terms of l^* using $w = c_1/(1 - \rho)^3$ in (I, 9). Then A can be written explicitly as

$$A = \mu(l^*) \frac{p_0}{3} N^{1/3} w_s (1 - \rho)^3 \quad (\text{VII, 2})$$

Since $\mu(l^*)$ was shown to be approximately constant over most of the time range in both simulation and differential equations in Fig.(V, i) and

Fig. (VI, vi), we can consider A to be constant. In equation (VII, 1) we assume that $c(l, t)$ is a smooth function of continuous variables, chosen such that $c(l, t) = c_l(t)$ when l is an integer.

Equation (VII, 1) is only valid when l and l^* are both large. For small l , the small clusters obey the steady state distribution (I, 6). We can therefore introduce a size L so that clusters larger than this size are considered to be large and to obey (VII, 1), whereas clusters smaller than this size are considered small and obey (I, 6). The conservation of mass condition can then be written as

$$\rho_L(w) + \int_L^\infty lc(l, t) dl = \rho = \text{constant} \quad (\text{VII, 3})$$

where $\rho_L(w)$ was defined in (I, 8). The value of L therefore should satisfy the inequality $1 \ll L < l^*$. The latter inequality follows because the steady state formula (I, 6) does not apply to clusters larger than l^* . Then $\rho_L(w)$ signifies the number of particles in the small clusters at supersaturation w , which can be expressed in terms of l^* from (I, 9). In the integral in (VII, 3), $c(l, t)$ is given by (VII, 1). The quantity l^* therefore controls both $\rho_L(w)$ and the integral in (VII, 3). Lifshitz and Slyozov treat l as a continuous variable from the beginning and do not distinguish between w and the density of the vapour, $\rho_L(w)$. Instead of (VII, 3), therefore, they took the simpler equation

$$w + \int_L^\infty lc(l, t) dl = \rho$$

The quantity l^* was found in Chapters V and VI to be linear both in the simulation and in the differential equations, so that we can write in general

$$l^* = K(t + t_1) \quad (\text{VII, 4})$$

where K and t_1 are constants independent of time. Since l^* is such an important quantity in this theory, we change variables from t to l^* in equation

(VII, 1), as was done in Penrose (1978). Using (VII, 4), (VII, 1) can be solved by the method of characteristics after this further substitution

$$g(l, l^*) = \int_l^\infty c(\lambda, l^*) d\lambda \quad (\text{VII, 5})$$

The function $g(l, l^*)$ stands for the total number per lattice site of clusters larger than l at a certain value of l^* . The new equation can then be written

$$\frac{\partial g(l, l^*)}{\partial l^*} + \frac{A}{K} \frac{\partial}{\partial l} \left[\left(\frac{l}{l^*} \right)^{1/3} - 1 \right] \frac{\partial g(l, l^*)}{\partial l} = 0 \quad (\text{VII, 6})$$

The characteristics of (VII, 6) are the solutions of

$$\frac{dl}{dl^*} = \frac{A}{K} \left[\left(\frac{l}{l^*} \right)^{1/3} - 1 \right] \quad (\text{VII, 7})$$

This formula is identical to (I, 13) with $\bar{l} \equiv l^*$ and $A \equiv 4\pi D\alpha$. From (VII, 7), treating l^* as linearly increasing in t , clusters of size greater than l^* tend to grow, whereas clusters smaller than l^* tend to shrink. The solution f of (VII, 7), denoting the natural logarithm by \ln , is

$$f \equiv \ln(l^*) + \phi\left(\frac{l}{l^*}\right) = \text{constant} \quad (\text{VII, 8})$$

where

$$\phi(x) = \int_0^x \frac{dy}{y + \frac{A}{K}(1 - y^{1/3})} \quad (\text{VII, 9})$$

The general solution of (VII, 6) is therefore

$$g(l, l^*) = \psi\left(\ln(l^*) + \phi\left(\frac{l}{l^*}\right)\right) \quad (\text{VII, 10})$$

where ψ is an arbitrary function.

VII. 2 Comparison of A , K , A/K for simulation and differential equations.

We can check the validity of (VII, 10) by plotting $g(l, l^*)$ against the argument $f \equiv \ln(l^*) + \phi\left(\frac{l}{l^*}\right)$. We do this in Fig. (VII, i) for $\rho = 0.075$ for the range $50 < l^* < 200$. If (VII, 10) is correct, plots of $g(l, l^*)$ against this argument for various values of l^* , or time t , will all lie on one curve. This is indeed the case when one takes A/K to be 4.0, the value obtained by the ‘table’ method described in Penrose et al. (1978). In Fig. (VII, i), we give these plots for our differential equations, and also for the simulation for various values of l^* . On the same graph, we plot ψ from Table VII in the same paper. We must bear in mind, however, that the function ψ is not defined the same as ours, and in fact it can be shown that our argument, $\ln(l^*) + \phi\left(\frac{l}{l^*}\right)$, is equal to the argument in this cited paper, $\ln(t) + \phi\left(\frac{l}{t}\right)$, diminished by 3.33. As is to be expected, this curve is an average of the coordinates for the simulation. The differential equation curve is always very near this curve, the error being at worst 15%.

We now compare the quantities A , K , A/K with the same quantities obtained from the simulation. Taking a mean value of $\mu(l^*)$ to be about 2.5 from (VI, 27) in the expression (VII, 2) for A , and using the value $K = 0.028$ given in (VI, 25) for the differential equations for density $\rho = 0.075$, will give

$$A = 0.11, \quad K = 0.028, \quad A/K = 3.94 \quad (\text{VII, 11})$$

as compared with the simulation values (op. cit.)

$$A = 0.15, \quad K = 0.038, \quad A/K = 3.97 \quad (\text{VII, 12})$$

It can be seen from Fig. (VII, i), that there are certain consistent differences

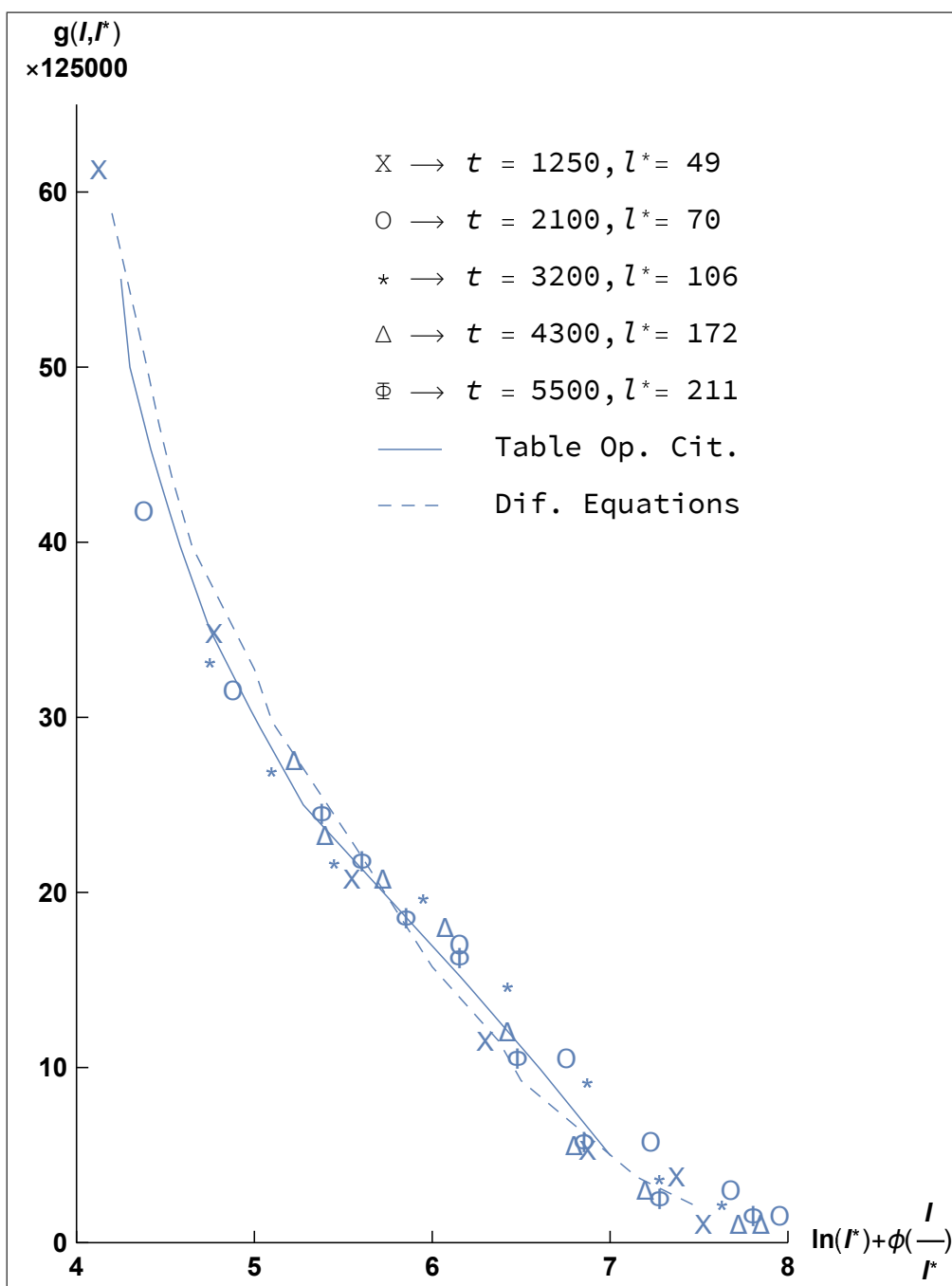


Fig. (VII, i). Graph of $g(l, l^*)$ against $\ln(l^*) + \phi\left(\frac{l}{l^*}\right)$ for the simulation at various (simulation) values of l^* , and for the differential equations. The constant A/K is taken to be 4.0. This is a 'universal' curve independent of the value of l^* . $\rho = 0.075$.

between the simulation curve and the differential equation curve. The simulation curve has a point of inflexion at $f \equiv \ln(l^*) + \phi\left(\frac{l}{l^*}\right) = 5.8$ and the curves intersect at this point approximately. The slopes are appreciably different at this point of inflexion. The slope of these curves are important because the concentrations c_l at a certain value of l^* can be obtained by differentiating (VII, 5):

$$c(l, l^*) = -\frac{\partial}{\partial l}g(l, l^*) = -\frac{\partial g}{\partial f} \frac{\partial f}{\partial l} = -\frac{\partial g}{\partial f} \frac{1}{l + \frac{A}{K}l^* - \frac{A}{K}l^{*2/3}l^{1/3}} \quad (\text{VII, 13})$$

Equation (VII, 13) implies that since A/K is the same in both simulation and differential equations, $c_l \equiv c(l, l^*)$ is proportional to $\frac{\partial g}{\partial f}$, which is the slope of the curves in Fig. (VII, i). We therefore find the slopes of the simulation and the differential equation curves in Fig. (VII, i) and plot them against the quantity $f \equiv \ln(l^*) + \phi\left(\frac{l}{l^*}\right)$ in Fig. (VII, ii). This graph gives us a summary of how well the differential equations predict c_l for the simulation, when the value of l^* is the same in both. It can be seen from Fig. (VII, ii) that the agreement is reasonably good, apart from the significant minimum in the simulation curve, which we plot as a histogram. This minimum features also in the simulation histograms for $\rho = 0.075$ in the relevant plots in Fig. (V, ii).

The function ψ in (VII, 10) can be found explicitly as a function of the argument $f \equiv \ln(l^*) + \phi\left(\frac{l}{l^*}\right)$. This is done in a way similar to that employed in Penrose et al. (1978), but using l^* instead of t . Essentially, this implies treating $\rho - \rho_L(w)$ in (VII, 3) as a function of l^* using the steady state distribution of small clusters (I, 6) and equation (I, 8) which gives w in terms of l^* . Thus $\rho - \rho_L(w)$ can be accurately approximated by a polynomial in $\frac{1}{l^{*1/3}}$. For $\rho = 0.075$, this polynomial is analogous to equation (41) in this

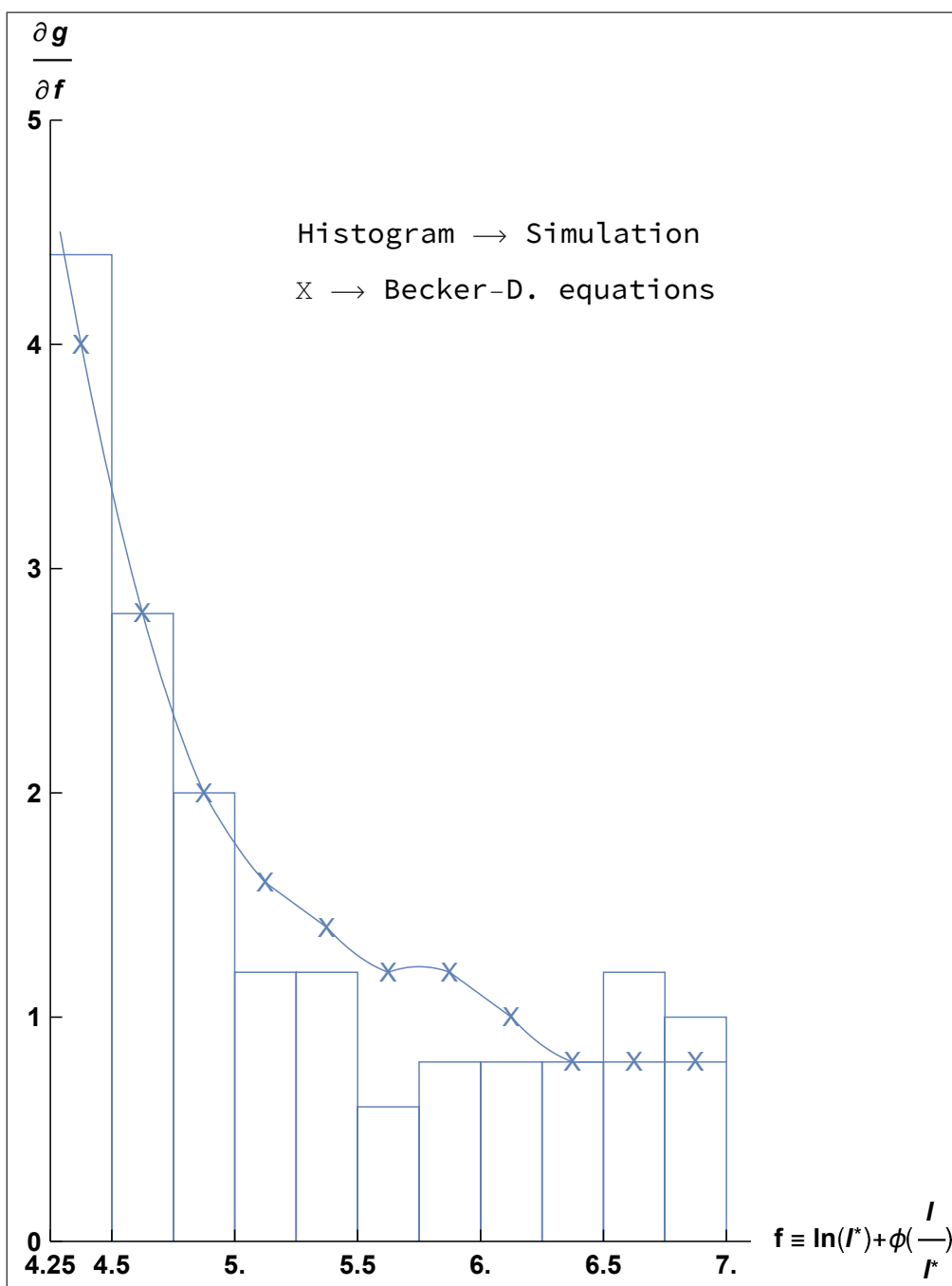


Fig. (VII, ii). Graph of $\frac{\partial g}{\partial f}$ against $f \equiv \ln(l^*) + \phi\left(\frac{l}{l^*}\right)$ for the simulation and the Becker-Döring equations. For a given value of A/K , the concentrations $c(l, l^*)$ are proportional to $\frac{\partial g}{\partial f}$, which is the slope of the previous graph. $\rho = 0.075$.

cited work, and is given by:

$$\rho - \rho_{20}(w) = 0.06316 - \frac{0.02859}{l^* 1/3} - \frac{0.18686}{l^* 2/3} \quad (\text{VII, 14})$$

The integral in the conservation of mass condition (VII, 3) can be integrated by parts using the fact that $c_l = -\frac{\partial g_l}{\partial l}$. In fact it can be shown (op. cit.) that to an accuracy of $\frac{1}{l^* 1/3}$, we can write (VII, 3) as

$$\rho - \rho_L(w) = \int_0^\infty \psi \left(\ln(l^*) + \phi \left(\frac{l}{l^*} \right) \right) dl \quad (\text{VII, 15})$$

Since $\rho - \rho_L(w)$ approaches the constant $\rho - \rho_L(w_s)$ for large times, it can be argued that the integral on the right is essentially independent of t , and hence that $\psi(f)$ is proportional to e^{-f} . For the times considered, however, ρ_{20} is still varying appreciably and so one assumes that $\psi(f)$ is given approximately by (op. cit.)

$$\psi(f) = c_0 e^{-f} - c_1 e^{-4f/3} - c_2 e^{-5f/3} \quad (\text{VII, 16})$$

Substituting (VII, 14) in the left hand side of (VII, 15), and (VII, 16) in the right hand side of (VII, 15), one can obtain the constants c_0 , c_1 and c_2 as

$$c_0 = \frac{0.06316}{\int_0^\infty e^{-\phi(x)} dx}, \quad c_1 = \frac{0.02859}{\int_0^\infty e^{-4/3 \phi(x)} dx}, \quad c_2 = \frac{0.18686}{\int_0^\infty e^{-5/3 \phi(x)} dx} \quad (\text{VII, 17})$$

We integrated $e^{-\phi(x)}$ by Simpson's Rule using (VII, 9) with $A/K = 4$. The range from 0 to ∞ in (VII, 17) was replaced by the range $0 \leq x \equiv \frac{l}{l^*} \leq 5$, because there were no clusters of size $l > 5l^*$. We then obtain for $\psi(f)$ the formula

$$g(l, l^*) = \psi(f) = 0.05134e^{-f} - 0.02947e^{-4f/3} - 0.2307e^{-5f/3} \quad (\text{VII, 18})$$

This holds approximately for both simulation and differential equations because A/K is the same in both. In Table (VII, i), we compare the prediction of (VII, 18) with the simulation values of g given in Table VII, (op. cit.), remembering that x as defined in this table is equal to $f + 3.33$. The agreement is better than 15% over most of the range of x or f .

Table (VII, i). Comparison of our equation (VII, 18) with simulation values of g obtained from Table VII from Penrose et al. (1978).

x	12500 ψ_{sim} from Table VII (op.cit.)	$f = x - 3.33$	125000 $\psi(f)$ from (VII, 18)
7.54	55	4.21	56.0
7.65	50	4.32	52.2
7.76	45	4.43	48.5
7.91	40	4.58	43.6
8.09	35	4.76	38.2
8.32	30	4.99	31.9
8.61	25	5.28	25.1
9.04	20	5.71	17.3
9.51	15	6.18	11.4
9.92	10	6.59	7.80
10.31	5	6.98	5.38

VII. 3 Comparison of the cluster size distribution predicted by our equations with that of real alloys.

In this section, we compare the predictions of the Becker-Döring equations and of the Lifshitz-Slyozov theory with the cluster distribution in real alloys (Ardell, 1966; Pedder 1978).

It was found in the previous section that the dimensionless constant A/K is very well predicted by the differential equations, and that its value is about 4.0. This differs from the value predicted by Lifshitz and Slyozov. They predict that the denominator in (VII, 9) must have a double zero, which would imply that A/K is 6.75, which is considerably greater than our estimate of 4.0. For this value of $A/K = 6.75$, the Lifshitz-Slyozov distribution has an explicit formula (Wagner, 1961 and Ardell, 1969). If $r = \left(\frac{l}{l^*}\right)^{1/3}$, then the Lifshitz-Slyozov distribution $d(r)$ is given explicitly by

$$\begin{cases} d(r) \propto r^2 \left(\frac{3}{3+r}\right)^{7/3} \left(\frac{3}{3-2r}\right)^{11/3} \exp\left(\frac{-2r}{3-2r}\right) & \text{for } r \leq \frac{3}{2} \\ d(r) = 0 & \text{for } r > \frac{3}{2} \end{cases} \quad (\text{VII, 19})$$

The cluster size distribution for several Ni-Al alloys was extensively studied by Ardell and Nicholson (Ardell, 1966). They considered alloys with different Al content: 6.35% Al, which was quenched to 625°C, and 6.71% Al quenched to 750°C and 775°C. The cluster size distribution was found at different times after the quench. A series of histograms is presented in Fig. 6 of their paper. The abscissa in their histograms is taken to be $\left(\frac{l}{l^*}\right)^{1/3}$, and the area under the curve is proportional to the total number of clusters.

In Fig. (VII, iii), therefore, we plot $l^{*1/3}l^{2/3}c_l$ against $\left(\frac{l}{l^*}\right)^{1/3}$ for the differential equations at density $\rho = 0.075$ for various values of l^* . The area under such a graph also gives the total number of clusters. A continuous curve is then plotted through these points to get an ‘average’ distribution for the differential equations (BD in the graph). On the same graphs, we superimpose the Lifshitz-Slyozov distribution (LS in the graph) and points from three histograms in Fig. 6 of Ardell (Ardell, 1966). Since we are now more interested in the shape of the distribution rather than the actual concentrations c_l , we adjust the scales so that all ordinates at $l = l^*$ in Fig. (VII, iii) are equal to 1.

It can be seen that the distribution predicted by the Becker-Döring equations fits the alloy data very well. This distribution is broader than that predicted by Lifshitz and Slyozov, which is more highly peaked, and which predicts no clusters with $\left(\frac{l}{l^*}\right)^{1/3} \geq 3/2$. Besides, our distribution is quite accurate for $l < l^*$.

Our distribution also models successfully the coarsening of isoamylalcohol droplets in water. This coarsening was studied by Kahlweit (Kahlweit, 1963). The distribution of droplet sizes of the alcohol is shown in Fig. 7 of Ardell (Ardell, 1966). The distribution is broader than that predicted by Lifshitz and Slyozov, and is much nearer to our distribution.

Fig. (VII, iii) shows that the smaller A/K is, the broader the distribution is. This discrepancy in the value of A/K is probably due to the fact that we take the number of particles in the small clusters to be given by the w -formula (I, 8), whereas Lifshitz and Slyozov take this to be equal to w . It is also important to note that A/K is independent of $\mu(l^*)$.

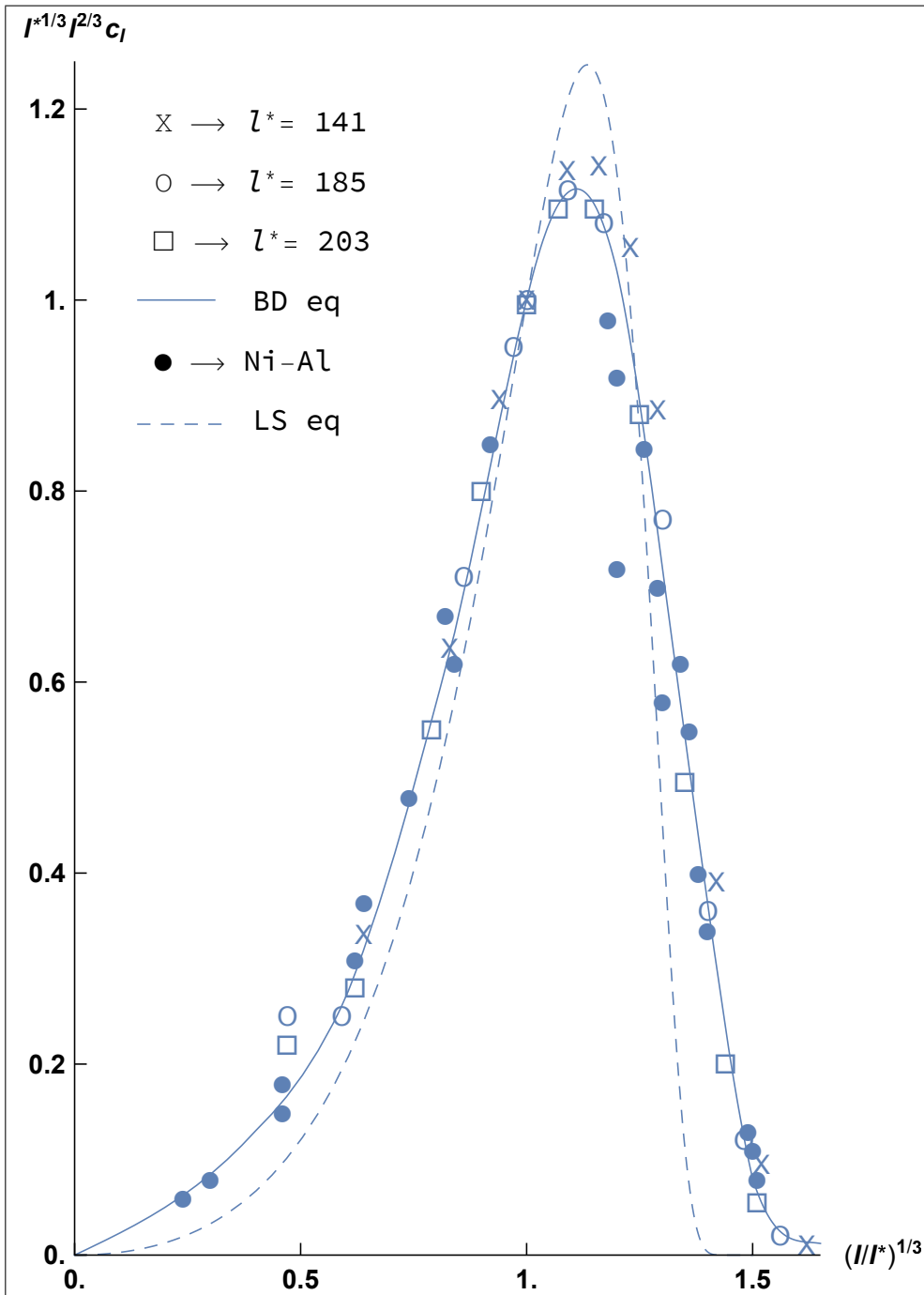


Fig. (VII, iii). Graph of $l^{*1/3} l^{2/3} c_l$ against $(l/l^*)^{1/3}$ for the Becker-Doring Equations (BD) and for an Ni-Al alloy. The predictions of the Lifshitz Slyozov (LS) theory are also given. All ordinates at $l = l^*$ are scaled down to 1. $\rho = 0.075$.

Lifshitz and Slyozov predict that the nucleation rate, $\frac{dl^*}{dt}$, should vary, if not strongly, with density ρ at fixed temperatures. This is confirmed in the differential equations and the simulations for densities $\rho = 0.075$ and 0.10 , as can be seen from the different gradients in Fig. (VI, iv) and Fig. (VI, v). This seems to be true also for NiAl alloys as evidenced in Table 1 of Ardell (1966). Conversely, the rate of coarsening of copper (Cu) in an α -Fe matrix does not depend on the volume fraction of the copper (Speich, 1965).

In practice, the rate of coarsening is heavily dependent on temperature through the constant D (or $p_0/3$) which satisfies Arrhenius Law, $\ln D \propto \frac{1}{T}$, in many systems including Cd-Ag (Pedder, 1979), Mn-Mg (Smith, 1967), and Si-Ni alloys (Ardell, 1969).

Discussion and Conclusions

The Becker-Döring system of differential equations, or some generalisation of it, was used by various authors to predict the time variation of the cluster size distribution. These authors include Courtney (1962), Abraham (1969), and Miold and Binder (1977). However, in these calculations, $a_l(0)$ was taken to be proportional to $l^{2/3}$, that is to the surface area of a sphere of volume l , rather than to $l^{1/3}$ as required by the diffusion mechanism of Lifshitz-Slyozov. Besides, the concentration of monomers, c_1 , is assumed to be constant in Courtney and in Abraham. For these reasons, their results are not readily comparable to ours.

The comparisons made in Chapter VII give some confirmation of the method used in Chapters III and IV for calculating the coefficients in the Becker-Döring kinetic equations for nucleation. This method was to calculate coefficients for cluster sizes 1 to 6, using a diffusion model, and then to extrapolate to larger values of l using the idea of Lifshitz and Slyozov that these coefficients should be proportional to $l^{1/3}$ for large cluster sizes l .

Our work shows that our system of differential equations is helpful in representing the behaviour of both real and simulated clusters, for a three dimensional lattice gas at temperature $0.59T_c$ and density $\rho = 0.075$. As shown in Chapter VII, the cluster size distribution is very well predicted in terms of l/l^* , where l^* is the critical cluster size, and our theory is an improvement on that of Lifshitz and Slyozov which predicts that there are no clusters with $(l/l^*)^{1/3} > 3/2$.

The success of our theory is due in part to the density corrections which

are applied to the various quantities in our analysis. The empirical formula (I, 6), which involves the density, gives a good description of the steady state distribution of small clusters in a lattice gas in terms of the supersaturation w , which is in turn related via (I, 9) to the critical cluster size l^* . The kinetic coefficients a_l and b_l also depend on density via equations (II, 4) and (II, 8), ensuring that the small clusters satisfy detailed balancing even in the steady state.

The quantity $l^*(t)$ is found to be approximately linear in both the differential equations and the simulation under steady state conditions, as predicted by Lifshitz and Slyozov. For density $\rho = 0.05$, $l^*(t)$ is well predicted by the differential equations. Unfortunately, however, for the higher densities $\rho = 0.075, 0.10$, the rate of growth of $l^*(t)$ is underestimated by the differential equations by a factor of 0.3. The reason for this discrepancy in the time scale is not understood at present, but it appears that the low-density theory upon which our calculations is based needs amendment before it can be applied at densities as high as 0.075.

In our work, the only processes considered were the absorption or emission of a monomer by a given cluster. However, at higher densities, a significant fraction of the particles are in dimers and larger clusters, so that processes such as the absorption or emission of dimers, ignored in this work, may have a significant effect on the transport of matter near a cluster. In this thesis, these density effects were lumped together in the empirical parameter μ , whose value appears to depend mainly on the concentration of monomers rather than the overall density. Further investigation is required to determine whether this procedure is theoretically justified, and if so, whether μ can be calculated from first principles.

References

- Abraham F. F. (1969) *J. Chem. Phys.* 51, 1632.
- Abraham F.F. (1974) *Homogeneous Nucleation Theory*, Academic Press, New York.
- Ardell A. J. (1969) *Experimental Confirmation of the Lifshitz-Wagner theory of Particle Coarsening in The Mechanics of Phase Transformations in Crystalline Solids*, Monograph 33, Page 111-116. Institute of Metals, London.
- Ardell A. J. and Nicholson R. B. (1966) *J. Phys. Chem. Solids* 27, 1793.
- Bauer S. H., Wilcox C. F. and Russo S. (1978) *J. Phys. Chem.* 82, 59.
- Becker R. and Döring W. (1935) *Ann. Der Phys.* 24, 719-752.
- Binder K. and Stauffer D. (1974) *Phys. Rev. Lett.* 33, 1006.
- Binder K. and Stauffer D. (1976) *Adv. Phys.* 25, 346.
- Cahn J. W. (1961) *Acta Metall.* 9, 795.
- Cahn J. W. (1962) *Acta Metall.* 10, 179.
- Chandrasekhar S. (1954) *Stochastic Processes in Physics and Astronomy* in the book *Noise and Stochastic Processes* edited by Wax N., Dover Publications, New York.
- Courtney W. G. (1962) *J. Chem. Phys.* 51, 1632.

- Fisher M. E. (1967) J. Appl. Phys. 38, 981.
- Fisher M. E. and Essam J. W. (1961) J. Math. Phys. 2, 609.
- Frenkel J. (1946) *Kinetic Theory of Liquids*, Dover, New York.
- Glauber R. (1963) J. Math. Phys. 4, 294.
- Greenwood G. W. (1969) *Particle Coarsening in The Mechanics of Phase Transformations in Crystalline Solids*, Monograph 33, Page 103-110. Institute of Metals, London.
- Huang J. S., Goldburg W. I. and Bjerkaas A. W. (1974) Phys. Rev. Lett. 32, 921.
- Huang J. S. and Goldburg W. I. (1976) Bull. Am. Phys. Soc. 21, No. 1, 55.
- Isaacson E. and Keller H. B. (1966) *Elements of Numerical Methods*, Wiley, New York.
- Ising E. (1925) Z. Phys. 31, 253.
- Kahlweit M. (1963) Z. Phys. Chem., 36, 292.
- Kalos M. H., Lebowitz J. L., Penrose O. and Sur A. (1978) J. Stat. Phys, 18, 39.
- Kawasaki K. (1966) Phys. Rev. 145, 224.
- Kawasaki K. (1972) *Kinetics of Ising Models* in Domb C. and Green M. S., *Phase Transitions and Critical Phenomena*, vol. 2, Academic Press, N. York.

- Lebowitz J. L. and Kalos M. H. (1976) *Scripta Metall.* 10, 9.
- Lebowitz J. L. and Penrose O. (1977) *J. Stat. Phys.* 16, 321.
- Lifshitz I. M. and Slyozov V. V. (1961) *J. Phys. Chem. Solids* 19, 35.
- Lothe J. and Pound G. M. (1962) *J. Chem. Phys.* 36, 2080.
- Marro J. (1976) Private communication to O. Penrose.
- Marro J., Bortz A.B., Kalos M.H. and Lebowitz J.L. (1975) *Phys. Rev. B* 12, 2000.
- Mirolid P. and Binder K. (1977) *Acta Metall.* 25, 1435.
- Pedder D. J. (1978) *Metall. T. A.* 9, 659.
- Penrose O. (1978) *Sections Notes in Physics*, 84 in *Stochastic Processes in Nonequilibrium Systems* edited by Garrido L., Springer, Berlin.
- Penrose O. (1979) Private communication to A. Buhagiar.
- Penrose O., Lebowitz J. L., Marro J., Kalos M. H. and Sur A. (1978) *J. Stat. Phys.* 19, 243.
- Penrose O. and Lebowitz J. L. (1979) *Towards a rigorous theory of metastability* in the series *Studies in Statistical Mechanics VIII*, edited by Montroll E. W. and Lebowitz J. L., North Holland, New York.
- Reiss H. (1974) *The Replacement Free Energy in Nucleation Theory* in *Nucleation II*, edited by Zettlemoyer A. C., M. Dekker, New York.

Smith A. F. (1969) *Acta Metall.* 15, 1867.

Smoluchowski M. (1916) *Phys. Z.* 17, 385.

Speich G. R. and Oriani R. A. (1965) *Trans. AIME.* 233, 623.

Sur A., Lebowitz J. L., Marro J. and Kalos M. H. (1977) *Phys. Rev.* B15, 535.

Sykes M. (1976) Private communication to O. Penrose.

Wagner C. (1961) *Z. Electrochem.* 65, 581.

Zarzycki J. and Naudin F. (1969) *J. of Non-Cryst Solids* I, 215-234.